

NASA Contractor Report 3784

Att. yes
R.B. in back
SPC

Fracture Behavior of Thick, Laminated Graphite/Epoxy Composites

C. E. Harris and D. H. Morris

GRANT NAG1-264
MARCH 1984

DEPARTMENT OF DEFENSE
PLASTICS TECHNICAL EVALUATION CENTER
ARRADCOM, DOVER, N. J. 07801

19960229 139

NASA

DTIC QUALITY INSPECTED 1

DISTRIBUTION STATEMENT A

Approved for public release;
Distribution Unlimited

PLASTEC
2/16/86

NASA Contractor Report 3784

Fracture Behavior of Thick, Laminated Graphite/Epoxy Composites

C. E. Harris and D. H. Morris

*Virginia Polytechnic Institute and State University
Blacksburg, Virginia*

Prepared for
Langley Research Center
under Grant NAG1-264

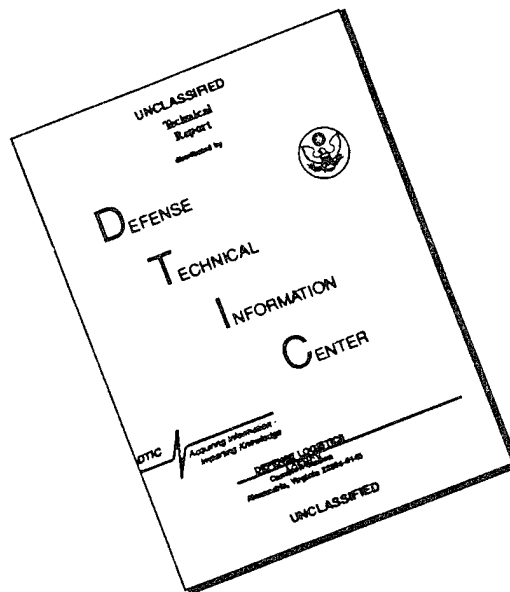


National Aeronautics
and Space Administration

**Scientific and Technical
Information Office**

1984

DISCLAIMER NOTICE



THIS DOCUMENT IS BEST QUALITY AVAILABLE. THE COPY FURNISHED TO DTIC CONTAINED A SIGNIFICANT NUMBER OF PAGES WHICH DO NOT REPRODUCE LEGIBLY.

Table of Contents

	<u>Page</u>
LIST OF FIGURES.....	v
LIST OF TABLES.....	x
SUMMARY.....	xi
1.0 INTRODUCTION.....	1
2.0 LITERATURE REVIEW.....	4
2.1 Formulation of the Characteristic Problem (Failure Criteria).....	4
2.2 Fracture Toughness Measurements.....	11
2.2.1 Review of Investigative Studies.....	12
2.2.2 Center-Cracked Tension Specimen Testing....	16
2.2.3 Three-Point Bend Specimen Testing.....	18
2.2.4 Compact Tension Specimen Testing.....	18
2.2.5 Effect of the Specimen Notch Root Radius on Test Results.....	18
2.2.6 Effects of Specimen Thickness on Toughness Values.....	22
2.3 Summary and Conclusions.....	23
3.0 DESCRIPTION OF THE RESEARCH PROGRAM.....	25
3.1 Specimen Test Program.....	25
3.2 Damage Evaluation Program.....	26
3.3 Evaluation of Postulated Prediction Models.....	29
4.0 METHODOLOGY AND PROCEDURES.....	31
4.1 Fracture Test Procedure.....	31
4.2 Enhanced X-ray Procedure.....	35
4.3 Specimen Depley Procedure.....	36
4.4 Determination of Fracture Toughness by the Stress Analysis Method.....	37
5.0 RESULTS AND DISCUSSION.....	39
5.1 Finite Element Stress Analysis of the Fracture Specimens.....	39
5.1.1 Description of the Finite Element Code.....	40
5.1.2 Description of the Finite Element Models...	40
5.1.3 Laminate Material Properties.....	45
5.1.4 Relationship Between Strain Energy Release Rate and Stress Intensity Factor.....	49
5.1.5 Results.....	51

5.2	Characteristics of the Load-COD Curves.....	55
5.3	The Effect of Laminate Thickness.....	59
5.3.1	The $[0/\pm 45/90]_{ns}$ Laminate.....	60
5.3.2	The $[0/90]_{ns}$ Laminate.....	82
5.3.3	The $[0/\pm 45]_{ns}$ Laminates.....	97
5.4	Comparison of the Test Results from the Center-Cracked Tension, Compact Tension and Three-Point Bend Specimen Types.....	113
5.5	Concluding Remarks.....	127
6.0	A CRITICAL ASSESSMENT OF THE APPLICABILITY OF CURRENT POSTULATED FRACTURE MODELS TO THICK LAMINATES.....	129
6.1	Description of Models.....	130
6.1.1	The Inherent Flaw Model.....	130
6.1.2	The Point Stress Model.....	132
6.1.3	The Average Stress Model.....	134
6.1.4	General Toughness Parameter.....	136
6.1.5	Mar-Lin Curve Fit Model.....	138
6.1.6	Determination of Strength and the Finite Width Correction Factor.....	138
6.2	Prediction of Notched Strength of Thin Laminates..	141
6.3	Application to Thick Laminates.....	149
7.0	SUMMARY AND CONCLUSIONS.....	155
	REFERENCES.....	159
	APPENDIX A	

LIST OF FIGURES

	<u>Page</u>
Fig. 3.1 Drawing of the Specimen Geometry with Dimensions (a) Center-Cracked Tension, (b) Compact Tension, (c) Three-Point Bend.....	28
Fig. 4.1 Center-Cracked Tension Test Setup.....	32
Fig. 4.2 Compact Tension Specimen Test Setup.....	33
Fig. 4.3 Three-Point Bend Specimen Test Setup.....	34
Fig. 5.1 8-Node Symmetric Crack-Tip Element [35].....	41
Fig. 5.2 Finite Element Model of the Center-Cracked Tension Specimen in the Crack Region.....	42
Fig. 5.3 Half-Symmetry Model of the Compact Tension Specimen.....	43
Fig. 5.4 Half-Symmetry Model in the Crack Region of the Three Point Bend Specimen.....	44
Fig. 5.5 Typical Plot of Load Versus COD for $[0/\pm 45/90]_s$ Laminates (Center-Cracked Tension Specimen).....	56
Fig. 5.6 X-ray Photographs of the Crack-Tip Damage (a) Just Before and (b) Just After a Large COD Discontinuity (Center-Cracked Tension Specimen).....	57
Fig. 5.7 Load Versus COD Records for the $[0/\pm 45/90]_{ns}$ Laminate at Various Thicknesses (Center-Cracked Tension Specimen).....	61
Fig. 5.8 Comparison of the Crack-Tip Damage in the 8 Ply and 64 Ply $[0/\pm 45/90]_{ns}$ Laminate at the First COD Discontinuity (Center-cracked Tension Specimens)	62
Fig. 5.9 Fracture Toughness Versus Laminate Thickness for the $[0/\pm 45/90]_{ns}$ Laminate, $2a/w = 0.5$ (Center- Cracked Tension Specimen).....	64
Fig. 5.10 Comparison of Fracture Toughness at the Maximum Load and at the Critical Load as a Function of Thickness for the $[0/\pm 45/90]_{ns}$ Laminate $2a/w =$ 0.5 (Center-Cracked Tension Specimen).....	65
Fig. 5.11 Fracture Toughness as a Function of $2a/w$ for $[0/\pm 45/90]_{ns}$ Laminates at 8 Plies and 120 Plies (Center-Cracked Tension Specimen).....	68

Fig. 5.12	X-ray Radiograph of the $[0/\pm 45/90]_S$ Specimen (Before Deply) at 77% of Average Failing Load (Center-Cracked Tension Specimen).....	69
Fig. 5.13	Documentation of the Through-the-Thickness Damage in a $[0/\pm 45/90]_S$ Specimen by Deply at 77% of Average Failing Load (Not Drawn to Scale), (Center-Cracked Tension Specimen).....	71
Fig. 5.14	Photograph of the $0/+45$ Delamination, Marked by Gold Chloride, at 20x Magnification.....	72
Fig. 5.15	Photograph of the 45° Line of Broken Fibers in the 0° Surface Ply at 20x Magnification.....	73
Fig. 5.16	Photograph of the $+45^\circ$ Line of Broken Fibers in the 0° Surface Ply at 200x and 400x Magnifications...	74
Fig. 5.17	Crack Tip Damage in the $[0/\pm 45/90]_S$ Specimen at 85% of Failing Load (Center-Cracked Tension Specimen).....	75
Fig. 5.18	Photograph of the Fracture Surface of a $[0/\pm 45/90]_S$ Specimen.....	76
Fig. 5.19	X-ray Radiograph of the $[0/\pm 45/90]_{15S}$ Specimen Before Deply, at 91% of Average Failing Load (Center-Cracked Tension Specimen).....	78
Fig. 5.20	Documentation of the Through-the-Thickness Damage in the $[0/\pm 45/90]_{15S}$ Specimen by Deply at 91% of Average Failing Load (Not Drawn to Scale) (Center-Cracked Tension Specimen) (a) First 8 Plies from Surface (b) Interior 6 0° Plies from Midplane....	79,80
Fig. 5.21	Photographs of the Final Fracture Surface of Two $[0/\pm 45/90]_{15S}$ Specimens.....	81
Fig. 5.22	Fracture Toughness as a Function of Laminate Thickness for the $[0/90]_{ns}$ Laminate; $2a/w = 0.5$ (Center-Cracked Tension Specimen).....	83
Fig. 5.23	Fracture Toughness as a Function of $2a/w$ for a $[0/90]_{ns}$ Laminate (Center-Cracked Tension Specimen)	85
Fig. 5.24	Crack Tip Damage in a $[0/90]_{2S}$ Specimen at 60% of Failing Load (Center-Cracked Tension Specimen)	86
Fig. 5.25	Crack Tip Damage in a $[0/90]_{2S}$ Specimen at 92% of Failing Load (Center-Cracked Tension Specimen)	87
Fig. 5.26	X-ray Radiograph of the $[0/90]_{2S}$ Specimen Before Deply at 71% of Average Failing Load (Center-Cracked Tension Specimen).....	89

Fig. 5.27	Documentation of the Through-the-Thickness Damage in the $[0/90]_{2s}$ Specimen by Deply at 71% of Average Failing Load (Not Drawn to Scale).....	90
Fig. 5.28	Comparison of the Load Versus COD Record for an 8 Ply and 32 Ply $[0/90]_{ns}$ Specimen (Center-Cracked Tension Specimen).....	91
Fig. 5.29	Photograph of a Fractured $[0/90]_{2s}$ Specimen.....	94
Fig. 5.30	Photograph of the Fracture Surface of a $[0/90]_{30s}$ Specimen.....	95
Fig. 5.31	X-ray Radiograph of a $[0/90]_{24s}$ Specimen at 96% of the Failing Load.....	96
Fig. 5.32	X-ray Radiograph of Crack Tip Damage in a $[0/90]_{24s}$ Compact Tension Specimen (a) Just After the First Load Reduction (b) After Final Load Reduction with Surface Ply Partially Peeled.....	98
Fig. 5.33	Fracture Toughness Versus Laminate Thickness for the $[0/\pm 45]_{ns}$ Laminate (Center-Cracked Tension Specimen).....	100
Fig. 5.34	Fracture Toughness as a Function of $2a/w$ for the $[0/\pm 45]_{ns}$ Laminates (Center-Cracked Tension Specimen).....	101
Fig. 5.35	Comparison of Typical Load Versus COD Records for the 6, 60 and 120 Ply $[0/\pm 45]_{ns}$ Laminates (Center-Cracked Tension Specimen).....	102
Fig. 5.36	X-ray Radiograph of the $[0/\pm 45]_s$ Specimen Before Deply at 83% of Average Failing Load (Center-Cracked Tension Specimen).....	105
Fig. 5.37	Documentation of the Through-the-Thickness Damage in the $[0/\pm 45]_s$ Specimen by Deply at 83% of Average Failing Load (Not Drawn to Scale), (Center-Cracked Tension Specimen).....	106
Fig. 5.38	Photograph of a Fractured $[0/\pm 45]_s$ Specimen.....	108
Fig. 5.39	X-ray Radiograph of the 120 Ply $[0/\pm 45]_{ns}$ Specimen Before Deply at 92% of Average Failing Load (Center-Cracked Tension Specimen).....	109
Fig. 5.40	Documentation of the Through-the-Thickness Damage in the $[0/\pm 45]_{20s}$ Specimen by Deply at 92% of Average Failing Load (Not Drawn to Scale), (Center-Cracked Tension Specimen) (a) First 7 Plies from the Surface (b) Interior 6 0° Plies from the Midplane.....	110

Fig. 5.41	Photographs of the Fracture Surface of Several 120 Ply $[0/\pm 45]_{ns}$ Specimens.....	112
Fig. 5.42	Comparison of Typical Load Versus COD at 64 Plies for: (a) Center-Cracked Tension Specimen (b) Three Point Bend Specimen (c) Compact Tension Specimen.....	115
Fig. 5.43	Comparison of Damage at the First COD Discontinuity for the $[0/90]_{ns}$ Laminate at 64 Plies (a) Center-Cracked Tension at 96% of Failing Load (b) Compact Tension (c) Three Point Bend.....	117
Fig. 5.44	Comparison of Damage at the First COD Discontinuity for the $[0/\pm 45/90]_{ns}$ Laminate at 64 Plies (a) Center-Cracked Tension at 92% of Failing Load (b) Compact Tension (c) Three Point Bend.....	118
Fig. 5.45	Comparison of the Fracture Toughness of the $[0/\pm 45/90]_{ns}$ Laminate for the Center-Cracked Tension, Compact Tension and the Three Point Bend Specimens; $2a/W = 0.50$	119
Fig. 5.46	Comparison of the Fracture Toughness of the $[0/90]_{ns}$ Laminate for the Center-Cracked Tension, Compact Tension and the Three Point Bend Specimens; $2a/W = 0.50$	120
Fig. 5.47	Comparison of the Fracture Toughness of the $[0/\pm 45]_{ns}$ Laminate for the Center-Cracked Tension, Compact Tension and the Three Point Bend Specimens; $2a/W = 0.50$	121
Fig. 5.48	Development of Crack Tip Damage in the Three Point Bend Specimen of the $[0/\pm 45]_{ns}$ Laminate (a) Just After the First Load Reduction, (b) After the Final Load Reduction.....	125
Fig. 5.49	Development of Crack Tip Damage in the Compact Tension Specimen of the $[0/\pm 45]_{ns}$ Laminate (a) Just After the First Load Reduction (b) Just After the Final Load Reduction.....	126
Fig. 6.1	"High Intensity Energy Zones" Postulated by Waddoups, Eisenmann and Kaminski [5].....	131
Fig. 6.2	Point Stress Model of Whitney and Nuismer [6]....	133
Fig. 6.3	Average Stress Model of Whitney and Nuismer [6]..	135

Fig. 6.4	Comparison of Experimental and Predicted Values of Notched Laminate Strength of the 8 Ply and 120 Ply $[0/\pm 45/90]_{ns}$ Laminates.....	143
Fig. 6.5	Comparison of the Experimental and Predicted Values of Notched Laminate Strength of the 8 Ply and 96 Ply $[0/90]_{ns}$ Laminates.....	144
Fig. 6.6	Comparison of the Experimental and Predicted Values of Notched Laminate Strength of the 6 Ply and 90 Ply $[0/\pm 45]_{ns}$ Laminates.....	145
Fig. 6.7	Comparison of the Experimental and Predicted Values of Notched Laminate Strength at the Critical Load for the $[0/90]_{2s}$ Laminate.....	147
Fig. 6.8	Comparison of the Mar-Lin Curve Fit at the Critical Load and Maximum Load for the Thin Laminates.....	148
Fig. 6.9	Comparison of the Mar-Lin Curve Fit at the Maximum Load for the Thin and Thick Laminates.....	153

LIST OF TABLES

	<u>Page</u>
Table 2.1 Summary of Fracture Toughness Tests Utilizing the Center-Cracked Tension Specimen.....	17
Table 2.2 Summary of Fracture Toughness Tests Utilizing the Three Point Bend Specimen.....	19
Table 2.3 Summary of Fracture Toughness Tests Utilizing the Compact Tension Specimen.....	20
Table 2.4 Summary of the Specimen Notch Root Radii.....	21
Table 3.1 Fracture Toughness Test Matrix.....	27
Table 5.1 Measured Lamina Stiffness Properties.....	47
Table 5.2 Laminate Engineering Stiffness Properties.....	48
Table 5.3 Finite Element Analysis Stress-Strain Anisotropic Material Property Input.....	50
Table 5.4 Orthotropic Relationship Between Strain Energy Release Rate and Stress Intensity Factor for Mode I.....	52
Table 5.5 Comparison of the Finite Element Analysis Results to the ASTM Standards [1,2] for an Isotropic, Plane Strain Analysis for 1.0 in. (25.4 mm) Thick Specimens.....	53
Table 5.6 The Effects of Material Anisotropy on the Plane Stress and Plane Strain Stress Intensity Factors	54
Table 5.7 Test Data for the $[0/90]_{2S}$ and $[0/90]_{8S}$ Laminates	93
Table 5.8 Crack Tip Damage Zone Size.....	104
Table 6.1 Characteristic Distances Computed from Thin Laminate Data.....	142
Table A-1 Notched Specimen Test Data for the $[0/\pm 45/90]_{ns}$ Laminates.....	A-2
Table A-2 Notched Specimen Test Data for the $[0/\pm 45]_{ns}$ Laminates.....	A-6
Table A-3 Notched Specimen Test Data for the $[0/90]_{ns}$ Laminates.....	A-10

SUMMARY

The effect of laminate thickness on the fracture behavior of laminated graphite/epoxy (T300/5208) composites has been studied. The predominantly experimental research program included the study of the $[0/\pm 45/90]_{ns}$ and $[0/90]_{ns}$ laminates with thicknesses of 8, 32, 64, 96 and 120 plies and the $[0/\pm 45]_{ns}$ laminate with thicknesses of 6, 30, 60, 90 and 120 plies. The research concentrated on the measurement of fracture toughness utilizing the center-cracked tension, compact tension and three point bend specimen configurations. Fracture toughness was computed using the stress intensity factor results of a finite element stress analysis of each specimen geometry which treated the composite as homogeneous but anisotropic. The development of subcritical damage at the crack tip was studied nondestructively using enhanced x-ray radiography and destructively using the laminate delly technique.

The test results showed fracture toughness to be a function of laminate thickness. The fracture toughness of the $[0/\pm 45/90]_{ns}$ and $[0/90]_{ns}$ laminates decreased with increasing thickness and asymptotically approached lower bound values of $30 \text{ ksi}\sqrt{\text{in}}$ ($1043 \text{ MPa}\sqrt{\text{mm}}$) and $25 \text{ ksi}\sqrt{\text{in}}$ ($869 \text{ MPa}\sqrt{\text{mm}}$) respectively. The fracture toughness of the $[0/\pm 45/90]_{ns}$ laminate was independent of crack length at 8 and 120 plies. The fracture of the thin and thick $[0/\pm 45/90]_{ns}$ laminates were self-similar, macroscopically. However, the $[0/90]_{2s}$ laminate exhibited fracture toughness values that increased sharply as a function of increasing crack size. This was attributed to large axial splits which formed perpendicular to the crack tip in the 0° plies and extended in the direction of applied load. The fracture toughness of the $[0/90]_{ns}$ laminate was independent of crack length at 90 plies. The axial splits

in the 0° plies of the thicker specimens were confined to the surface and the final fracture was self-similar. For both the $[0/\pm 45/90]_{NS}$ and $[0/90]_{NS}$ laminates, the center-cracked tension, three-point bend and compact tension specimens gave comparable results.

In contrast to the other two laminates, the fracture toughness of the $[0/\pm 45]_{NS}$ laminate increased sharply with increasing thickness but reached an upper plateau value of $40 \text{ ksi}\sqrt{\text{in}}$ ($1390 \text{ MPa}\sqrt{\text{mm}}$) at 30 plies. Fracture toughness was independent of crack size at 6 and 90 plies. The 6 ply specimens failed by an apparent uncoupling mechanism where the two interior -45° plies delaminated from the adjacent $+45^\circ$ plies and failed by matrix splitting parallel to the fibers. The surface 0° plies failed by broken fibers along a $+45^\circ$ line in association with matrix splitting parallel to the fibers in the $+45^\circ$ plies. The thick $[0/\pm 45]_{NS}$ laminates exhibited a surface boundary layer in which 45° fiber breaks and splits were evident along with delaminations. However, the interior of the specimens failed in a self-similar manner with fibers in the 0° plies breaking along a line collinear with the starter notch. The compact tension and three-point bend specimens defined a constant fracture toughness at about 15% below the plateau exhibited by the center-cracked tension specimens.

The general toughness parameter model, a strain criterion developed by C. C. Poe, Jr. of NASA Langley, was the only candidate thin laminate failure criterion that was successful in using thin laminate parameters to predict the fracture of thick laminates. The "universal" general toughness parameter value of $1.5 \sqrt{\text{mm}}$ quite closely predicted the fracture of the thick laminates.

1.0 INTRODUCTION

Fiber reinforced composite materials have a superior strength-to-weight ratio as well as other mechanical and thermal property advantages over isotropic metals such as steel or aluminum. This has led to increased utilization of these materials as major structural components in many practical applications. Examples can be found in the automotive and aerospace industries, such as the payload bay doors of the space shuttle.

The mechanics of laminated composite structures is theoretically highly developed. However, experimental studies confirming these theories have been conducted almost exclusively on thin laminates generally less than one-tenth of an inch in thickness. In contrast, many structural components are substantially thicker; often five or ten times thicker. As an example, the horizontal stabilizers on the U.S. Air Force F-18's are approximately 160 plies thick.

In general, geometry effects such as thickness variations do not affect the determination of material properties and are easily addressed by applied mechanics theories. This is not necessarily the case in the area of fracture mechanics. For isotropic metals the state-of-the-art of fracture mechanics is highly developed and the plane strain fracture toughness is treated as a material property. However, no such fracture toughness material property has been identified for laminated composite materials. Also the measured fracture toughness of composites has shown variations with specimen configuration and specimen geometry such as width and thickness. Furthermore, the correlation between thin laminate fracture characteristics and the fracture behavior of thick laminates has not been established.

Most composite laminates are notch sensitive. Therefore, when a structural component is damaged such as by a dropped tool or has a designed cutout such as a bolt hole, the composite laminate loses much of its original strength. The designer must be cognizant of the fracture mechanics considerations and must know the fracture toughness of the material to properly design a "damage tolerant structure." Because of the wide variation in composite laminate materials and ply layups, it is not practical to determine the fracture toughness of every laminate. Therefore, a general fracture toughness material property that can be used in conjunction with a failure criterion for composite structures is greatly needed by the structural designer.

The relationship between fracture toughness and specimen thickness has been established for isotropic materials. Fracture toughness is a decreasing function of increasing specimen thickness. A lower bound toughness value corresponding to a condition of plane strain at the crack-tip is asymptotically approached. Discussions of this relationship and the implications thereof can be found in references such as ASTM STP 410 [1] and STP 463 [2]. The crack-tip state-of-stress is directly related to the relationship between the size of the plastic zone at the crack-tip and the specimen thickness. If the specimen thickness is large relative to the size of the crack-tip plastic zone, sufficient constraint in the interior will be present to produce plane strain conditions. Plane stress conditions prevail when the specimen is too thin to provide constraint in the interior. However, no such relationship between fracture toughness and laminate thickness has been established for fiber reinforced laminated composites.

The first specimen configurations utilized for fracture toughness testing of metals and composites were the center-cracked and double-edge notched tension specimens. Problems associated with testing these configurations began to surface when test results identified the dependence of fracture toughness on specimen thickness. The thick specimens required higher loads that exceeded the load capacity of many testing machines. Also, problems developed with regard to gripping the specimens. (The gripping problem is especially acute for laminated composites.) The three-point bend and compact tension specimens were proposed as alternative configurations and were verified as being acceptable for plane strain fracture toughness testing by the ASTM [1,2]. Primarily because most laminated composites testing has been confined to thin sheets, no such verification of the similarity of test results from the three specimen configurations has occurred for composite materials.

The primary objective of this research is to investigate the fracture characteristics of thick laminated composites. The fracture behavior of thick laminates will be compared to that of thin laminates. The experimental phase of the program will concentrate on the measurement of the fracture toughness of thick laminates utilizing the center-cracked tension, compact tension and three point bend specimen configurations. Also, the modes of damage development and the type of final fracture will be studied and documented. The analytical phase of the research will investigate the applicability of several candidate thin laminate fracture criteria to the prediction of the fracture failure of thick laminated composites.

2.0 LITERATURE REVIEW

The literature review summarized herein has emphasized the characterization of fracture or failure of laminated composites, measurement of fracture strength and toughness, and the development and employment of analytical models to predict fracture strength and toughness. The summary is divided into two primary areas. The first is the characterization of fracture, development of failure criteria, and the associated analytical models. The second primary area is the measurement of fracture strength and toughness. A number of investigative studies are summarized with the emphasis on attempts to identify and measure a material property, effects of laminate configuration on the failure mode of the specimen, and the effects of specimen type and geometry on measured toughness values. The literature review also emphasized the fracture characterization of thick laminates and the effects of specimen thickness on the measurement of fracture toughness.

Only selected articles and studies are summarized herein. The summary traces the key developments in the characterization of fracture of laminated composites. These developments have occurred primarily over the past fifteen years. The literature survey placed special emphasis on the time period of 1976 to the present.

2.1 Formulation of the Characteristic Problem (Failure Criteria)

In the late 1950's and early 1960's several investigators modified linear elastic fracture mechanics (LEFM) for a homogeneous anisotropic material. Paris and Sih [3] developed expressions for the crack tip stress field using Hooke's law for a homogeneous linear anisotropic material for the cases of plane strain and pure shear. The crack tip

stress field exhibited the same $r^{-1/2}$ singularity and the expressions for stress are analogous to those for the isotropic case. The stress intensity factors K_I , K_{II} , and K_{III} were exactly the same as for the isotropic case. Wu [4] found that linear elastic fracture mechanics was applicable to composite laminates if self-similar crack growth occurred and the anisotropic stress distribution and stress intensity factors were defined consistently with the isotropic case.

Perhaps the earliest attempt to employ LEFM to address the behavior of a composite laminate was not a typical cracked body problem but rather had to do with paradoxical data from fatigue tests of graphite-epoxy laminates with stress concentrations [5]. The residual strength after 5×10^6 cycles was greater than the static strength in laminates with through holes and notches. Also even though the material was brittle, through cracks did not nucleate and grow as for isotropic metals. Waddoups, et al. [5] postulated the existence of a "high intensity energy region" adjacent to the holes and at the tip of notches which could be represented by a characteristic dimension, a . The characteristic dimension was then utilized much like Irwin's plastic zone correction factor for isotropic materials to modify the stress intensity factors and hence the stress distribution. The critical stress or strength of the laminate was then computed from K_{IC} and a , given the geometry and stress intensity factor. This approach of characterizing the damage zone and modifying the LEFM stress intensity factors became known as the inherent flaw model.

Recognizing that single cracks do not nucleate and grow under fatigue loading in composites as they do in metals led investigators to question the general applicability of LEFM to composite laminates. The

question became one of defining the characteristic problem. This prompted some investigators to postulate non-fracture mechanics stress fracture criteria and others to conduct fundamental exploratory programs into the nature of composite fractures. Whitney and Nuismer [6,7] postulated several two-parameter models based on a critical stress value and the stress distribution adjacent to discontinuities such as circular holes and straight cracks. The "point stress model" postulated failure to occur when the stress at some distance, d_0 , from the discontinuity reached the fracture stress, σ_0 , of an unnotched specimen. The "average stress model" postulated failure to occur when the average stress at some distance, a_0 , from the discontinuity reached the critical stress, σ_0 . Whitney and Nuismer further postulated that the distances d_0 and a_0 may characterize some critical damage state for a given composite and thus be a material property. Measurements of a_0 and d_0 were made and the models were found to work well for some laminates and not so well for others.

Mandell, et al. [8] conducted an analytical and experimental study of prenotched [45/-45/-45/45] graphite/epoxy laminates. They observed that the specimens did not fail by self-similar crack growth. There was extensive subcritical splitting parallel to the fibers and some delamination of the plies. This may lead to natural crack tip blunting and caused the investigators to question the existence of the $r^{-1/2}$ singularity at the crack tip and the applicability of LEFM to these laminates. During the same time period Cruse and Osias [9] were conducting an exploratory study of a number of different angle-ply laminates of graphite/epoxy. Their objectives were to answer fundamental questions concerning the failure modes, applicability of LEFM, the existence of a

fracture strength independent of specimen configuration and geometry, and models to predict the fracture strength. Their test results indicated that asymptotic values of toughness could be measured, inhomogeneous effects such as fiber size and ply thickness were not significant, and that simple macromechanics models based on LEFM could be employed to predict fracture. Cruse and Osias developed a model based on a special form of the boundary integral equation (BIE) method of analyzing cracked-body geometries. The BIE model uses boundary data on the surface of an arbitrary body, excluding the crack surfaces, and Green's influence function to solve the cracked-body problem.

Zweben [10] and Goree and Gross [11] developed shear-lag models to predict the behavior of unidirectional fiber-reinforced composites which were susceptible to matrix splitting ahead of the crack tip rather than fiber breaks. The basic two-dimensional model assumed that the fibers supported all of the axial force because they had a much higher elastic modulus than the matrix. The matrix, in turn, supported shear forces and transverse normal forces. Both investigators reported close agreement between the model predictions and experimental results for cases that split axially in the matrix and those that did not. A modified version of the shear lag model [12] can also be employed to predict the behavior of angle-ply laminates such as $[0/\pm\theta]_s$ by treating the plies adjacent to the 0° ply as a constraint layer in the model. For example, this type of model has been used to qualitatively predict the fracture strength of $[0/90]_{2s}$ laminates [13].

During the 1970's numerous investigations were conducted in which composite laminate fracture toughness or fracture strength were measured, modes of failure observed, and various models used to predict

fracture. In 1979, Yeow, et al. [14] published a correlative study of graphite/epoxy laminates. Measured data was obtained from $[0]_{8S}$, $[0/\pm 45/0]_{2S}$, $[0/90]_{4S}$ and $[\pm 45]_{4S}$ laminates. Fracture was predicted using the inherent flaw model of Waddoups, et al. [5], the point and average stress models of Whitney and Nuismer [6] and the boundary integral equation model of Snyder and Cruse [15,16]. Experimentally, Yeow found that the $[0]_{8S}$ and $[\pm 45]_{4S}$ laminates failed by splitting parallel to fibers. The $[0/90]_{4S}$ laminate failed initially by crack propagation parallel to the fibers in the inner ply. The $[0/\pm 45/0]_{2S}$ laminates failed by fracture of the fibers in the outer ply. The analytical results were "generally poor" for the inherent flaw, point and average stress models but excellent for the boundary integral equation model with the exception of the $[0]_{8S}$ laminate where the failure mode was axial splitting.

Thus far, the discussion has concentrated on macromechanical models of fracture. In addition to the shear lag model there are several noteworthy micromechanical models. Sih, et al. [17] developed a low fiber volume and high fiber volume micromechanical model of fracture. Comparisons of predictions and measurements indicated, at least qualitatively, that the models have merit in addressing the relative fracture toughness of laminates. Griffith [18] et al., developed a finite element micromechanical model of an individual cracked ply where the region surrounding the crack tip was modeled to reflect its heterogeneous character. This allowed the crack predictions to be based on the fracture behavior and properties of the fibers, matrix and interfaces. Laminate behavior was then predicted by using fracture mechanics to trace the damage growth in each ply. The energy release rate approach was used to assess

crack growth both parallel to and normal to the fiber directions. Ueng et al. [19] also utilized the finite element method to demonstrate the potential of micromechanics modelling techniques to account for layering and heterogeneity in the crack tip region.

Micromechanics models are attractive because they would allow the prediction of laminate toughness directly from the properties of the constituents. However, a prediction of this nature necessitates a thorough knowledge of the state of stress at the crack tip. Because of the heterogeneity in the crack tip region this knowledge can only be postulated. Therefore, micromechanics models are generally viewed as having somewhat limited potential at the present.

In 1980-81, Poe [13,20] postulated a new composite laminate fracture criterion. Poe assumed that a laminate failed whenever the fiber strains (or stress) reached a critical value in the principle load-carrying laminae. Using laminate theory and linear elastic fracture mechanics, the expressions for singular zone strains in the i^{th} laminae

are

$$\begin{Bmatrix} \epsilon_1 \\ \epsilon_2 \\ \gamma_{12} \end{Bmatrix}_i = \frac{K}{E_y \sqrt{2\pi r}} \begin{Bmatrix} \xi_1 \\ \xi_2 \\ \xi_{12} \end{Bmatrix}_i$$

where

$$\begin{Bmatrix} \xi_1 \\ \xi_2 \\ \xi_{12} \end{Bmatrix}_i = [T]_i [\beta] \begin{Bmatrix} \sqrt{E_x E_y} \\ E_y \\ 0 \end{Bmatrix}$$

$[T]_i$ = Transformation matrix for the i^{th} laminae

$[\beta]$ = matrix of constitutive properties, plane stress

E_x, E_y = laminate stiffness properties with the y direction being the loading direction.

It is easily seen that $\epsilon_1 \sqrt{2\pi r}$ is a constant at failure. This yields a constant fracture toughness parameter, Q_C , defined as follows

$$Q_C = K_Q(\epsilon_1)_i / E_y$$

where K_Q is the stress intensity factor at failure, and $(\epsilon_1)_i$ is calculated for the principle load-carrying laminae. Q_C values were calculated from data obtained from center-cracked panel specimens of various boron/aluminum laminates. Q_C was independent of laminate orientation and varied proportionally with the critical stress intensity value, with the constant of proportionality being a function of the laminate constants only. This same result was found to be the case for other composite materials as well. Constant Q_C appears to hold whether fiber dominated or matrix dominated laminates are considered. Furthermore, when the fracture parameter, Q_C , is divided by the ultimate tensile strain of the fibers, ϵ_{tuf} , the ratio appears to be roughly constant ($\approx 1.5\sqrt{\text{mm}}$) for those laminates that exhibit self-similar fracture, regardless of material type and laminate stacking sequence. Finally, the ratio Q_C/ϵ_{tuf} can be shown to be proportional to the square root of a characteristic distance, d_0 , from the crack tip where $\epsilon_1 = \epsilon_{tuf}$. If Q_C/ϵ_{tuf} is constant then so will be d_0 . The values of d_0 determined in this manner are quite different from those obtained from the point stress or average stress models. However, strength values predicted by using d_0 compared quite well to measured strengths even for laminates such as $[\pm 45]_s$. Q_C/ϵ_{tuf} appears to be more universally applicable in predicting failure than is the point or average stress model. Poe's study and conclusions regarding Q_C and Q_C/ϵ_{tuf} were based on data from

center-cracked tension tests only. It should be noted that $Q_c/\epsilon_{tuf} \approx 1.5\sqrt{\text{mm}}$ was within normal data scatter for all specimens except those that did not fail due to self-similar crack growth. For specimens that split extensively or delaminated the value of Q_c/ϵ_{tuf} was significantly different.

Using an entirely different approach, in an attempt to define the characteristic problem for failure of composite laminates, statistical-strength theory models are being developed. As an example, Whitney and Knight [21] used a two-parameter Weibull model to address the failure strength of graphite/epoxy. The two parameters were the characteristic strength and a shape factor which characterized the flaw distribution in the material. While their results were inconclusive others, such as Bullock [22], have reported that the Weibull model is valid for graphite/epoxy. For these statistical models to be anything more than a curve fit the fundamental question to be addressed is whether or not the shape factor that characterizes the flaw distribution is a material property.

2.2 Fracture Toughness Measurements

Numerous experimental investigations of the fracture toughness of composite laminates have been conducted during the past decade. Representative programs have been selected and reviewed herein. They include investigations of a multitude of laminate configurations for graphite/epoxy, glass/epoxy and boron/aluminum materials. A brief summary is provided below in chronological order with the emphasis on specimen type and geometry effects as well as the effects of laminate failure modes on the measured fracture toughness or strength.

2.2.1 Review of Investigative Studies

In 1973 Mandell, et al. [8] conducted an exploratory program to evaluate fracture toughness and the applicability of LEFM to graphite/epoxy laminates. Single and double edge notched tensile specimens were tested from seven different laminates. Specimen geometry was not investigated. Mandell found that subcritical crack zones blunted the cracks and that general yielding in regions removed from the crack tip occurred. Some laminates failed in simple failure modes while the more complex laminates had associated complex failure modes. The test results led the investigators to question the applicability of LEFM to compute a meaningful toughness value.

Cruse and Osias [9] reported the results of an exploratory program in 1974. Three-point bend and center-cracked tension specimens from ten angle-ply laminates of graphite/epoxy were tested. It was generally concluded that the fracture toughness was independent of specimen geometry. Toughness data from center-cracked tension specimens indicated an asymptotic value of K_Q as the crack length, $2a$, approached one inch. Data from the two types of specimens of a $[0/\pm 45]_S$ laminate were comparable. Because the three-point bend and center-cracked specimens were of different thicknesses, it was concluded that the fracture strength was independent of specimen thickness. Cruse and Osias also concluded that the three-point bend specimen gave valid fracture toughness data that approached the asymptotic value from the center-cracked tension specimen tests.

Compact tension specimens were used by Slepetz and Carlson [23] to study seven glass/epoxy laminates and five graphite/epoxy laminates. The compact tension specimens appeared to give valid test results except

for the 0° case where splitting perpendicular to the notch occurred. The application of the compliance calibration technique was found to be limited to the 90° laminate and cross-ply laminates of graphite/epoxy and generally not applicable to cross-ply or angle-ply glass/epoxy. Slepetz and Carlson observed that unidirectional laminates had toughness dependent on crack length but cross-ply laminates did not. The compact tension toughness values were reasonably consistent with reported test data from other test methods.

Owen and Cann [24] reported test results on glass-reinforced plastics (GRP) from 12 investigators. They concluded that the critical fracture toughness (K_C) and critical strain energy release rate (G_C) values depended on specimen type, size and crack length. Correlations between K_C and G_C results were poor. Furthermore, conditions for valid fracture toughness testing of GRP had not yet been established.

In 1977 Sun and Prewo [25] reported the results of an investigation of four boron/aluminum laminates using compact tension specimens. Fracture toughness was determined using the compliance method and stress analysis methods. They found that both methods gave similar fracture toughness values provided the specimens exhibited collinear (self-similar) crack growth with the starter notch. They tested specimens of two different thicknesses and found that the thin specimen fracture toughness was dependent on the ratio of crack length to specimen width ($\frac{a}{W}$), whereas the fracture toughness of thick specimens was less dependent on $\frac{a}{W}$.

Hahn and Morris [26] used the resistance curve technique to generate fracture toughness resistance (K_R) curves for three graphite/epoxy laminates. Test specimens were center-cracked tension of three thick-

nesses. They found that the value of K_R at initiation of crack growth was fairly independent of initial crack length. They also concluded that the thickness did not seem to affect the fracture strength.

In 1978, Prewo [27] investigated the effects of layup sequence of 0° and 90° plies of boron/aluminum using both compact tension and center-cracked tension specimens. He reported a tendency of cracks to grow at right angles to the premachined notch in compact tension specimens. The tendency varied with the percent of 0° plies and with the specimen $(\frac{a}{W})$ ratio. Toughness data from the two specimen types did not agree. The toughness of the center-cracked specimens was considerably lower than the values from the compact tension specimens. Since the compact tension specimen toughness decreased with increasing $(\frac{a}{W})$ it was postulated that toughness values from the two specimen types may be the same at some high $(\frac{a}{W})$ value.

Yeow, Morris and Brinson [28] investigated the fracture behavior of four laminates of graphite/epoxy using center-cracked tension specimens of varying $(\frac{a}{W})$ values. Some laminates exhibited self-similar crack growth while the $[0]_{8S}$ and $[\pm 45]_{4S}$ laminates did not. There was some slight dependence on $(\frac{a}{W})$ ratios with toughness increasing with increasing $(\frac{a}{W})$.

In 1980 Reedy [29] reported the results of his study of specimen type and geometry effects on the fracture toughness of unidirectional, transverse notched boron/aluminum. Comparing the results from center-cracked tension, compact tension, and three point bend specimens, Reedy reported that the specimens did not exhibit the same failure modes and that the toughness varied with specimen geometry and type. He concluded that no material property had been defined in his investigation. Tough-

ness from three-point bend specimens was only 60% of the toughness from center-cracked tension specimens with both specimen types exhibiting collinear crack growth. The compact tension specimens did not exhibit collinear crack growth and had a substantially lower toughness. The center-crack tension specimens exhibited the greatest scatter band which was attributed in part to load induced bending and nonuniformity in the grip pressure. Three point bend test fixtures was also addressed. The toughness from roller supports was lower than for fixed supports. This was attributed to the high local yielding under the load ram and supports in the fixed case. Also the three point bend fracture toughness appeared to be independent of span length. Reedy's final observation of considerable yielding in regions not confined to the crack tip led him to question the applicability of LEFM to predict fracture toughness.

An investigation of 5 laminates of boron/aluminum using center-cracked tension specimens with various width and $(\frac{a}{W})$ values was reported by Poe and Sova [20] in 1980. Failure of all specimens was generally collinear with the starter notch. However, $[0]_{6T}$ specimens did exhibit matrix cracking that was perpendicular to and at the ends of the notch. Failure began as tensile failure of the fibers at the notch ends in the principle load carrying laminae. Most laminates showed some increase in toughness with increasing $(\frac{a}{W})$ and also with increasing width. These variations were not overly pronounced except in the $[0]_{6T}$ specimens where the toughness varied by about a factor of two. Poe [13] also reported data from three quasi-isotropic laminates of graphite/epoxy. Data obtained from center-cracked tension specimens with various widths but $\frac{a}{W} = 1/3$ showed some increase in toughness with increasing width.

Finally, in 1981 Shih and Logsdon [30] investigated the fracture toughness of a thick (2.125 in., 54.0 mm) quasi-isotropic graphite/epoxy laminate. Edge-notched, center-notched, and three point bend specimen tests were conducted on specimens with various $(\frac{a}{W})$ values. "Thin" specimens (0.25 in., 6.35 mm and 0.50 in., 12.7 mm) were cut from the thick laminate with the specimen notches oriented in the laminate thickness direction, i.e. the notches were not through the laminate thickness. The three point bend specimen toughness values were about twice those of the center-notched tension specimen. The three-point bend specimen toughness was dependent on the notch depth but the center-notched tension specimen toughness was not. Modes of failure included delamination and crack growth that was not self-similar. Delaminations perpendicular to the notch in the center-notched specimens caused deviations from linearity. Shih and Logsdon concluded that LEFM was not directly applicable to thick-section composites with cracks perpendicular to the fiber orientation.

2.2.2 Center-Cracked Tension Specimen Testing

Table 2.1 presents a summary of fracture toughness tests utilizing the center-cracked tension (CCT) specimen geometries including comments on geometry effects on toughness. The bulk of the composite laminate toughness testing has been performed using this specimen. This is largely due to the fact that the laminates are generally quite thin so the CCT specimens are the easiest to test. Results indicate that fracture toughness varies with both the width W , and the $(\frac{a}{W})$ ratio. However, toughness appears to approach an asymptotic value when the width

Table 2.1 Summary of Fracture Toughness Tests Utilizing the Center-cracked Tension Specimen

Investigation	Mat'l Type	Thickness in.(mm)	Width in.(mm)	2a/W	Comments
Hahn & Morris [26]	Gr/Ep	.035(.89) .065(1.65)	2.0(50.8) 2.0(50.8)	0.1-0.5 0.1-0.5	Negligible thickness effect
Yeow, et al. [14]	Gr/Ep	0.1(2.54)	1.0(25.4)	0.15-0.45	Minor variation with 2a/W
Shih & Logsdon [30]	Gr/Ep	0.25(6.35)	2.0(50.8)	0.40-0.60	Toughness independent of 2a/W
Poe [13]	Gr/Ep	16 Plies	0.87(22.1) -4.0(101.6)	0.30	Minor variation in toughness
		16 Plies	2.0(50.8) 2.0(50.8)	0.17	
		16 Plies	-4.0(101.6)	0.33	
Cruse & Osias [9]	Gr/Ep	.070(1.78) .074(1.88) .074(1.88)	0.5(12.7) 1.0(25.4) 2.5(63.5)	0.2 0.2 0.2	Reported an asymptotically approached K _{IC}
Mandell, et al. [8]	Gr/Ep	4-7 plies 4-7 plies	1.50(38.1) 2.0(50.8)	0.167, 0.125 0.167, 0.125	
Reedy [29]	Bo/Al	.20(5.08)	1.0(25.4)	0.5	Toughness increased with increasing width and 2a/W
Poe & Sova [20]	Bo/Al	6 plies 8 plies 8 plies	0.75(19.1) 2.0(50.8) 4.0(101.6)	.026, .068 .05-.50 .05-.50	
Prewo [27]	Bo/Al	.077(1.96)	1.38(34.3)	.09-.38	

is in the vicinity of 2 in. (50.8 mm) and $(\frac{a}{W})$ is in the vicinity of one-half. There are no other obvious geometry effects, such as thickness.

2.2.3 Three-Point Bend Specimen Testing

Table 2.2 presents a summary of fracture toughness tests utilizing the three-point bend (TPB) specimen including comments on geometry effects on toughness. Results indicate that toughness may vary with $(\frac{a}{W})$, crack depth, and span length. Also the type of load and support fixtures may affect the toughness, and thin laminate specimens tend to buckle out-of-plane.

2.2.4 Compact Tension Specimen Testing

Table 2.3 presents a summary of fracture toughness tests utilizing the compact tension (CT) specimen including comments on geometry effects on toughness. CT specimens exhibit some variation in toughness with $(\frac{a}{W})$. Also variations in toughness are more pronounced with thin specimens than with thicker specimens. Care must be exercised when testing thin laminate compact tension specimens as they exhibit a tendency to buckle out-of-plane. Finally, compact tension specimens appear more likely to not exhibit self-similar modes of failure than the other two specimen types.

2.2.5 Effect of the Specimen Notch Root Radius on Test Results

Table 2.4 summarizes the notch root radii of all three types of specimens from a number of selected investigations. None of the specimen tests reported herein contained fatigue induced sharp cracks or any other attempt to produce sharp cracks. In general there were no obvious effects on the toughness values as a result of the notch root radius. However, some investigators, Waddoups, et al. [5] and Poe [13], did

Table 2.2 Summary of Fracture Toughness Tests Utilizing the Three-Point Bend Specimen

Investigated	Mat'l Type	Span ¹ in.(mm)	Thickness in.(mm)	Width in.(mm)	a/W	Comments
Shih & Logsdon [30]	Gr/Ep	4.0(101.6)	0.5(12.7)	1.0(25.4)	0.35-0.65	Toughness increased with a/W
Cruse & Osias [9]	Gr/Ep	4.0(101.6)	0.35(8.89)	1.0(25.4)	0.4	
Reedy [29]	Bo/Al	3.2(81.3)	0.20(5.08)	0.80(20.3)	0.5	Toughness values were geometry dependent
		4.25(108.0)	0.20(5.08)	1.0(25.4)	0.5	
		1.57(39.9)	0.20(5.08)	0.40(10.2)	0.5	

¹Note: The span is the distance between the supports.

Table 2.3 Summary of Fracture Toughness Tests Utilizing the Compact Tension Specimen

Investigation	Mat'l Type	Thickness in.(mm)	Width in.(mm)	a/W	Comments
Slepetz & Carlson [23]	S-Gr/Ep Gr/Ep	12 plies 12 plies	3.25(82.6) 3.25(82.6)	0.115,0.231 0.115,0.231	
Sun & Prewo [25]	Bo/Al	0.15(3.81) 0.30(7.62)	3.50(88.9) 3.50(88.9)	0.2-0.6 0.2-0.6	Dependent on a/W
Prewo [27]	Bo/Al	0.15(3.81)	2.0(50.8)	0.3-0.63	Toughness varied with a/W
Reedy [29]	Bo/Al	0.20(5.08)	2.5(63.5)	0.5	

Table 2.4 Summary of the Specimen Notch Root Radii

Investigation	Material	Radius in.(mm)
Reedy [29]	Bo/Al	0.004 (0.102 to 0.006 (0.152)
Prewo [27]	Bo/Al	0.00015 (0.0038)
Sun & Prewo [25]	Bo/Al	0.00015 (0.0038)
Mandell, et al. [8]	Gr/Ep	0.005 (0.127) to 0.025 (0.625)
Cruse & Osias [9]	Gr/Ep	0.005 (0.127)
Hahn & Morris [26]	Gr/Ep	0.0025 (0.0625)
Yeow, et al. [14]	Gr/Ep	0.0025 (0.0625)
Shih & Logsdon [30]	Gr/Ep	0.001 (0.0254)

attempt to account for a damage zone (inherent flaw) at the tip of notches by increasing the starter notch size in toughness calculations similar to a crack tip plastic zone correction.

2.2.6 Effects of Specimen Thickness on Toughness Values

There have been several investigations where laminate or specimen thickness was a test variable. Hahn and Morris [26] tested center-cracked tension specimens of 0.035 in. (0.889 mm) and 0.065 in. (1.65 mm) of graphite/epoxy and reported no apparent effect on toughness due to specimen thickness. Cruse and Osias [9] compared toughness data from a three-point bend specimen with 0.363 in. (9.22 mm) thickness and a center-cracked tension specimen of 0.070 in. (1.78 mm) thickness of graphite/epoxy. They concluded that fracture was independent of specimen thickness. Owen and Cann [24] explored thickness effects with center-cracked tension specimens of polyester resin reinforced with glass chopped strand mats. With thicknesses of 3, 6 and 9 plies, they concluded that there were no thickness effects on fracture toughness. However, Sun and Prewo [25] found that thin, 0.15 in. (3.81 mm), compact tension specimens of boron/aluminum exhibited toughness values that were more dependent on $(\frac{a}{W})$ than were thick, 0.30 in. (7.62 mm), specimens. Finally, Shih and Logsdon [30] tested relatively large three point bend specimens, 0.50 in. (12.7 mm), and center-cracked tension specimens, 0.25 in. (6.35 mm) prepared from a 2.125 in. (54.0 mm), 370 ply quasi-isotropic graphite/epoxy laminates. However, the notches in these specimens were in the laminate thickness direction, with the notches only partially through the laminate thickness. This is contrary to the typical orientation where the notch is in the plane of the laminate with

the notch extending completely through the laminate thickness. In general the specimens did not exhibit self-similar crack growth and considerable delamination occurred. The fracture toughness from the two specimen types were quite different. These results led Shih and Logsdon to question the direct applicability of LEFM to thick section laminates.

2.3 Summary and Conclusions

There are both similarities and differences when comparing the fracture behavior of a composite laminate to that of an isotropic material. Laminate strength is substantially reduced by the presence of a notch. A singular stress zone may exist at the tip of cracks in a composite laminate as in an isotropic metal. However, it may not be characterized by an $r^{-1/2}$ singularity because of natural blunting due to matrix yielding and fiber pullout, etc. Since cracks do not grow under fatigue loading, sharp cracks of critical dimensions may not form in composite laminates as they do in metals. Also self-similar or collinear crack growth may not be the failure mode in notched laminates where delamination, matrix splitting, etc. may take place. Several failure criteria have been postulated but their applicabilities are generally limited to specific laminate orientations and usually to situations where the failure mode is self-similar. Poe's [13] criterion of laminate failure occurring when fibers break in the principle load carrying laminae and his associated general fracture toughness parameter appears to be the most promising criterion because of its more extensive applicability. However, the universal value (1.5/mm) of Poe's general toughness parameter is valid only when self-similar crack growth takes place.

Fracture toughness testing has failed to yield a clearly identifiable material property. The preponderance of data has been generated from the center-cracked tension (CCT) specimen although limited testing has shown that compact tension and three-point bend specimens may also yield "valid" toughness data. In general, though, test results indicate that specimen geometry as well as specimen type affects toughness measurements. Toughness data from CCT specimens varies with specimen width and $(\frac{a}{W})$ ratio, but toughness may approach an asymptotic value. Also specimen failure modes may vary with specimen type and with laminate orientation.

Specimen thickness effects on toughness data has not been thoroughly addressed. There have been no test programs conducted in which specimen thickness was a primary test variable. There have been several tests where specimen thickness was varied but all thicknesses (6, 12, 18 plies, etc.) were still in the thin laminate range. These tests reported no apparent effect on toughness or failure mode due to specimen thickness. Other test programs have compared results from thin center-cracked tension specimens to thicker compact tension or three point bend specimens and reached mixed conclusions.

Only one test has been conducted on a thick laminate, 2.125 in. (54.0 mm). The notches were oriented in the laminate thickness direction as opposed to the usual orientation. Specimens exhibited considerable delamination prior to failure which was not, in general, self-similar.

3.0 DESCRIPTION OF THE RESEARCH PROGRAM

Many unresolved issues were raised in the literature review in the previous chapter. Several of these issues will be addressed by the research program described herein. The primary objective of the program is to study the effect of laminate thickness on the fracture behavior of graphite/epoxy composites. The study has been performed by conducting three general research activities. The first activity was the testing of a large number of fracture test specimens prepared from three representative laminate stacking sequences. The specimen test variables were laminate thickness, specimen configuration and crack size. The second research activity was the documentation of the development of damage and final fracture of thin and thick laminates. The nondestructive enhanced x-ray radiography technique and the destructive deply technique has allowed the determination of the type of damage as well as the through-the-thickness variation in damage at intermediate test loads as well as at final fracture. The final research activity was the evaluation of the applicability of several fracture criteria, developed from thin laminate investigations, to the prediction of thick laminate fracture. The details of each of these three research activities are described in the following paragraphs.

3.1 Specimen Test Program

The measurement of fracture toughness and the study of damage development and final fracture was conducted by performing the static fracture of a large number of fracture test specimens. (The test procedure is described in Section 4.1.) The specimens were obtained from three basic laminate types. These laminates were the $[0/\pm 45/90]_{ns}$,

$[0/90]_{ns}$ and $[0/\pm 45]_{ns}$, where ns means multiple stacks of the repeated sequence symmetric about the laminate midplane. The laminates were all prepared from graphite/epoxy (T300/5208) using a prepreg tape layup and autoclave curing process. The three laminate stacking sequences were selected because it was felt that they were representative of the range of thin laminate fracture behavior reported in the literature. (Laminate stiffness properties are presented in Article 5.1.3.)

The complete specimen test matrix is shown in Table 3.1. For each laminate type, center-cracked tension specimens were tested at 5 thicknesses, ranging from 6 or 8 plies, depending on laminate type, to 120 plies. For a thin and thick laminate, 4 crack sizes were tested, ranging from $\frac{2a}{W} = 0.25$ to 0.625, where $2a$ is the crack length and W is the specimen width. (See Figure 3.1.) At the 3 highest laminate thicknesses, compact tension and three-point bend specimens were also tested. Three or four replicate tests were conducted at each entry in the test matrix. Figure 3.1 presents drawings of the three specimen configurations along with their respective dimensions. It should be noted that the dimensions of each specimen shown in Figure 3.1 were the same for all specimen thicknesses.

3.2 Damage Evaluation Program

The primary objective of the damage evaluation program was to compare the damage development and final fracture of thick laminates to thin laminates and to compare damage in the three specimen configurations. This was accomplished by a combination of nondestructive and destructive examinations. Specimens were examined nondestructively by enhanced x-ray radiography. (The procedure is described in Section 4.2.)

Table 3.1 Fracture Toughness Test Matrix

Laminate Type A $[0/\pm 45/90]_{ns}$

Number of Spec. Type ¹ / Plies	8	32	64	96	120
CCT	16 ²	4	4	4	16 ²
CT			4	4	4
TPB			4	4	4

Laminate Type B $[0/\pm 45]_{ns}$

Number of Spec. Type ¹ / Plies	6	30	60	90	120
CCT	16 ²	4	4	16 ²	3
CT			4	4	4
TPB			4	4	4

Laminate Type C $[0/90]_{ns}$

Number of Spec. Type ¹ / Plies	8	32	64	96	120
CCT	16 ²	4	4	16 ²	3
CT			4	4	4
TPB			4	4	4

Notes: 1. CCT = Center Cracked Tension

CT = Compact Tension

TPB = Three Point Bend

2. 4 CCT each at $2a/W = 0.25, 0.375, 0.50, 0.625$. For all other specimens $2a/W$ equals 0.50.

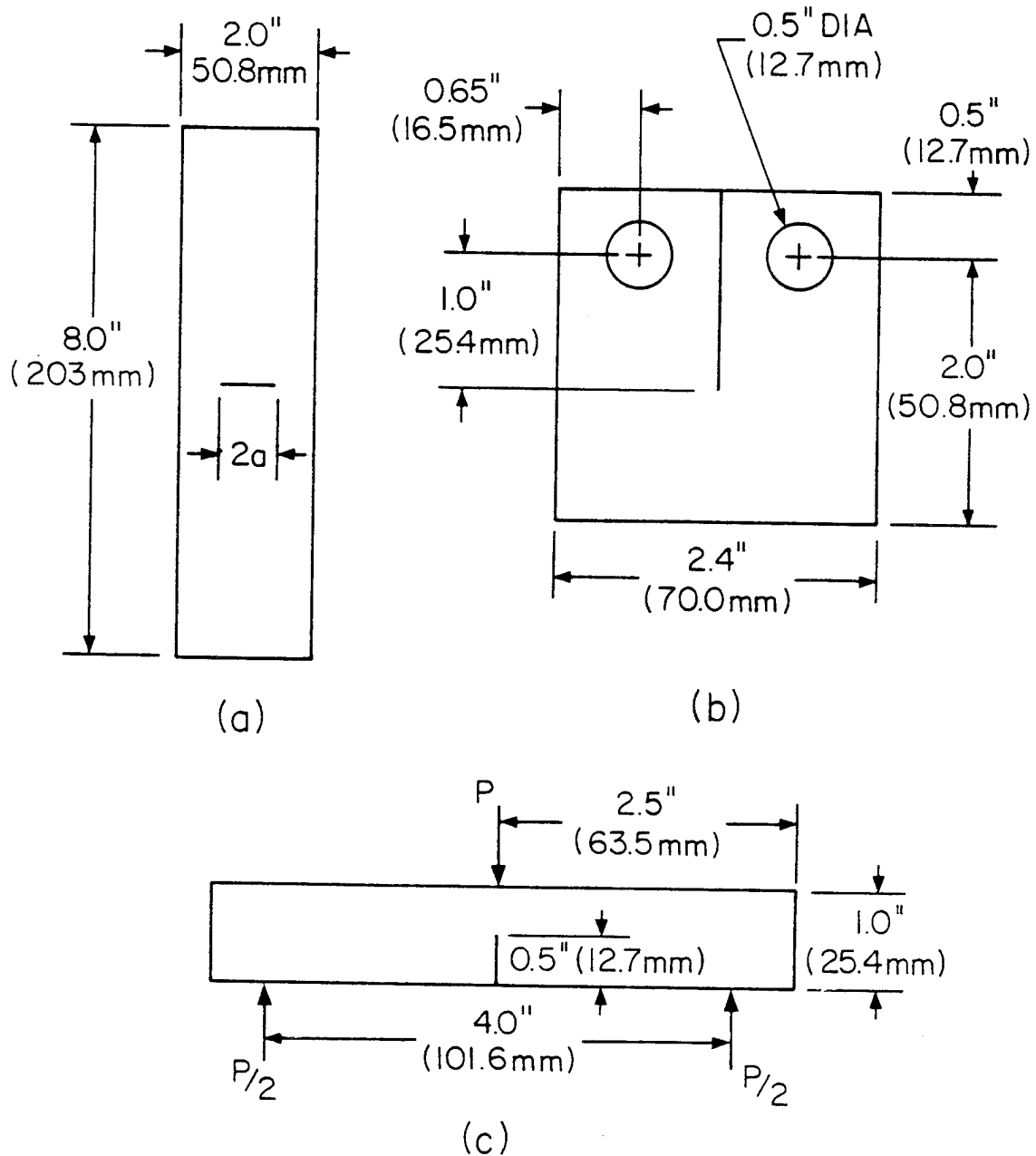


Figure 3.1 Drawing of the Specimen Geometry with Dimensions
 [(a) center-cracked tension, (b) compact tension,
 (c) three-point bend]

The x-ray examination provided a photographic documentation of the "in-plane" damage integrated through the specimen thickness. Matrix cracks and delaminations are clearly visible. Numerous x-rays were taken of at least one specimen from most laminate thicknesses and all specimen configurations. Examinations were made at intermediate load levels in order to document the progression of damage as the test load approached the final fracture load.

The destructive deply technique provided the documentation of damage through the thickness. For selected specimens, each individual ply was separated from the laminate and examined for damage. (The deply procedure is described in Section 4.3.) The technique was especially useful for determining the exact interface location of delaminations, which were marked by gold chloride prior to deply, and the extent of broken fibers in each ply. One center-cracked tension specimen at $\frac{2a}{W} = 0.50$ from each laminate type at 6 or 8 plies, depending on stacking sequence, and at 120 plies were selected for the deply study. The specimens were loaded to the load at the first discontinuity in the load versus crack-opening displacement record. (This test condition is discussed in more detail in Section 5.2.) The specimens were then x-rayed and deplyed to provide a direct x-ray-deply examination correlation. Each ply was then examined for the type and extent of damage.

3.3 Evaluation of Postulated Prediction Models

The final activity of the research project was the evaluation of the applicability of postulated candidate failure criteria to the fracture of thick laminates. The failure criteria were critically evaluated on the basis of the appropriateness of the criteria, developed for thin

laminate data, to thick laminate applications. Several candidate criteria (prediction models) were selected for evaluation. The models selected for evaluation included the inherent flaw, point stress and average stress models which are based on stress criteria and the general toughness parameter model which is based on a strain criteria. (It should be noted that the evaluations were limited to macromechanical models since at this time most micromechanical models are too cumbersome to be applied to thick angle-ply laminates.)

4.0 METHODOLOGY AND PROCEDURES

This chapter describes the methods and procedures used to conduct the various research activities described in Chapter 3. The procedures for the fracture test data reduction tasks are described in Sections 4.4 and 4.5. (The use of the prediction models, associated with the fracture criteria described in Chapter 2, is described in detail in Chapter 6.)

4.1 Fracture Test Procedure

All fracture tests were conducted at a constant crosshead displacement rate of 0.05 in./min (0.02 mm/s). The thicker (90, 96, and 120 plies) center-cracked tension specimens were tested in a 120,000 lb (534 KN) Tinius-Olsen testing machine. All other tests were conducted in a 20,000 lb. (89 KN) Instron testing machine. The center-cracked tension specimens were held in 2 in. (51 mm) wide wedge-action friction grips such that the specimen length between grip ends was approximately 5 in. (127 mm). The test setup is shown in Figure 4.1. The thin specimens, 6 or 8 plies, were tested with an antibuckling support to prevent out-of-plane motion. The compact tension specimens, see Figure 4.2, were loaded through 3/8 in. (9.5 mm) loading pins. (Monitoring of the specimen during the test and x-ray examinations did not reveal any evidence of local damage around the loading hole or out-of-plane buckling of the compact tension specimen.) The three-point bend specimens, see Figure 4.3, were point supported on 1 in. (25.4 mm) diameter cylindrical rods. The rods were positioned 4.0 in. (101.6 mm) apart and spring loaded to allow proper initial positioning and free movement once the test commenced. The load ram had a 3/4 in. (19 mm) radius. (Observations and x-ray examinations of three-point bend specimen did not reveal any

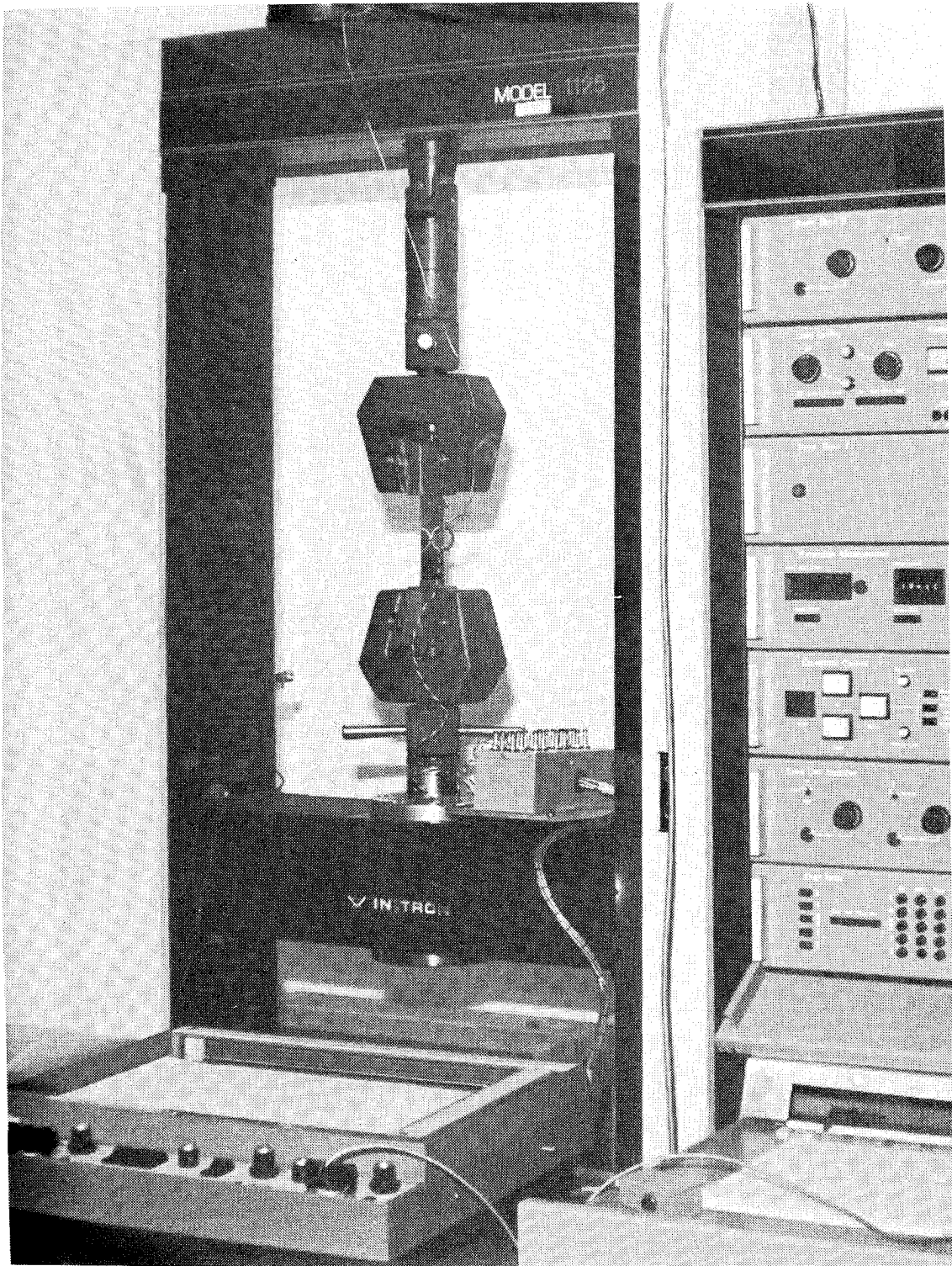


Figure 4.1 Center-Cracked Tension Test Setup

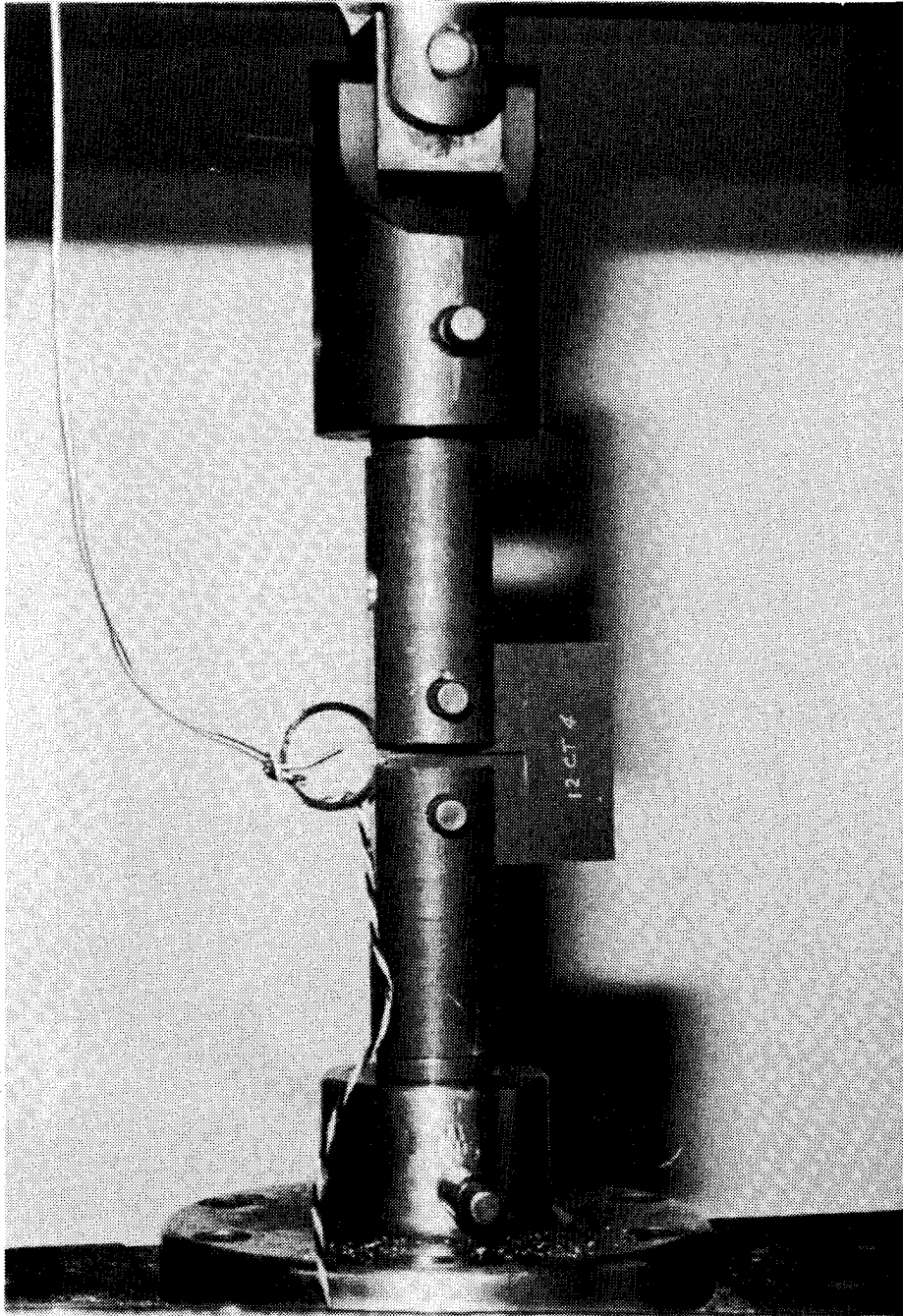


Figure 4.2 Compact Tension Specimen Test Setup

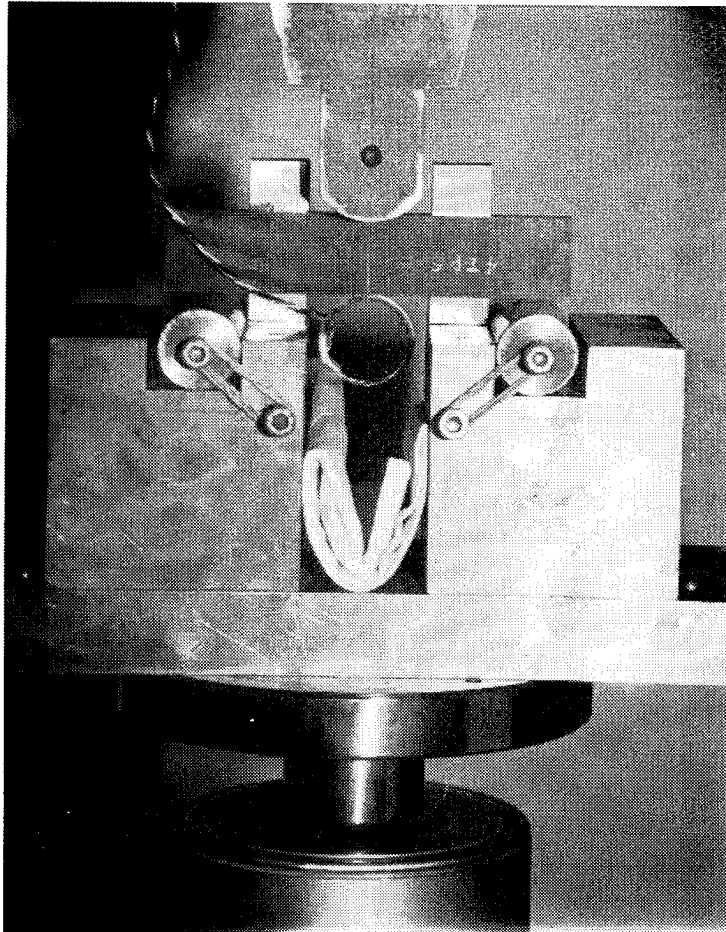


Figure 4.3 Three-Point Bend Specimen Test Setup

measurable amount of crushing underneath the loading points or out-of-plane buckling.)

The recorded test data included a plot of crack-opening displacement (COD) versus load. The split ring type COD clip gage was held directly in the crack (machined slot) by machined knife edge tabs. (This is shown in Figures 4.1-4.3.) The ring is initially compressed and the tabs inserted into the slot. The load output voltage and COD clip gage output voltage were recorded on an x-y plotter and calibrated frequently throughout the testing periods.

4.2 Enhanced X-Ray Procedure

An industrial type "soft" x-ray machine was used to make all x-ray radiographs. Damaged areas of the specimen were enhanced by the use of zinc iodide which penetrates the regions of matrix cracks and delaminations. The zinc iodide retards the penetration of the x-rays thus enhancing the damage regions. The specimens were typically subjected to the zinc iodide by placing a piece of tape over the notch on one surface and filling the notch cavity with zinc iodide. After several minutes the excess zinc iodide was drained away and the surfaces were cleaned with acetone to remove any excess zinc iodide. The specimen was then placed directly on the film (type M double emulsion) and onto the sensor assembly shelf of the x-ray cabinet. The x-ray voltage was 20 KVP for all examinations and the exposure time for an 8 ply specimen was 30 seconds. The exposure times for all other thicknesses were determined by multiplying 30 seconds by the ratio of the number of plies to 8.

4.3 Specimen Deply Procedure

The specimen deply technique is a relatively simple destructive examination method for determining individual ply damage as well as the precise interface location of delaminations. The interlaminar bond strength of the laminate is broken down by partially pyrolyzing the resin matrix in an oven. This allows the individual intact plies of the laminate to be separated. The microscopic examination of individual plies reveals the extent of fiber breaks. By subjecting the damaged region to a marking agent (before pyrolyzing), delaminations are also clearly visible. The procedure described below was originally developed by Freeman [31].

Interply delaminations and matrix splits were marked by a gold chloride enhancing agent. A 9.2 weight-percent solution of gold chloride in diethyl ether (the carrier agent) was applied to the damaged specimen in the same manner as the zinc iodide for x-ray examinations. After subjecting the specimen to the gold chloride solution for about 30 minutes, the excess diethyl ether residue was driven off to prevent gas bubble formation during the pyrolysis. This was accomplished by heating the specimen to 140°F for about one hour.

The pyrolysis procedure for graphite/epoxy, T300/5208, requires a temperature of 785°F (418°C). The time required for an 8 ply laminate is 30 minutes and the time for thicker laminates is 30 minutes times the ratio of the number of plies to 8. The pyrolysis was accomplished in an electric tube oven in an argon gas environment that was vented to the outside. Since the specimen emits noxious fumes during the process, it was necessary to purge the oven chamber using the argon gas. The specimen was allowed to cool in the oven for a time and then cooled to room

temperature outside the oven. Just enough matrix remained to keep the fibers together. Adhesive tape was applied to the surface of a ply for ease of removal and for additional reinforcement. Occasionally there was a small amount of bonding between plies, but the plies could easily be separated with a little prodding by a small knife edge probe.

The examination of the individual separated plies was accomplished in two phases. First, a Bausch and Lomb zoom microscope was used to examine the plies for delaminations. At a magnification of 20x to 30x, the extent of the gold chloride markings were clearly visible. Illumination of the specimen with the proper angle of reflected light was essential. At higher magnifications the gold chloride particles were too dispersed for examination. Second, fiber breaks were observed in a UNITRON, Series N #54748 microscope at magnifications between 200x-400x. The details of broken fibers were clearly visible along with the pattern of fiber breaks. Well defined lines of broken fibers extending from the starter notch were also clearly visible at 20x-30x magnification. Photographic documentation of broken fibers at the higher magnification was difficult. The separated plies were rough and uneven so it was impossible to achieve a properly focused photograph over the entire field of view. In general, the damage documentation took the form of recorded personal observations because of the large number of plies examined. Typical photographs of the magnified views of damage are presented in Chapter 5 together with the recorded personal observations.

4.4 Determination of Fracture Toughness by the Stress Analysis

Method

The stress analysis method was used to compute the fracture toughness from the test data of all three specimen types. A finite element analysis of each of the three specimen configurations and at the four $2a/W$ test values for the center-cracked tension specimen was performed. (The results of the finite element analyses are presented in Article 5.1.) The computer code, developed by the Lockheed-Georgia company for NASA [35], utilizes a special crack element that contains the crack tip and performs the singular zone stress analysis. The code performs analyses for either plane stress or plane strain on the basis of linear elastic fracture mechanics for fracture modes I and II. The crack element allows either isotropic material behavior or homogeneous anisotropic material behavior. The computer output included mode I & II stress intensity factors and strain energy release rates for an applied unit load. For a given test load the corresponding fracture toughness, K_{Ic} , was then determined by multiplying the test load by the stress intensity factor for a unit load.

5.0 RESULTS AND DISCUSSION

The results from the experimental phases of the program are presented in this chapter. In order to facilitate data comparisons and the discussions of the influence of the various test parameters, the results are segregated and presented in a topical format. The first article presents the results of the finite element stress analysis. Also included in the first article is a discussion of all laminate material properties used in the calculations. The second article discusses characteristics of the load-COD records that are similar for all three laminate types. The third article presents the effects of thickness on the fracture behavior of the three laminates. The final article compares the test results for the three specimen configurations. For each topic, the results from each of the three laminate types studied are presented and discussed individually.

5.1 Finite Element Stress Analysis of the Fracture Specimens

In order to compute the fracture toughness, the relationship between applied load, specimen geometry, material properties and the crack-tip stress intensity factor must be known. The finite element method has been previously demonstrated to yield very accurate expressions for the stress intensity factor of fracture test specimens [1]. The existing analytical expressions for the stress intensity factor of standard fracture test specimens [2] have been generated for isotropic materials. These expressions are not directly applicable to anisotropic composite materials because the stress-strain relationship effects the governing elasticity equations. Therefore, a solution is required that includes the effects of material anisotropy. This article describes the

finite element analysis of the center-cracked tension, compact tension and three-point bend specimens. Also described are all laminae material properties necessary to compute fracture toughness by either the stress analysis method or from the strain-energy release rate.

5.1.1 Description of the Finite Element Code

The "Finite Element Computer Program to Analyze Cracked Orthotropic Sheets" was developed by the Lockheed-Georgia Company for NASA [35]. The finite element code performs plane strain and plane stress analyses of plates with through-the-thickness cracks. Both isotropic and homogeneous anisotropic material properties are allowed by the code. Two special crack elements, for symmetric and nonsymmetric applications, account for the singular stress field at the crack tip. The stress intensity factor and strain energy release rate are computed for mode I (opening mode) and mode II (sliding mode) using standard linear elastic fracture mechanics. The special crack element surrounds the crack tip and the remaining structural geometry is modeled by plane stress or plane strain triangular membrane elements.

5.1.2 Description of the Finite Element Models

Since the test specimens of interest possess both load and geometric symmetry, it was necessary to use only the symmetric crack-tip element, see Figure 5.1. Finite element models of a center-cracked tension specimen ($\frac{2a}{W} = 0.625$), compact tension specimen ($\frac{a}{W} = 0.50$) and a three-point bend specimen ($\frac{a}{W} = 0.50$) are pictured in Figures 5.2-5.4, respectively. A relatively fine mesh was used in the region surrounding the crack and a coarse mesh (not shown in Figures 5.2 or 5.4) was used away

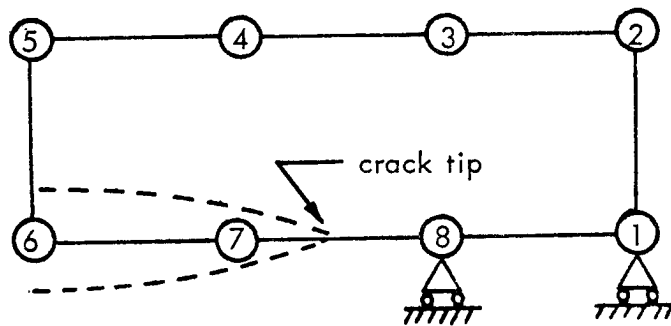


Figure 5.1 8-Node Symmetric Crack-Tip Element [35]

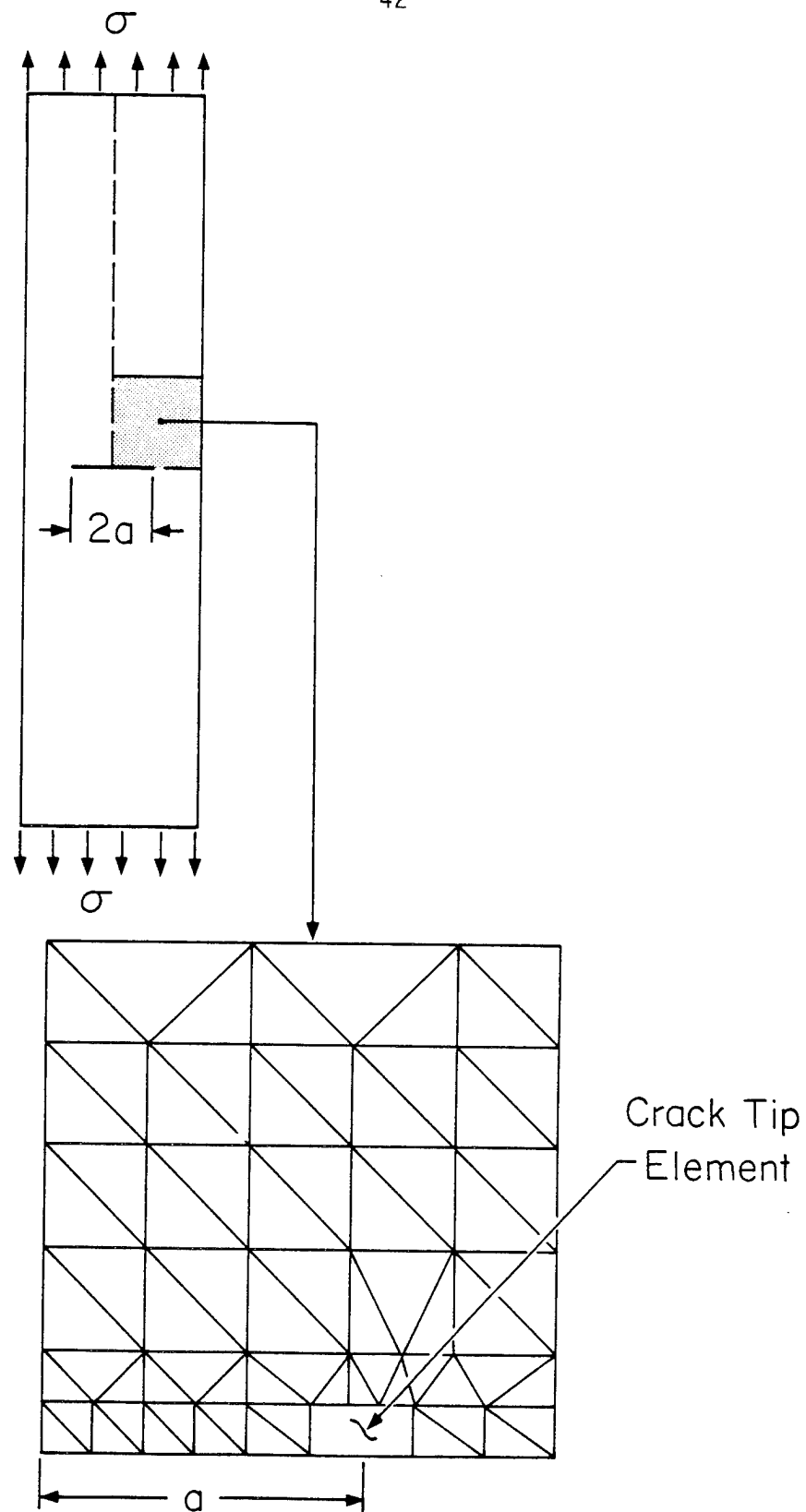


Figure 5.2 Finite Element Model of the Center-cracked Tension Specimen in the Crack Region

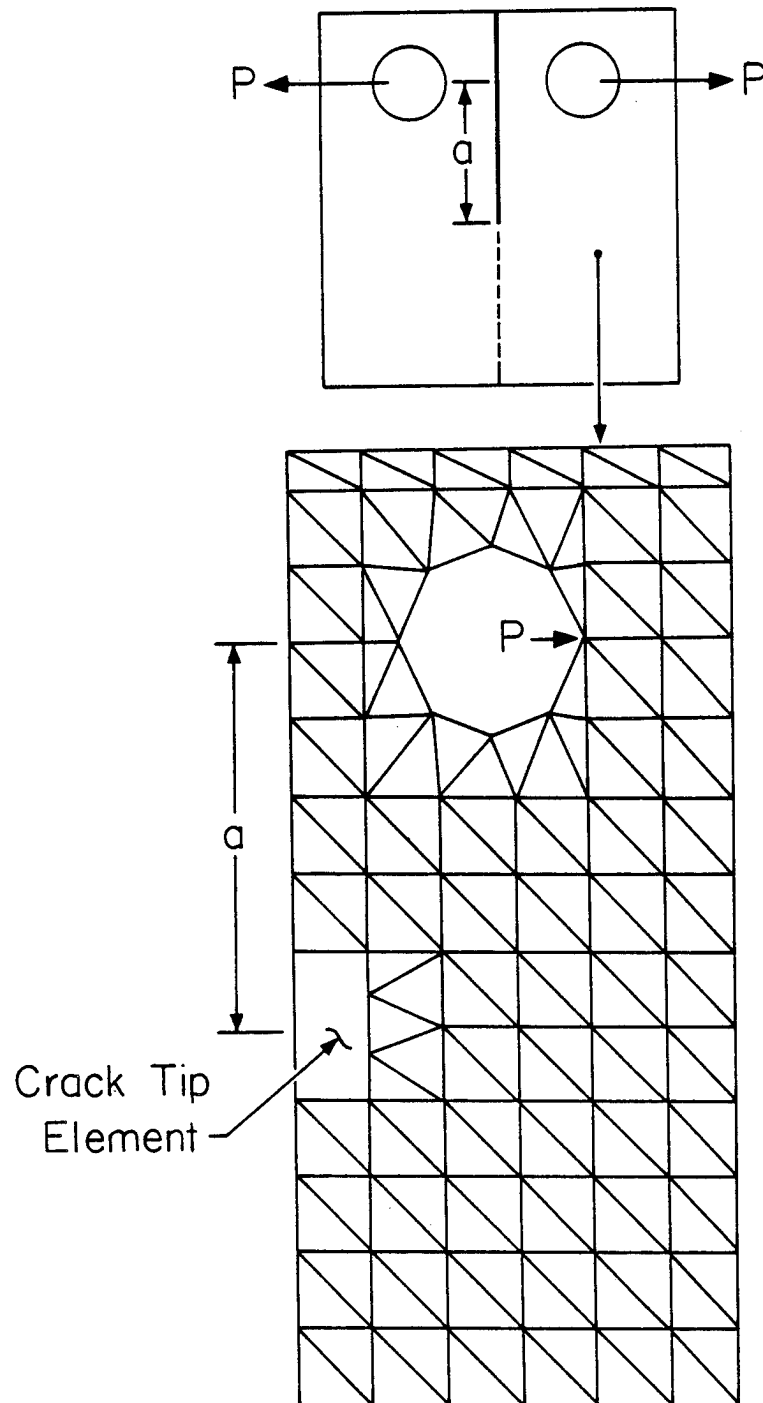


Figure 5.3 Half-Symmetry Model of the Compact Tension Specimen

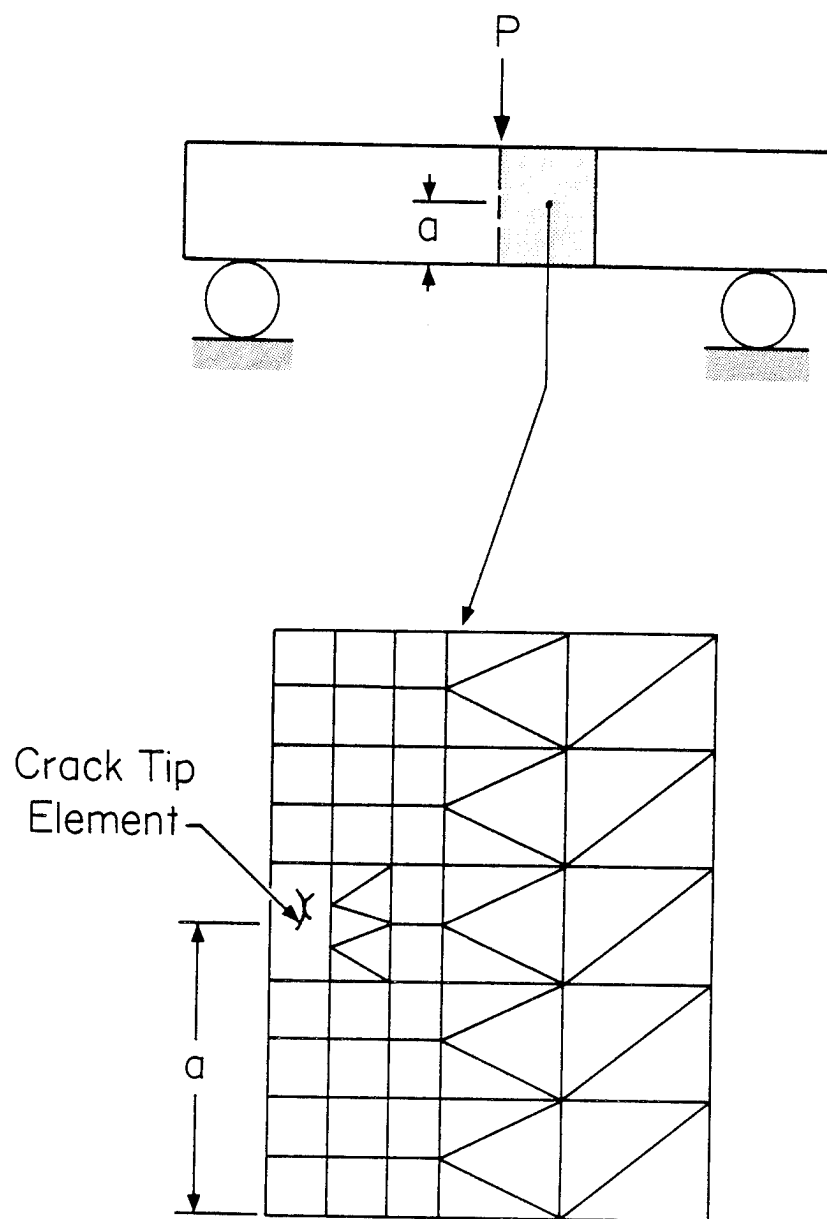


Figure 5.4 Half-Symmetry Model in the Crack Region of the Three Point Bend Specimen

from the crack-tip region. (Since the code has an automatic mesh generator and bandwidth reducer, the finite element model was set up for ease of geometry data specification.) Roller type support boundary conditions were specified along the symmetry boundaries of the model. The roller point support provided by the three-point bend test fixture was so modeled. The distributed load applied by the friction grips on the center-cracked tension specimen was represented by fractional concentrated forces acting at the nodes forming the end boundary of the center-cracked geometry. The pin loading on the compact tension specimen was represented by a single concentrated force located as shown in Figure 5.3. Each analysis was performed for a unit applied load of one pound (4.448 N). Since the analysis is linear elastic, the stress intensity factor and strain energy release rate at any desired load level is obtained by multiplying the unit load values by the desired load.

5.1.3 Laminate Material Properties

The laminated composite was represented as a homogeneous anisotropic material. Therefore, the stress-strain relationship required by the finite element code is a function of the laminate engineering stiffness constants, E_x , E_y , ν_{xy} and G_{xy} where y is the loading direction and x is the transverse direction. These constants were calculated from basic lamina data using standard macromechanical laminate stiffness equations [34]. The basic lamina data was determined experimentally from unidirectional stiffness coupons. The $[0]_8$ laminate yielded E_{11} and ν_{12} where the subscript 1 refers to the direction parallel to the fibers and 2 refers to the transverse direction. The $[90]_8$ laminate yielded E_{22} and the $[\pm 45]_{2s}$ laminate yielded G_{12} [36]. Four or five replicate tests

were conducted at a constant cross-head displacement of 0.05 in./min (0.02 mm/s) and the test results are presented in Table 5.1. The computed engineering constants are tabulated in Table 5.2 for the $[0/\pm 45/90]_{NS}$, $[0/90]_{NS}$ and $[0/\pm 45]_{NS}$ laminates.

The finite element code requires the following stress-strain material property input:

$$\{\sigma\} = [A]\{\epsilon\}$$

where $\{\sigma\}$ = stress tensor

$\{\epsilon\}$ = strain tensor

$[A]$ = laminate constitutive properties relating stress and strain

For plane stress $[A]$ is related to the laminate engineering constants as follows [34]:

$$A_{11} = \frac{E_x}{1 - \nu_{xy}\nu_{yx}}$$

$$A_{12} = \frac{\nu_{xy}E_y}{1 - \nu_{xy}\nu_{yx}} = \frac{\nu_{yx}E_x}{1 - \nu_{xy}\nu_{yx}}$$

$$A_{22} = \frac{E_y}{1 - \nu_{xy}\nu_{yx}}$$

$$A_{16} = A_{26} = 0$$

$$A_{66} = G_{xy}$$

Defining $[a] = [A]^{-1}$, $\{\epsilon\} = [a]\{\sigma\}$ is the plane stress and $\{\epsilon\} = [\bar{a}]\{\sigma\}$ is the plane strain strain-stress relationship. By manipulation of the plane strain stress-strain equations, the following relationship between the plane strain and plane stress constants is obtained:

Table 5.1 Measured Lamina Stiffness Properties

Specimen ID	E_{11} 10 ⁶ psi (GPa)	ν_{12}	Specimen ID	E_{22} 10 ⁶ psi (GPa)	Specimen ID	G_{12} 10 ⁶ psi (GPa)
25-0-1	20.51 (141.4)	0.318	25-90-1	1.57 (10.83)	26-45-1	0.791 (5.45)
25-0-2	20.36 (140.4)	0.333	25-90-2	1.54 (10.62)	26-45-2	0.879 (6.06)
25-0-3	20.44 (140.9)	0.304	25-90-3	1.55 (10.69)	26-45-3	0.879 (6.06)
25-0-4	19.42 (133.9)	NA	25-90-4	1.58 (10.89)	26-45-4	0.917 (6.32)
25-0-5	19.80 (136.5)	0.318	25-90-5	1.57 (10.83)		
Average	20.11 (138.7)	0.318	Average	1.56 (10.77)	Average	0.867 (5.98)

Table 5.2 Laminate Engineering Stiffness Properties

Property	$[0/\pm 45/90]_{ns}$	$[0/90]_{ns}$	$[0/\pm 45]_{ns}$
E_x 10^6psi (GPa)	8.057 (55.6)	11.07 (76.3)	3.893 (26.8)
E_y 10^6psi (GPa)	8.057 (55.6)	11.07 (76.3)	8.952 (61.7)
ν_{yx}	0.302	0.0410	0.694
G_{xy} 10^6psi (GPa)	3.094 (21.33)	0.871 (6.006)	3.835 (26.4)

$$\bar{a}_{ij} = a_{ij} - \frac{a_{i3}a_{j3}}{a_{33}} \quad (i, j = 1, 2, 6)$$

The values of a_{13} , a_{23} , and a_{33} are determined by assuming transverse isotropy such that the transverse (3 direction) properties of the laminate are taken to be the same as the in-plane transverse properties of a 0° lamina. Therefore, $\nu_{xz} = \nu_{yz} = \nu_{12}$ and $E_z = E_{22}$. One can now write the plane strain stress-strain relationship as

$$\{\sigma\} = [\bar{A}]\{\epsilon\}$$

$$\text{with } [\bar{A}] = [\bar{a}]^{-1}$$

The components of $[A]$ and $[\bar{A}]$ are tabulated in Table 5.3.

5.1.4 Relationship Between Strain Energy Release Rate and Stress

Intensity Factor

The strain energy release rate for mode I, G_I , is related to the stress intensity factor, K_I , by

$$G_I = cK_I^2$$

for linear elastic fracture mechanics [33]. For homogeneous orthotropic laminates ($A_{16} = A_{26} = 0$) the plane stress expression for c is

$$c = \left(\frac{a_{11}a_{22}}{2}\right)^{1/2} \left[\left(\frac{a_{22}}{a_{11}}\right)^{1/2} + \frac{2a_{12} + a_{66}}{2a_{11}} \right]^{1/2}$$

Table 5.3 Finite Element Analysis Stress-Strain Anisotropic Material Property Input

Layup Property	$[0/\pm 45/90]_{ns}$	$[0/90]_{ns}$	$[0/\pm 45]_{ns}$
Plane Stress			
A_{11} 10^6psi (GPa)	8.866 (61.13)	11.09 (76.47)	4.925 (33.96)
A_{12} 10^6psi (GPa)	2.678 (18.46)	0.4545 (3.134)	3.419 (23.57)
A_{22} 10^6psi (GPa)	8.866 (61.13)	11.09 (76.47)	11.320 (78.05)
A_{66} 10^6psi (GPa)	3.094 (21.33)	0.8710 (6.006)	3.835 (26.44)
Plane Strain			
\bar{A}_{11} 10^6psi (GPa)	10.91 (75.22)	11.11 (76.60)	5.773 (39.80)
\bar{A}_{12} 10^6psi (GPa)	4.720 (32.54)	0.4748 (3.274)	13.10 (90.32)
\bar{A}_{22} 10^6psi (GPa)	10.91 (75.22)	11.11 (76.60)	20.25 (139.6)
\bar{A}_{66} 10^6psi (GPa)	3.094 (21.33)	0.8710 (6.006)	3.835 (26.44)

where the components of $[a]$ are related to the laminate engineering constants as outlined in the previous section. For plane strain (\bar{c}), a_{ij} is replaced by \bar{a}_{ij} in the above expression. Values of c and \bar{c} are presented in Table 5.4.

5.1.5 Results

In order to investigate the accuracy of the finite element models, a plane strain isotropic analysis was performed using each model. The results are tabulated in Table 5.5 and compared to the ASTM standard stress intensity factor expressions [1,2]. The last column presents the percentage difference between the finite element analysis and the ASTM standard. This is interpreted to be a measure of the model accuracy. The models were considered to be acceptably accurate even though the percent differences were somewhat higher than those for the computer code test cases reported in reference 35. The model inaccuracies are attributed to using a finer mesh in the crack-tip region which requires the use of more triangular membrane elements. The numerical approximations of the triangular membrane element are less accurate than the numerical approximations of the special crack-tip element. Because of the ASTM studies of the validity of the numerical solutions [1,2] and the above discussion, the finite element stress intensity factors used to compute fracture toughness were adjusted according to the percentages in the last column of Table 5.5.

The primary reason for generating the finite element stress intensity factor solutions was to incorporate the effects of material anisotropy. The $[0/\pm 45]_{ns}$, $[0/90]_{ns}$ and $[0/\pm 45/90]_{ns}$ laminate analyses for each specimen geometry are summarized in Table 5.6. (The stress-

Table 5.4 Orthotropic Relationship Between Strain Energy Release Rate and Stress Intensity Factor for Mode I

Laminate	\bar{c} Plane Stress Psi^{-1} $(\text{GPa})^{-1}$	\bar{c} Plane Strain Psi^{-1} $(\text{GPa})^{-1}$
$[0/\pm 45/90]_{ns}$	1.2411×10^{-7} (18.00)	1.1279×10^{-7} (16.36)
$[0/90]_{ns}$	1.7274×10^{-7} (25.05)	1.7255×10^{-7} (25.03)
$[0/\pm 45]_{ns}$	1.114×10^{-7} (16.16)	1.0351×10^{-7} (15.01)

Table 5.5 Comparison of the Finite Element Analysis Results to the ASTM Standards [1,2] for an Isotropic, Plane Strain Analysis for 1.0 in. (25.4 mm) Thick Specimens

Specimen Geometry	2a/W	K_I		Model Accuracy % Difference $\frac{ASTM - FEA}{ASTM} \times 100$
		ASTM Standard ksi $\sqrt{\text{in.}}$ MPa $\sqrt{\text{mm}}$	Finite Element Analysis ksi $\sqrt{\text{in.}}$ MPa $\sqrt{\text{mm}}$	
Compact Tension	0.50	6.789 (236)	6.917 (240.4)	-1.9
Three-Point Bend	0.50	10.66 (370.4)	10.20 (354.5)	4.3
Center-Cracked Tension	0.25	0.4593 (15.96)	0.4779 (16.61)	-4.0
	0.375	0.5897 (20.49)	0.6143 (21.35)	-4.2
	0.50	0.7403 (25.73)	0.7765 (26.18)	-4.9
	0.625	0.9376 (32.58)	0.9590 (33.33)	-2.3

Table 5.6 The Effects of Material Anisotropy on the Plane Stress and Plane Strain Stress Intensity Factors

Specimen Geometry	2a/W	Laminate Type	1 K_I Isotropic PL Strain ksi \sqrt{in} (MPa \sqrt{mm})	2 K_I Anisotropic PL Strain ksi \sqrt{in} (MPa \sqrt{mm})	3 K_I Anisotropic PL Stress ksi \sqrt{in} (MPa \sqrt{mm})	Anisotropic Effect % Difference $\frac{1-2}{1} \times 100$
Compact Tension	0.50	[0/±45] _{ns}	6.917 (240.4)	6.873 (238.8)	6.736 (234.1)	0.6%
		[0/90] _{ns}		7.182 (249.6)	7.181 (249.5)	-3.8%
		[0/±45/90] _{ns}		6.866 (238.6)	7.088 (246.3)	0.7%
Three-Point Bend	0.50	[0/±45] _{ns}	10.20 (354.5)	10.18 (353.8)	10.22 (355.1)	0.2%
		[0/90] _{ns}		9.954 (345.9)	9.955 (345.9)	2.4%
		[0/±45/90] _{ns}		10.21 (354.8)	10.57 (367.3)	0.1%
Center-Cracked Tension	0.25	[0/±45] _{ns}	0.4779 (16.61)	0.4842 (16.83)	0.4805 (16.70)	-1.3%
		[0/90] _{ns}		0.4410 (15.32)	0.4410 (15.32)	7.7%
		[0/±45/90] _{ns}		0.4784 (16.62)	0.4967 (17.26)	0.1%
	0.375	[0/±45] _{ns}	0.6143 (21.35)	0.6281 (21.83)	0.6178 (21.47)	-2.2%
		[0/90] _{ns}		0.5703 (19.82)	0.5703 (19.82)	7.2%
		[0/±45/90] _{ns}		0.6148 (21.36)	0.6415 (22.29)	-0.1%
	0.50	[0/±45] _{ns}	0.7765 (26.98)	0.7934 (27.57)	0.7753 (26.94)	-2.1%
		[0/90] _{ns}		0.7313 (25.41)	0.7317 (25.43)	5.8%
		[0/±45/90] _{ns}		0.7775 (27.02)	0.8054 (27.99)	-0.1%
	0.625	[0/±45] _{ns}	0.9590 (33.33)	0.9784 (33.99)	0.9694 (33.69)	-2.0%
		[0/90] _{ns}		0.9023 (31.35)	0.9027 (31.37)	5.9%
		[0/±45/90] _{ns}		0.9601 (33.36)	0.9947 (34.57)	-0.1%

intensity-factors in Table 5.6 are not adjusted for model inaccuracies). The plane-strain and plane-stress stress-intensity-factors for a unit load of 1.0 lb (4.448 N) and 1.0 in. (25.4 mm) thickness are compared. Note that there are slight numerical differences between the isotropic and anisotropic solutions for the quasi-isotropic case. The computer code uses different subroutines and numerical schemes to analyze the isotropic and anisotropic cases and this causes slightly different results. The last column of Table 5.6 presents the percentage difference between the finite element plane strain isotropic and anisotropic stress intensity factors. This is a measure of the effects of anisotropy on the stress-intensity-factor. The results show that the anisotropic effects are greater for the $[0/90]_{ns}$ laminate than for the $[0/\pm 45]_{ns}$ laminate. The effect of anisotropy reported here for the center-cracked tension specimens of the $[0/90]_{ns}$ laminate appears to be in good agreement with the results of Yeow, et al. [14] generated by the boundary integral equation method for the same case.

The stress-intensity-factor results in Table 5.6 are proportional to the applied load and inversely proportional to the specimen thickness because the analysis is 2-D and linear, elastic. Therefore, the stress-intensity-factor at any load and at any specimen thickness is obtained accordingly.

5.2 Characteristics of the Load-COD Curves

A typical load versus crack-opening displacement (COD) record is shown in Figure 5.5 for a center-cracked tension specimen. There are several discontinuities in the loading record which correspond to the formation of damage at the crack tip. For example, Figure 5.6 shows

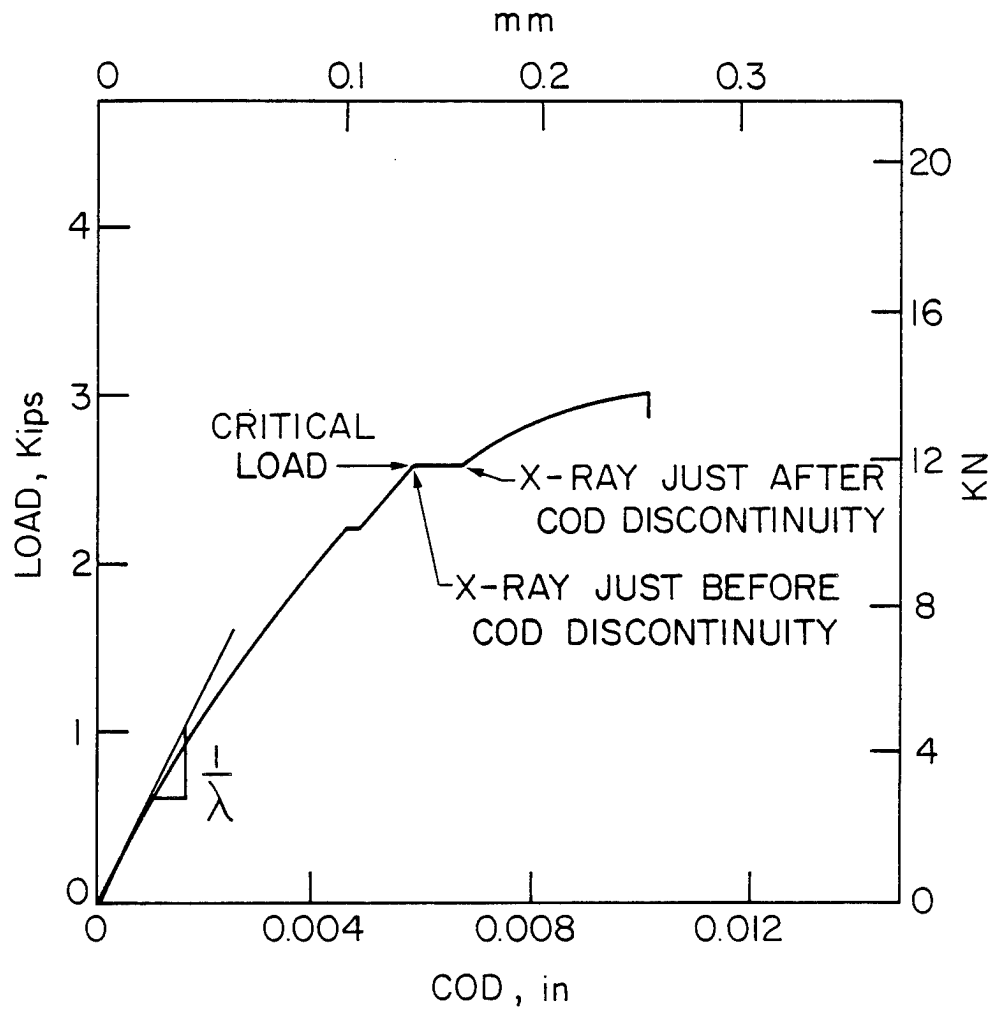


Figure 5.5 Typical Plot of Load Versus COD for $[0/\pm 45/90]_s$ Laminates (Center-Cracked Tension Specimen)

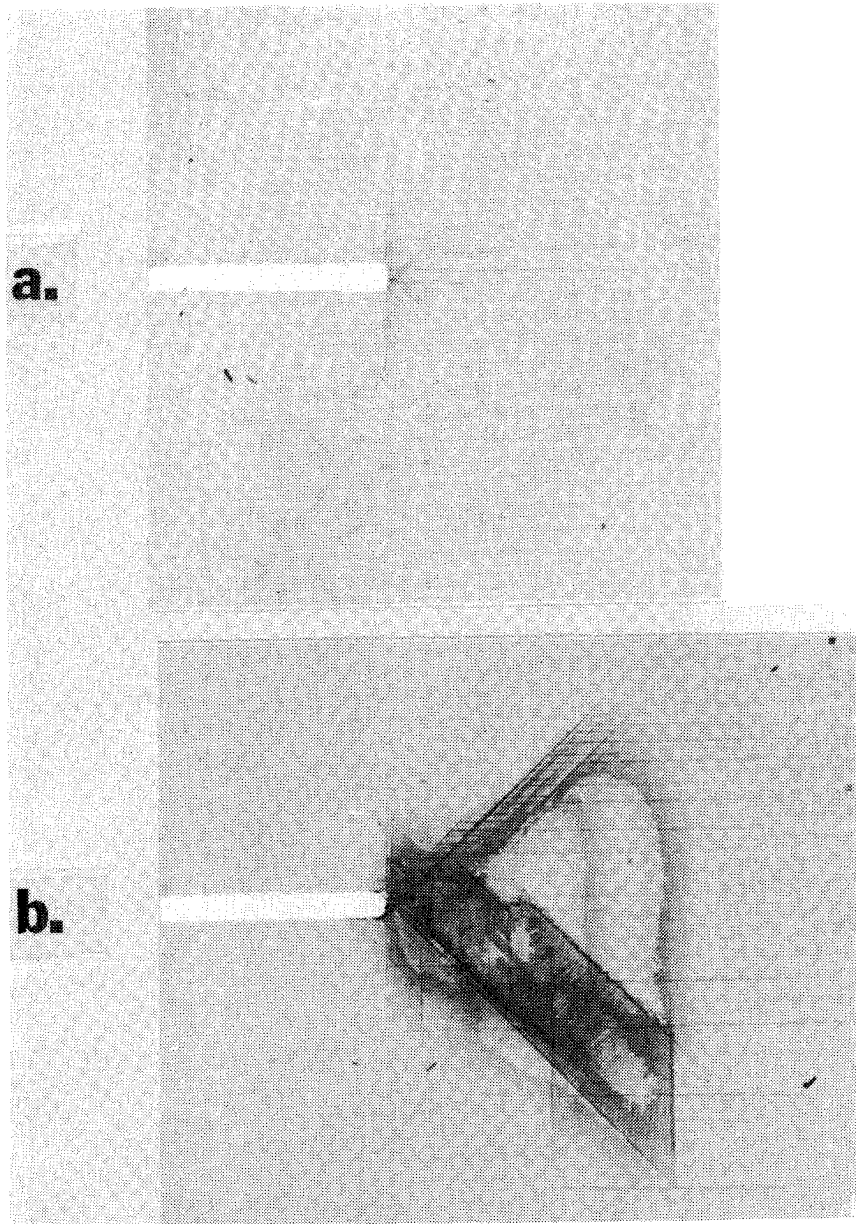


Figure 5.6 X-ray Radiographs of the Crack-Tip Damage
(a) Just Before and (b) Just After a Large
COD Discontinuity. (Center-Cracked Tension
Specimen)

enhanced x-ray radiographs of the crack-tip damage just before and just after a COD discontinuity. The formation of substantial subcritical crack-tip damage changes the specimen compliance and alters the original crack. These discontinuities are a fundamental characteristic of the load-COD records of the laminates described herein. This led the authors to speculate that perhaps there is a "critical load" at which substantial damage forms that may give rise to a material or design property. This "critical load" is somewhat subjectively defined as the load beyond which the compliance is "significantly" changed and the amount of crack tip damage is "significant." This usually corresponds to the first large COD discontinuity. These values are included in the appendix along with the maximum test load. The stress intensity factor at the critical load will sometimes be compared to the fracture toughness (stress intensity factor at the maximum load) for interpretive purposes.

The presence of the crack-tip damage prior to catastrophic failure can be addressed by adjusting the crack length used to compute the fracture toughness. The adjusted expression of fracture toughness is

$$K = Y\sigma\sqrt{\pi(a + \rho)}$$

where Y = specimen finite width correction factor

σ = applied stress at fracture

a = original crack half-length

ρ = size of damage zone at fracture.

By setting $a = 0$ and the notched laminate strength equal to the unnotched laminate strength, $Y\sigma = \sigma_0$, and the critical crack-tip damage is given by

$$\rho = \frac{1}{\pi} \left(\frac{K}{\sigma_0} \right)^2 .$$

It may be noted that this is analogous to the Irwin plastic zone correction factor for metals except the unnotched laminate strength is used rather than the yield strength of the metal.

Substantial subcritical crack-tip damage usually developed prior to final fracture in all three laminate types. This was especially the case for the thin laminates. Therefore, the values of fracture toughness computed at the maximum load may be somewhat questionable. This is because the stress intensity factors were computed on the assumption of linear elastic behavior. Adjusting the linear elastic value of fracture toughness to account for the damage zone, ρ , as previously outlined, is one typical approach used by composite fracture mechanics. The validity of this approach has not been fully demonstrated and is a fundamental issue under investigation. (The treatment of the subcritical damage zone will also be addressed in Chapter 6 where the failure criteria and mathematical models are discussed.)

5.3 The Effect of Laminate Thickness

The study of the fracture behavior of composites as a function of laminate thickness has concentrated on the behavior of the center-cracked tension specimen geometry. (The study of specimen configuration was conducted for only the thicker laminates and is discussed in the next section.) In this section and the next fracture toughness is

defined as the value of the stress intensity factor at the maximum test load which corresponds to catastrophic failure. It should be noted that the values of fracture toughness presented hereinafter have not been adjusted for the presence of the damage zone. (If the adjustments were made it would have a negligible effect on the fracture toughness trend curves presented herein.)

5.3.1 The $[0/\pm 45/90]_{ns}$ Laminate

Baseline data for the $[0/\pm 45/90]_{ns}$ laminate study were generated from an 8 ply laminate. Center-cracked tension specimens were tested at crack size-to-width ratios of 0.25, 0.375, 0.50 and 0.625. The toughness values experimentally determined by the stress analysis method (section 5.2) fell within the range of toughness values reported in the literature [13,26,30] for $[0/\pm 45/90]_s$ graphite-epoxy laminates. The load-COD record shown in Figure 5.7 and the damage illustrated by the enhanced x-ray photograph in Figure 5.8(a) are typical for the 8 ply replicate tests.

There is a similarity between the load versus COD records of the 8, 32, 64, 96 and 120 ply $[0/\pm 45/90]_{ns}$ laminates of Figure 5.7. (Note that in Figure 5.7 the load scale is different for each thickness whereas the COD scale is the same for each thickness.) There is one subtle difference in the load records of Figure 5.7. The critical load, P_c , where significant damage develops at the crack tip, is a greater percentage of the maximum load, P_m , as the specimen thickness increases. For example, at 8 plies P_c is 81% of P_m while at 64 plies P_c is 92% of P_m . However, the type and magnitude of damage associated with P_c is essentially the same. Comparing the enhanced x-rays of Figure 5.8(a) for a typical 8

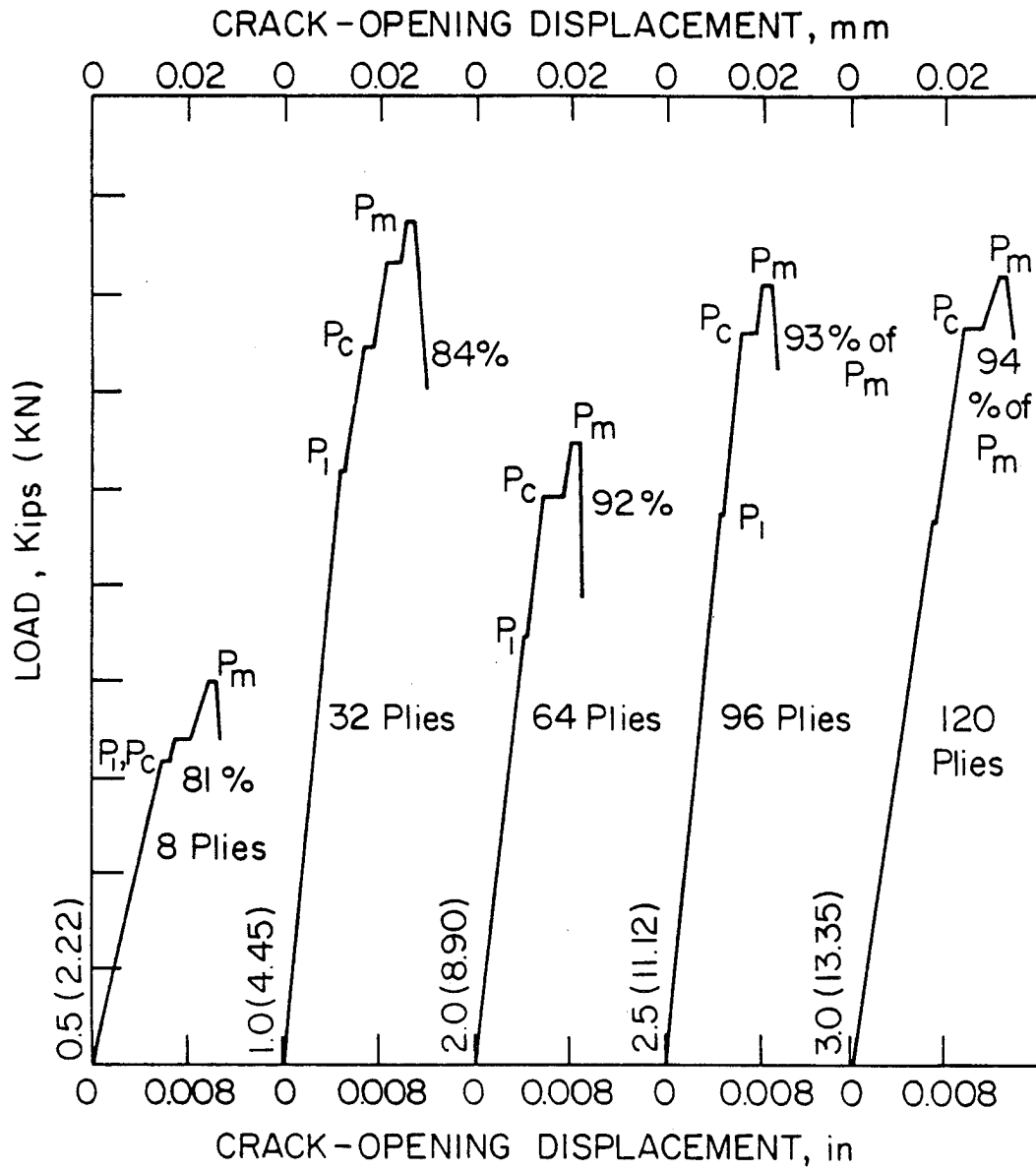
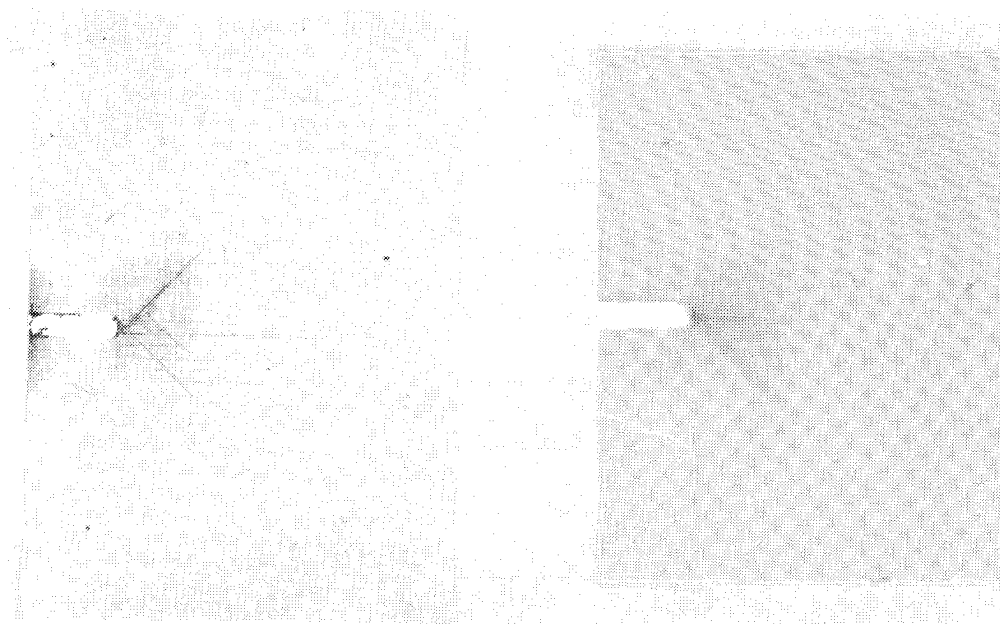


Figure 5.7 Load versus COD Records for the $[0/\pm 45/90]_{ns}$ Laminate at Various Thicknesses (Center-Cracked Tension Specimen)



(a) 8 Plies

(b) 64 Plies

Figure 5.8 Comparison of the Crack-Tip Damage in the 8 ply and 64 ply $[0/\pm 45/90]_{ns}$ Laminate at the First COD Discontinuity (Center-Cracked Tension Specimen)

ply specimen, and Figure 5.8(b) for a typical 64 ply specimen, it is obvious that both damage zones are comprised of matrix cracks in each fiber direction and delaminations more-or-less confined in a 45° triangle emanating from the crack tip. The damage appears more extensive in the 64 ply specimen but this is deceiving. The x-ray radiography is a thickness integrated record of damage. Since there are more plies in a 64 ply specimen, one would expect to see more damage in this specimen than in an 8 ply specimen. If the damage zone at each crack tip in Figure 5.8(a) and (b) were encircled the size of the zones would be essentially the same.

The fracture toughness of the $[0/\pm 45/90]_{ns}$ laminates at 8, 32, 64, 96 and 120 plies is shown in Figure 5.9 for a crack length-to-width ratio of 0.50. The circles represent the average of four replicate tests. The data scatter exhibited by a typical set of four replicate tests was 4-6% deviation from the average value. The $[0/\pm 45/90]_{ns}$ laminate exhibits a decrease in fracture toughness with increasing laminate thickness but appears to asymptotically approach a lower bound value beyond 64 plies. The lower bound value is approximately $30 \text{ ksi}\sqrt{\text{in}}$ ($1043 \text{ MPa}\sqrt{\text{mm}}$) and represents a 25% reduction in toughness from the 8 ply value.

The stress intensity factor computed at the critical load is compared to the fracture toughness computed at the maximum load in Figure 5.10. The symbols represent the average of four replicate tests. The data scatter (using the critical load) at 8 and 32 plies was approximately 14% deviation from the average while at 64, 96 and 120 plies it was less than 6%. The vertical dashed line in Figure 5.10 represents the ASTM isotropic metals specimen thickness requirement for plane

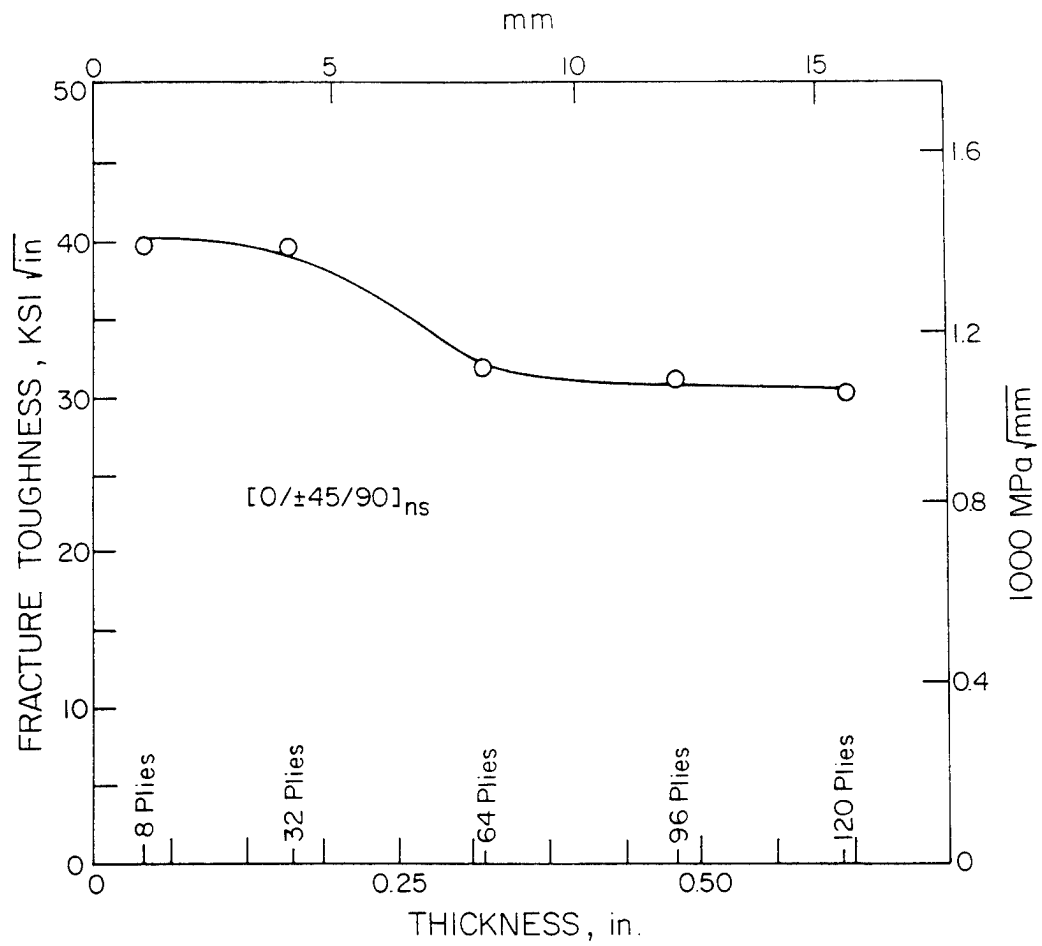


Figure 5.9 Fracture Toughness Versus Laminate Thickness for the $[0/\pm 45/90]_{ns}$ Laminate, $2a/W = 0.5$ (Center-Cracked Tension Specimen)

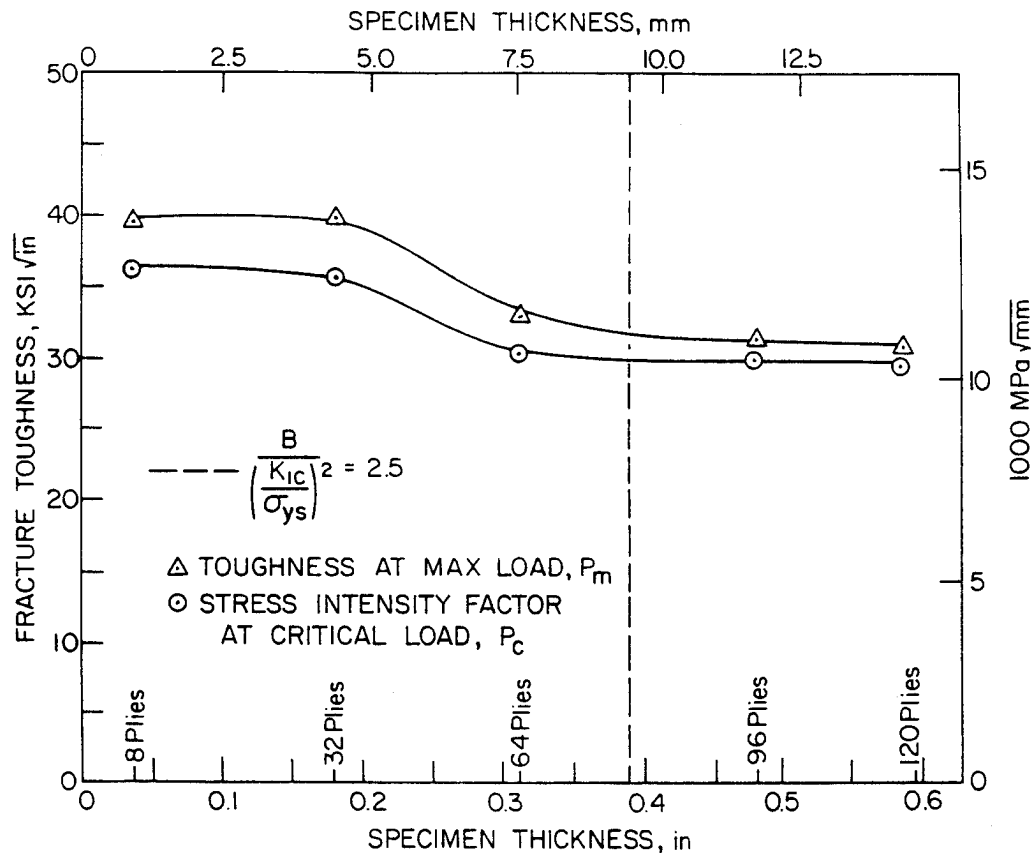


Figure 5.10 Comparison of Fracture Toughness at the Maximum Load and at the Critical Load as a Function of Thickness for the $[0/\pm 45/90]_{ns}$ Laminate, $2a/W = 0.5$ (Center-Cracked Tension Specimen)

strain fracture [2], $B \geq 2.5 \left(\frac{K_{Ic}}{\sigma_{ys}} \right)^2$

B = specimen thickness

K_{Ic} = plane strain fracture toughness

σ_{ys} = yield strength

(The yield strength was approximated by multiplying the laminate engineering stiffness in the loading direction, E_y , by the ultimate fiber strain, .010.) It is not suggested, herein, that this thickness requirement has any basis with respect to the fracture of laminated composites. It is simply of interest and facilitates the interpretation of the data trend curve. However, it does appear that the isotropic thickness requirement may be a reasonable indicator of the lower bound toughness behavior of the quasi-isotropic laminate.

Another interesting aspect of Figure 5.10 is the relationship between the maximum fracture toughness (K_m) and the critical stress intensity factor (K_c). For the 8 and 32 ply laminates the difference between K_c and K_m is greater than 10%. However, both curves appear to approach the same asymptotic value as the thickness increases. This is analogous to the pop-in phenomenon exhibited by some metals. It is believed [1,2] that pop-in is associated with a small increment of crack growth and arrest occurring in the interior region of the crack front; the crack growth appearance resembles plane strain crack growth. Therefore, the fracture toughness at pop-in is usually considered to be the plane strain fracture toughness. Variations in the fracture toughness, at pop-in, with specimen thickness exhibit about the same percentage change in toughness as the change in K_c shown in Figure 5.10 [37,38]. Thus,

there appears to be a number of similarities between the fracture behavior of an isotropic metal and the quasi-isotropic graphite/epoxy laminate.

Crack size was a test variable at 8 plies and at 120 plies. At each thickness the crack length-to-width ratios were 0.25, 0.375, 0.50 and 0.625. The fracture toughness (at the maximum load) for each crack size is shown in Figure 5.11. As already discussed the fracture toughness at 120 plies is lower than at 8 plies. The fracture toughness values of both the 8 ply laminate and 120 ply laminate are essentially independent of crack size.

To conclude the discussion of the effect of laminate thickness on the fracture behavior of the quasi-isotropic laminate, the examinations of crack-tip damage at intermediate loads and at final fracture will be described. Examinations prior to final fracture were performed using enhanced x-ray radiography and the specimen deply technique. The examination procedures for both methods were described in Chapter 4. A comparison of the damage development and final fracture of a typical 8 ply specimen and a typical 120 ply specimen is provided below.

The crack tip damage in an 8 ply specimen initiates as matrix cracks parallel to the fibers of the various plies at intermediate loads on the order of 50% of the final failure load. Damage formation increases dramatically at "damage events" that result in a discontinuity in the load-COD record. (See Figure 5.7.) An x-ray photograph of damage at the critical load, 77% of the maximum load, of an 8 ply specimen is shown in Figure 5.12. (The dark circular spot shown in Figure 5.12 just below the centerline of the crack is a slot cutting tool mark. These marks are also evident in the radiographs of Figures 5.24, 5.25, 5.26

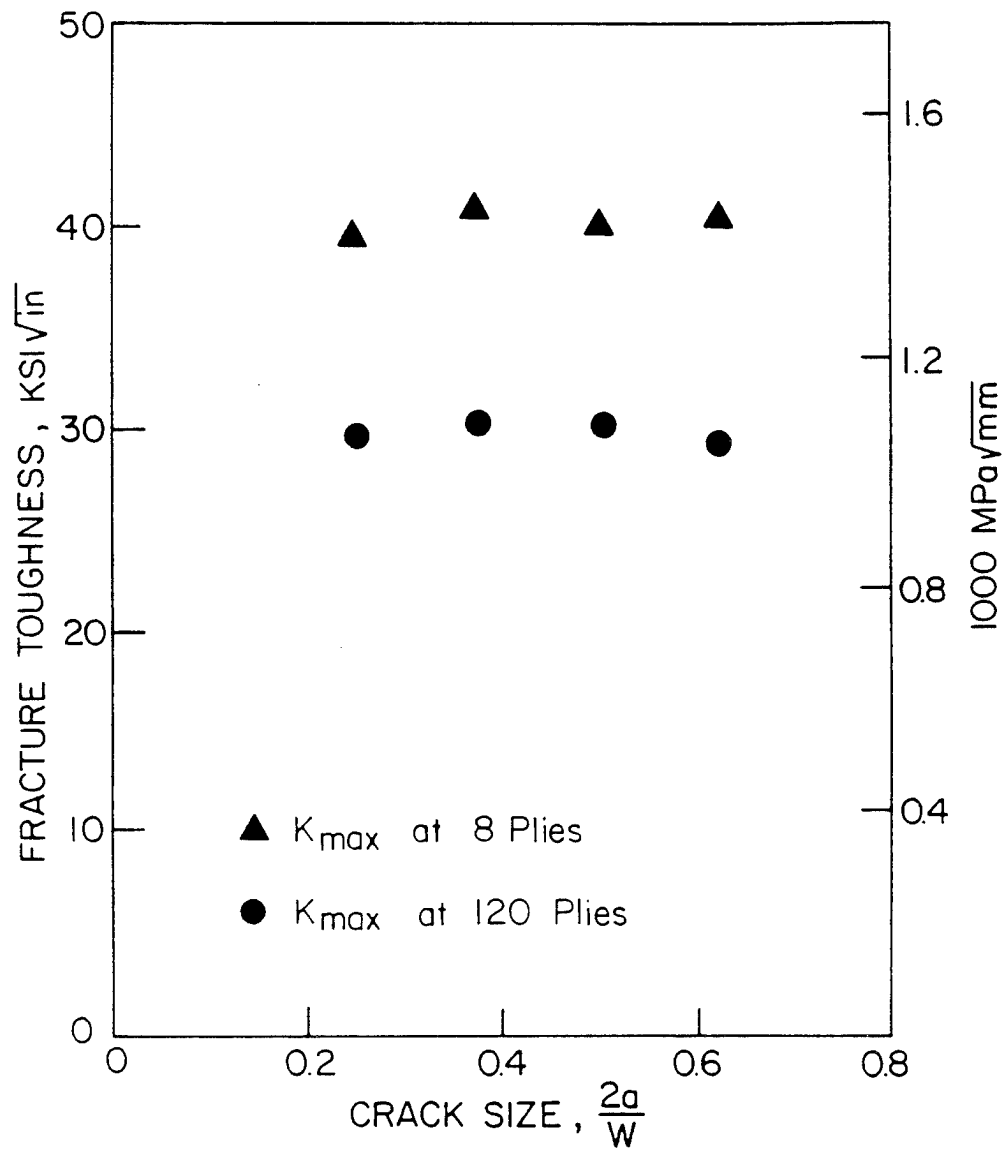
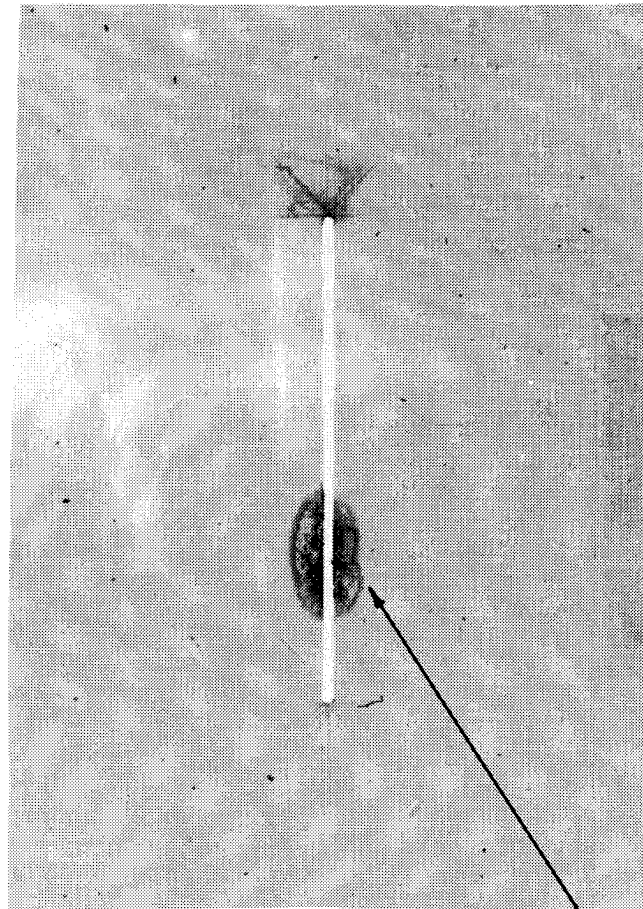


Figure 5.11 Fracture Toughness as a Function of $2a/W$ for $[0/\pm 45/90]_{ns}$ Laminates at 8 Plies and 120 Plies (Center-Cracked Tension Specimen)



Slot Cutting Tool Mark

Figure 5.12 X-ray Radiograph of a $[0/\pm 45/90]_S$ Specimen
(Before Deploy) at 77% of Average Failing Load
(Center-Cracked Tension Specimen)

and 5.36.) The radiographs reveal matrix cracks, delaminations and a dark jagged line at 45° to the starter notch. The corresponding deply of this specimen confirms that this dark jagged line visible in the radiographs is actually a line of broken fibers in the 0° surface ply. The documentation of the deply examination is provided in Figure 5.13. Typical photographs of magnified damage as viewed under the microscope are shown in Figures 5.14-5.16. Regions of delamination, Figure 5.14, are clearly marked by the gold chloride and are visible at low magnification. Well defined lines of broken fibers extending from the starter notch, Figure 5.15, are also visible at low (20-30x) magnifications. Examinations at high magnification (200x-400x), Figure 5.16, confirm the existence of the broken fibers. Extensive delaminations of the outside plies occur at the $0/+45$ and $+45/-45$ interfaces from both surfaces. A line of broken fibers in the 0° ply extend from the starter notch at 45° , parallel to the fibers in the adjacent layer. Matrix cracks between fibers are visible at the crack tip of most plies.

If the damage region in the radiographs (before deply) was encircled at the crack tip the diameter of the circle would be approximately 0.16 in. (4.0 mm). As the load increases toward the maximum load, the crack tip damage in an 8 ply specimen increases dramatically as illustrated in the radiograph shown in Figure 5.17. This radiograph was taken at 85% of the maximum load. Two lines of fiber breaks at $+45^\circ$ to the starter notch are visible along with extensive matrix cracking and delamination. If this damage region is encircled the diameter would be about 0.43 in. (11.0 mm). The final fracture surface of the 8 ply specimen is rough and uneven. However, macroscopically it is collinear with the starter notch (see Figure 5.18).

OUTSIDE 0 PLY 0/+45 INTERFACE	
+45 PLY 45/-45 INTERFACE	
-45 PLY -45/90 INTERFACE	
MIDPLANE 2@90 90/-45 INTERFACE	
-45 PLY -45/+45 INTERFACE	
+45 PLY +45/0 INTERFACE	
OUTSIDE 0 PLY +45/0 INTERFACE	

Figure 5.13 Documentation of the Through-the-Thickness Damage in a $[0/\pm 45/90]_s$ Specimen by Deply at 77% of Average Failing Load (Not Drawn to Scale), (Center-Cracked Tension Specimen)

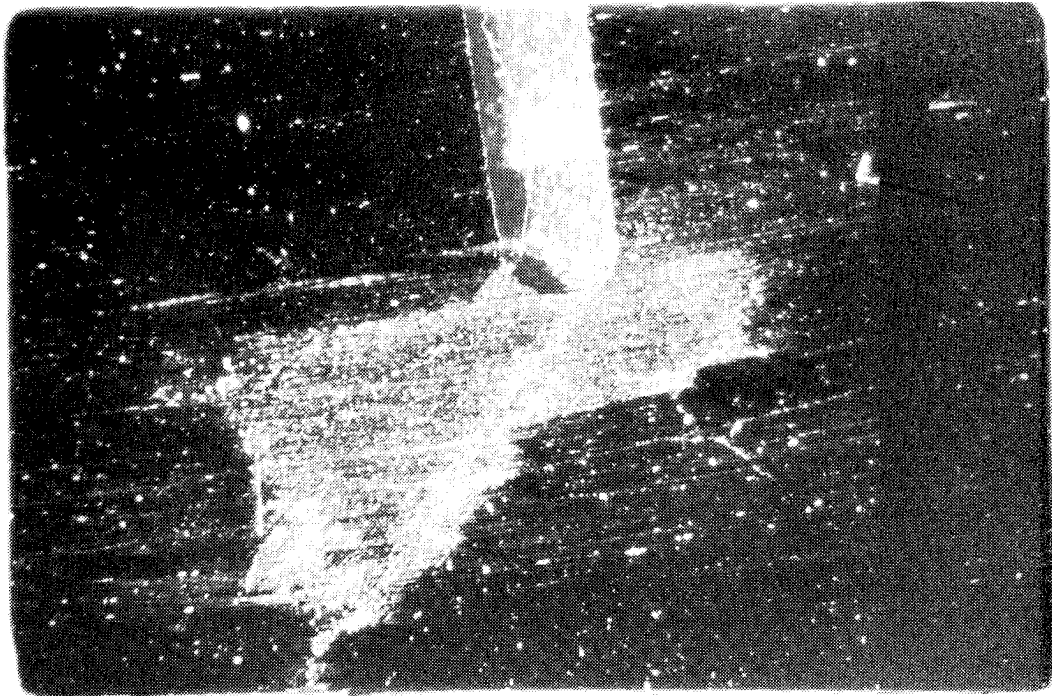


Figure 5.14 Photograph of the 0/+45 Delamination, Marked by Gold Chloride, at 20x Magnification

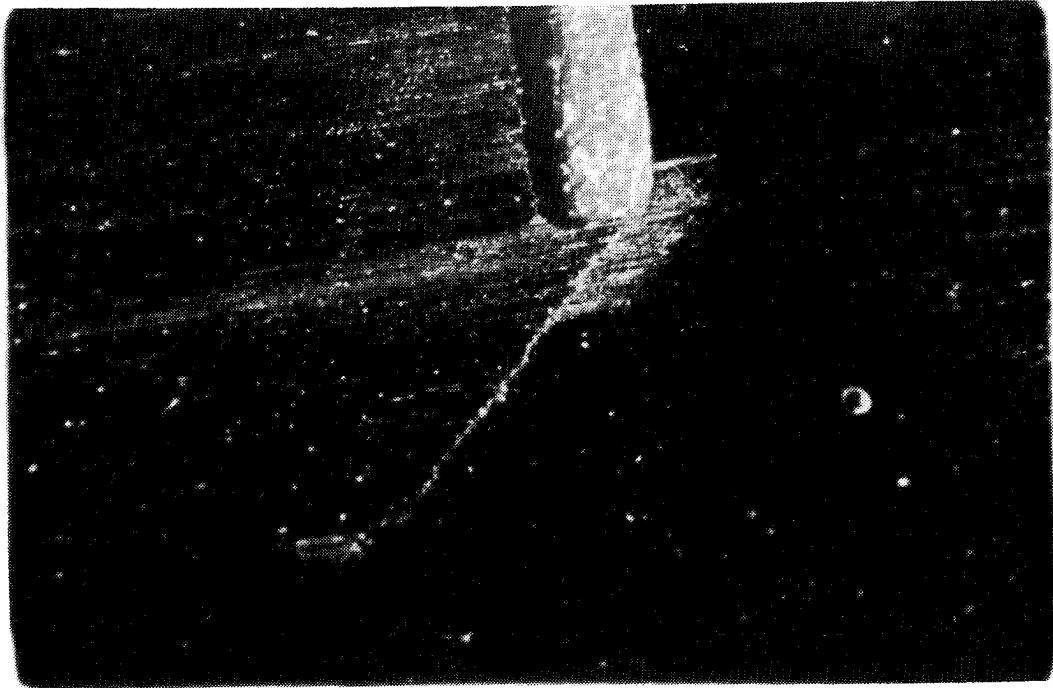


Figure 5.15 Photograph of the 45° Line of Broken Fibers
in the 0° Surface Ply at 20x Magnification

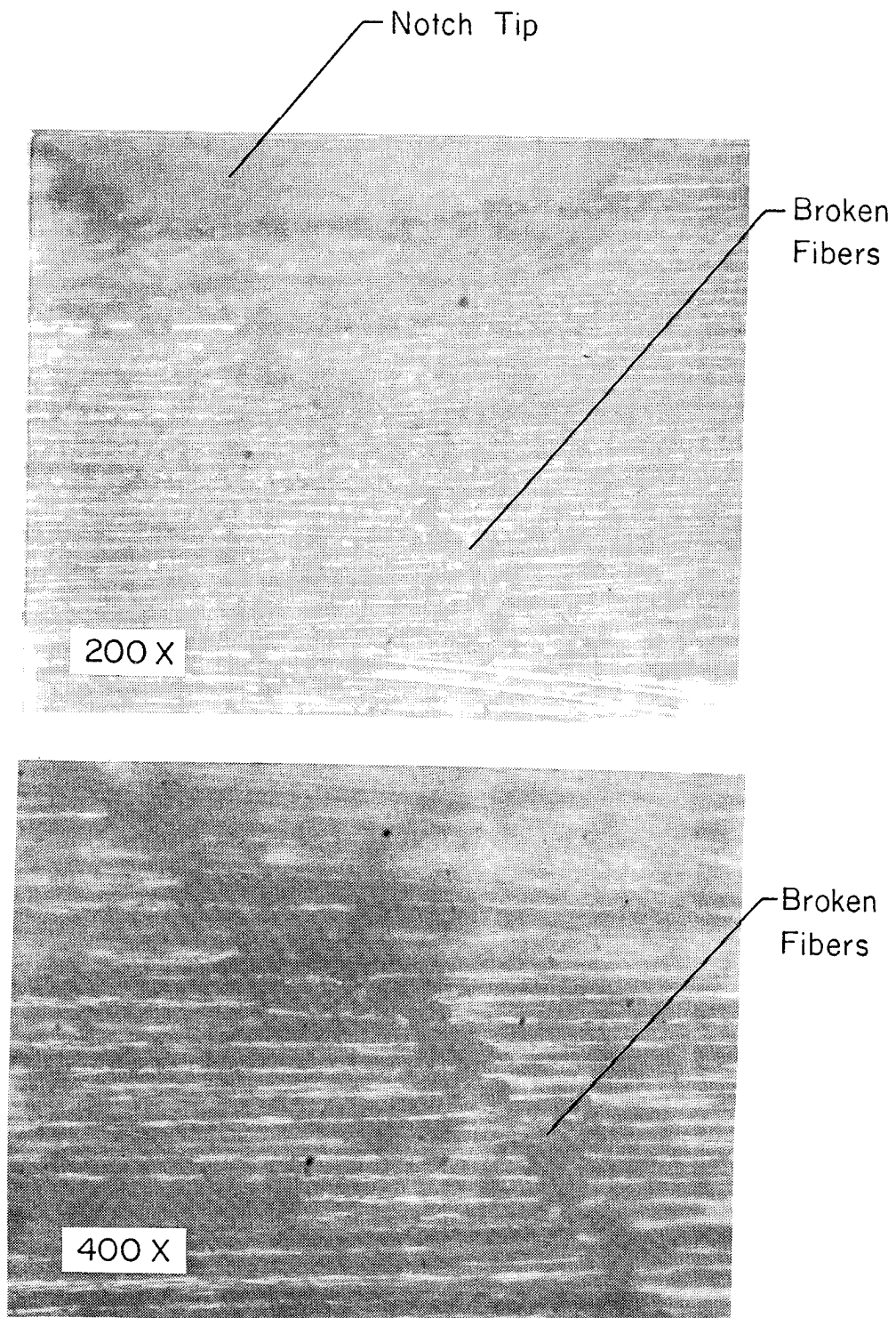


Figure 5.16 Photograph of the $+45^\circ$ Line of Broken Fibers in the 0° Surface Ply at 200x and 400x Magnifications

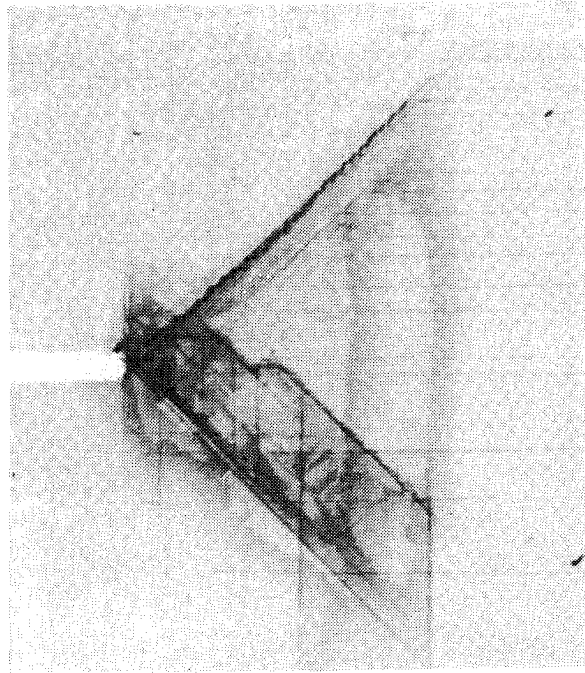


Figure 5.17 Crack Tip damage in the $[0/\pm 45/90]_s$ Specimen at 85% of Failing Load (Center-Cracked Tension Specimen)

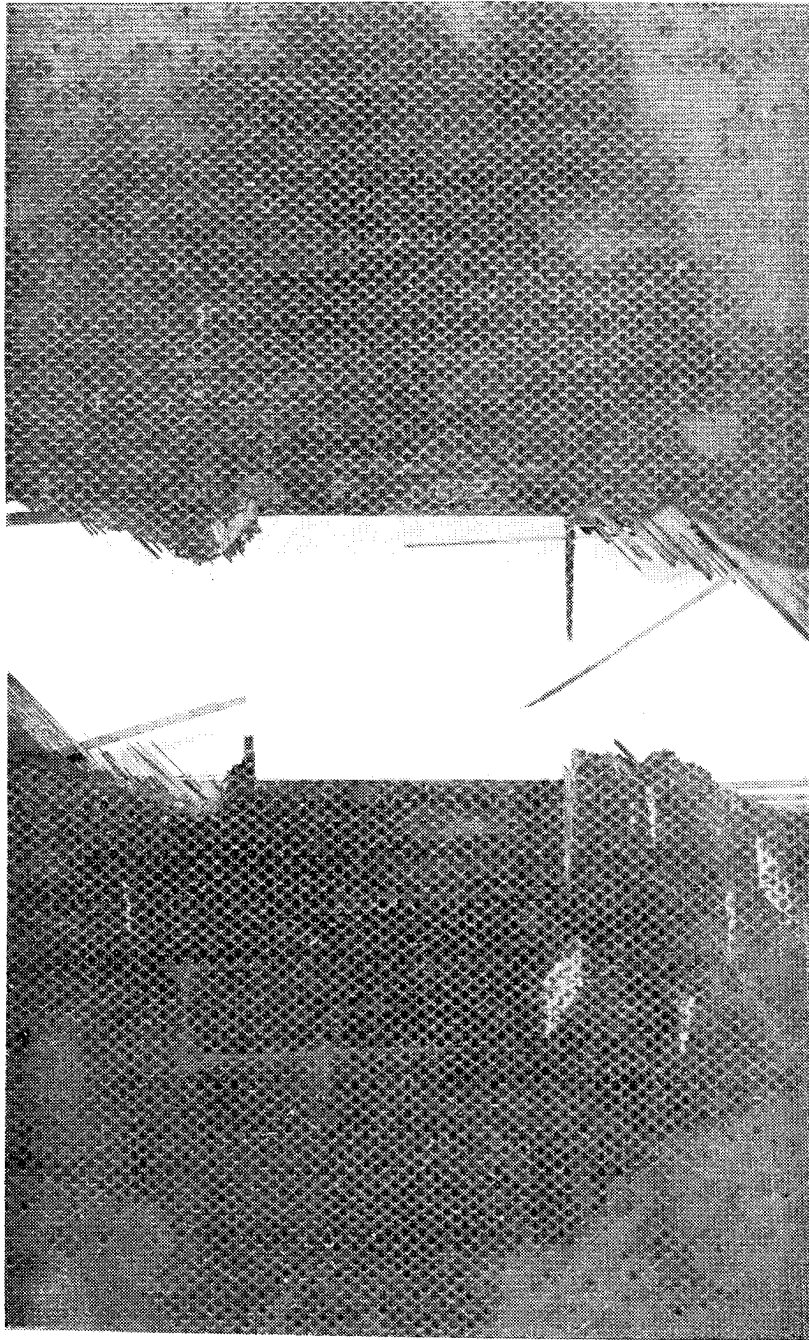


Figure 5.18 Photograph of the Fracture Surface of a $[0/\pm 45/90]_S$ Specimen

The x-ray photograph of Figure 5.19 shows the crack-tip damage in a 120 ply specimen at the critical load (91% of the maximum load). This damage region appears very similar to the damage region in the 8 ply specimen, Figure 5.12. If this damage region were encircled the diameter would be approximately 0.11 in. (2.8 mm) which is slightly smaller than the damage region in the 8 ply specimen at the critical load and much smaller than the damage shown in Figure 5.17 at 85% of the maximum load. The documentation of the deply examination of this specimen is presented in Figure 5.20. The deply examination reveals two significant findings. First, the regions of delamination and extensive matrix cracking are confined to plies near both surfaces. Major delaminations of the outside plies occurred at the 0/+45 and +45/-45 interfaces as was the case with the 8 ply specimen. Delaminations were not visible outside this "boundary layer." The damage in the interior of the specimen consists of short matrix cracks in the various fiber directions and a line of broken fibers in the 0° plies extending about 0.030" (0.76 mm) from the starter notch. The line of fiber breaks in the 0° surface plies extend in the 45° direction from the notch tip. This is parallel to the fibers in the adjacent layer and is exactly like the 8 ply specimen. Thereafter, each 0° ply has a +45° ply on one side and a 90° ply on the opposite side. This tends to "straighten" the line of fiber breaks. In the interior of the specimen, the starter crack appears to have extended a short distance in a collinear and stable manner. Indeed, the final fracture, Figure 5.21, of the 120 ply specimens are self-similar (collinear with the starter notch) and the fracture surface is relatively smooth compared to the 8 ply specimen. Each surface of the fractured 120 ply specimen exhibits a "shear lip" where the outside

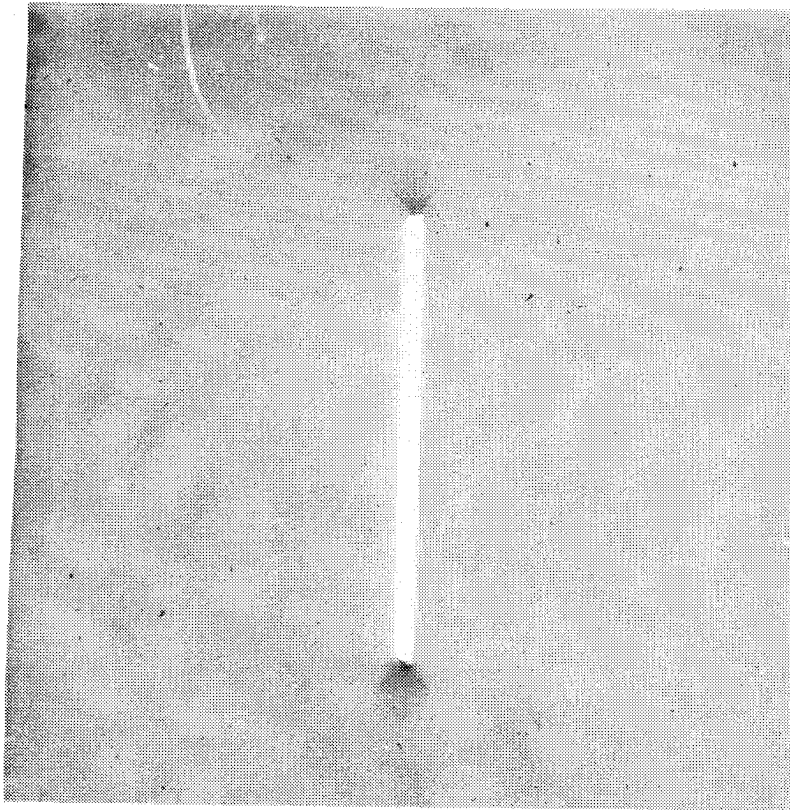
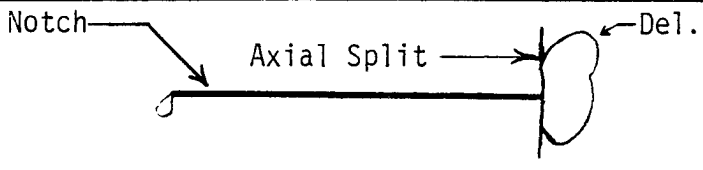
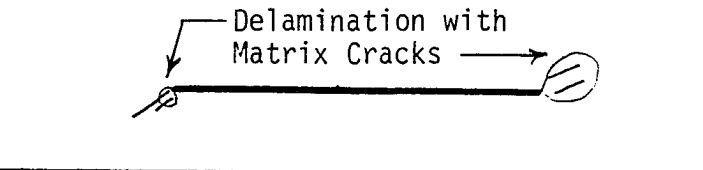
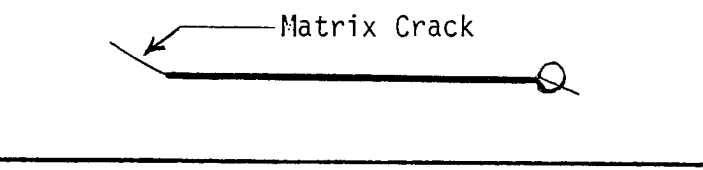
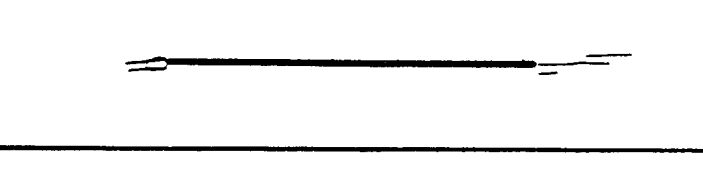
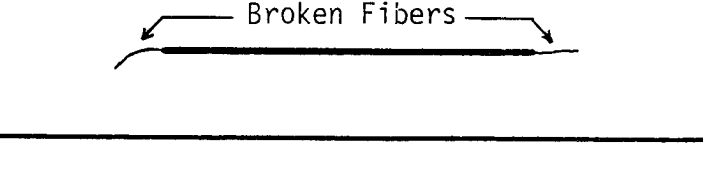
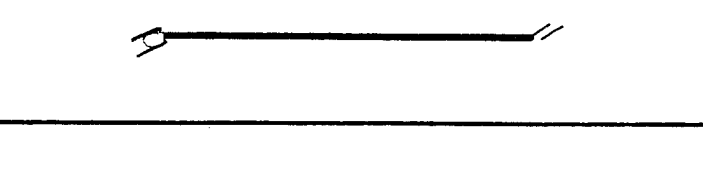
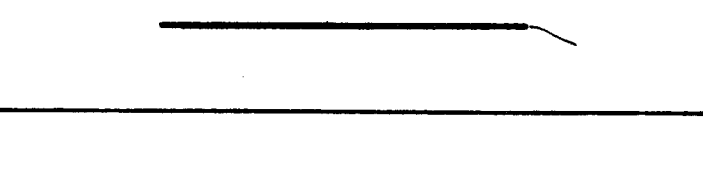

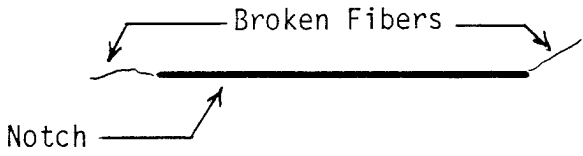







Figure 5.19 X-ray Radiograph of the $[0/\pm 45/90]_{15s}$ Specimen,
Before Deploy, at 91% of Average Failing Load
(Center-Cracked Tension Specimen)

Outside 0 Ply 0/+45 Interface	 <p>Notch — Axial Split — Del.</p>
#2 +45 Ply +45/-45 Interface	 <p>Delamination with Matrix Cracks —</p>
#3 -45 Ply -45/90 Interface	 <p>Matrix Crack —</p>
#4 90 Ply 90/0 Interface	
#5 0 Ply 0/+45 Interface	 <p>Broken Fibers —</p>
#6 +45 Ply +45/-45 Interface	
#7 -45 Ply -45/90 Interface	
#8 90 Ply 90/0 Interface	

a. First 8 Plies from Surface

Figure 5.20 Documentation of the Through-The-Thickness Damage in the $[0/\pm 45/90]_{15s}$ Specimen by Deply at 91% of Average Failing Load (Not Drawn to Scale) (Center-Cracked Tension Specimen)

#37 0 Ply 0/+45 Interface	 <p>Broken Fibers</p> <p>Notch</p>
#41 0 Ply 0/+45 Interface	
#45 0 Ply 0/+45 Interface	
#49 0 Ply 0/+45 Interface	
#53 0 Ply 0/+45 Interface	
JUST BEFORE MIDPLANE #57 0 Ply 0/+45 Interface	

b. Interior 6 0° Plies from Midplane

Figure 5.20 Documentation of the Through-The-Thickness Damage in the $[0/\pm 45/90]_{15s}$ Specimen by Deply at 91% of Average Failing Load; (Center-Cracked Tension Specimen)

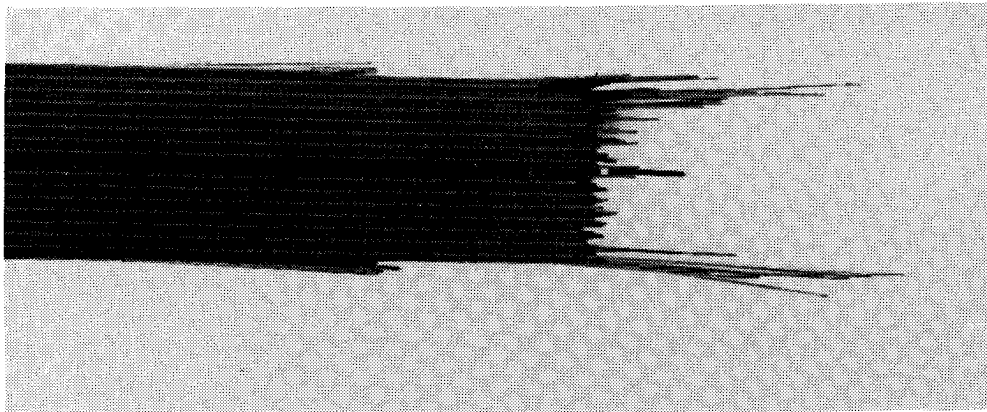
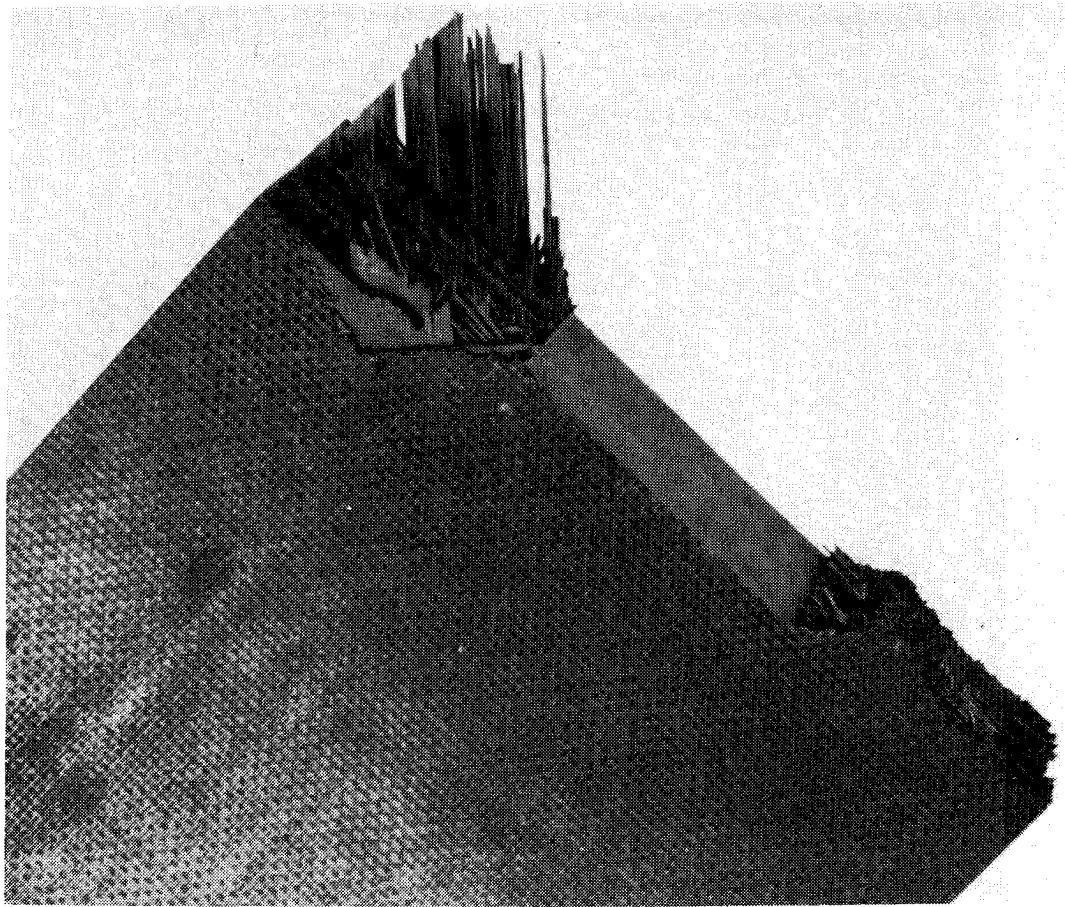


Figure 5.21 Photographs of the Final Fracture Surface
of Two $[0/\pm 45/90]_{15s}$ Specimens

0° ply breaks in a 45° direction and the boundary layer delaminations are evident.

The comparison of the damage regions in the thin and thick specimens allows for a consistent interpretation of the fracture toughness data. The thin (8 ply) specimens exhibit more extensive damage development in the form of delaminations and matrix cracking than do the thick specimens. This extensive damage region provides natural blunting to the crack tip thereby retarding crack extension. The damage in the thick specimens prior to final fracture is characterized by delaminations and splitting in the outside plies and by collinear fiber breaks in the interior. In effect the starter notch has extended collinearly in a stable manner. Therefore, the thin specimens have more crack growth resistance, and hence higher fracture toughness, than do the thick specimens. In conclusion, it appears likely that the reduction in fracture toughness of the quasi-isotropic laminate with increasing laminate thickness can be attributed to the differences in the subcritical damage region at the crack tip. This may be analogous to the effect of thickness on the size of the crack-tip plastic zone in isotropic metals.

5.3.2 The $[0/90]_{ns}$ Laminate

The fracture behavior of the $[0/90]_{ns}$ laminate is greatly affected by laminate thickness. Fracture toughness computed at the maximum load as a function of laminate thickness, $\frac{2a}{W} = 0.5$, is shown in Figure 5.22. The circles represent the average of four replicate tests. The maximum deviation from the mean value at 8 plies was 30% while the maximum deviation was less than 8% for all other thicknesses. Fracture toughness initially decreased sharply with increasing laminate thickness. Beyond

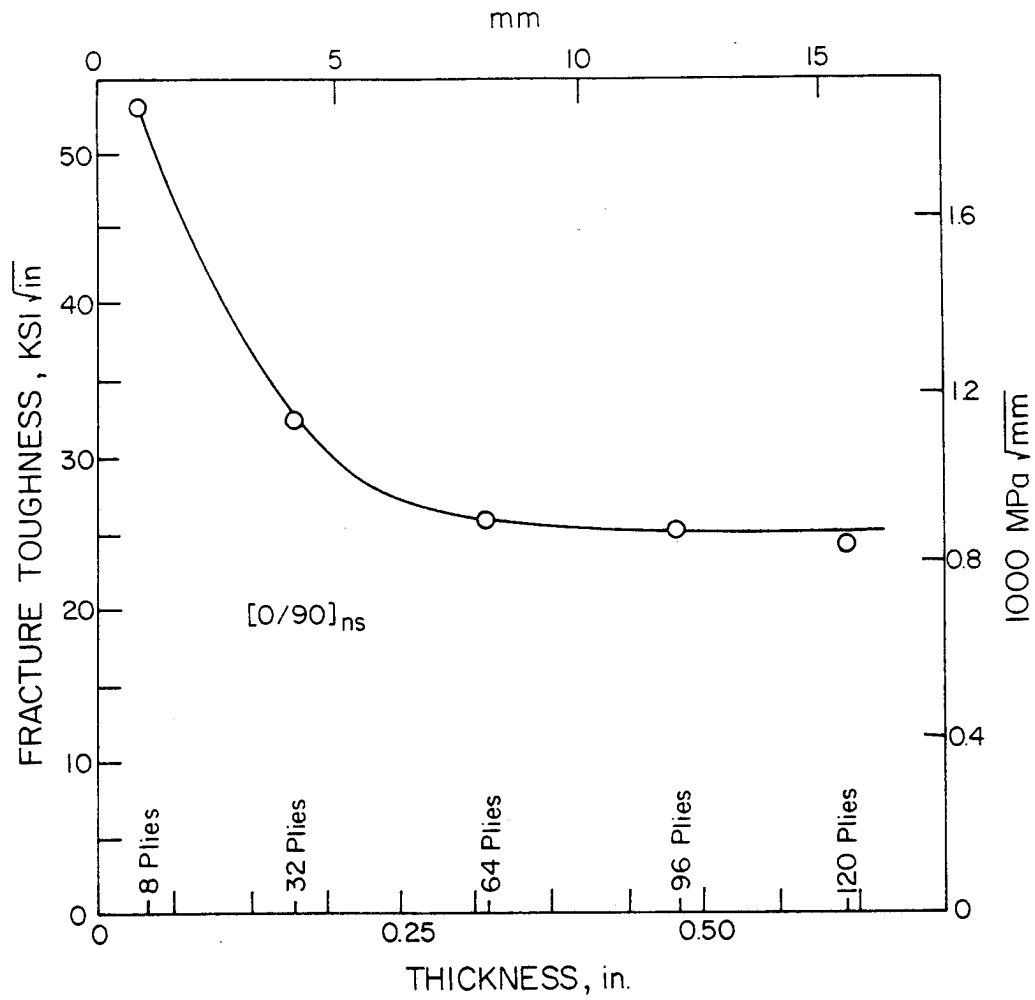


Figure 5.22 Fracture Toughness as a Function of Laminate Thickness for the $[0/90]_{ns}$ Laminate; $2a/W = 0.5$ (Center-Cracked Tension Specimen)

64 plies, fracture toughness asymptotically approaches a lower bound value of approximately $25 \text{ ksi}\sqrt{\text{in}}$ ($869 \text{ MPa}\sqrt{\text{mm}}$).

The crack length-to-width ratio was varied at 8 plies and at 96 plies. Fracture toughness was determined at $\frac{2a}{W}$ values of 0.25, 0.375, 0.50 and 0.625. These values are displayed in Figure 5.23. As previously stated the fracture toughness at 96 plies is substantially lower than the fracture toughness at 8 plies. Furthermore, the fracture toughness of the 96 ply laminate is practically independent of crack size while the fracture toughness of the 8 ply laminate sharply increases with increasing crack size.

Figures 5.22 and 5.23 illustrate two dramatic differences in the fracture toughness of thin and thick $[0/90]_{ns}$ laminates. Both the variations in fracture toughness with thickness and crack size are due to the differences in the formation of subcritical damage at the crack tip of thin and thick laminates. The examinations of damage in the $[0/90]_{2s}$ laminate of this study, as well as previous studies [12,13], show the 8 ply laminate to be highly susceptible to the formation of major axial splits at the crack tip extending in the direction of the applied load. This is clearly illustrated in Figures 5.24 and 5.25 where x-ray examinations of the same specimen were taken at 60% and 92% of the maximum load. These axial splits reduce the strength of the stress singularity at the crack tip and, therefore, raises the failure strength or fracture toughness. The axial splitting is more extensive for long starter cracks than for shorter cracks. Therefore, the fracture toughness increases with increasing crack length as illustrated in Figure 5.23.

The role of axial splitting also accounts for the dramatic reduction in fracture toughness with increasing laminate thickness. To fully

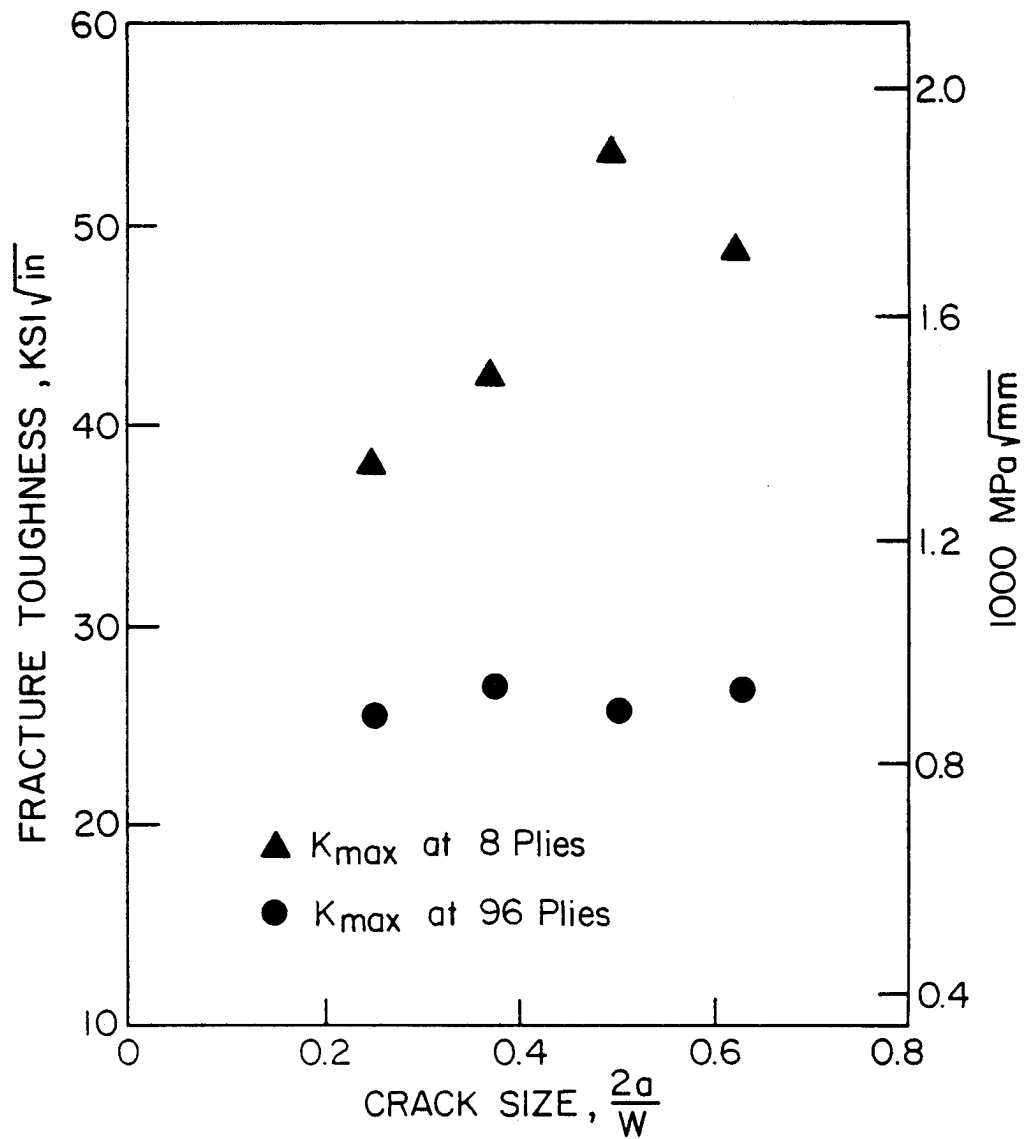


Figure 5.23 Fracture Toughness as a Function of $2a/W$ for a $[0/90]_{\text{ns}}$ Laminate (Center-Cracked Tension Specimen)

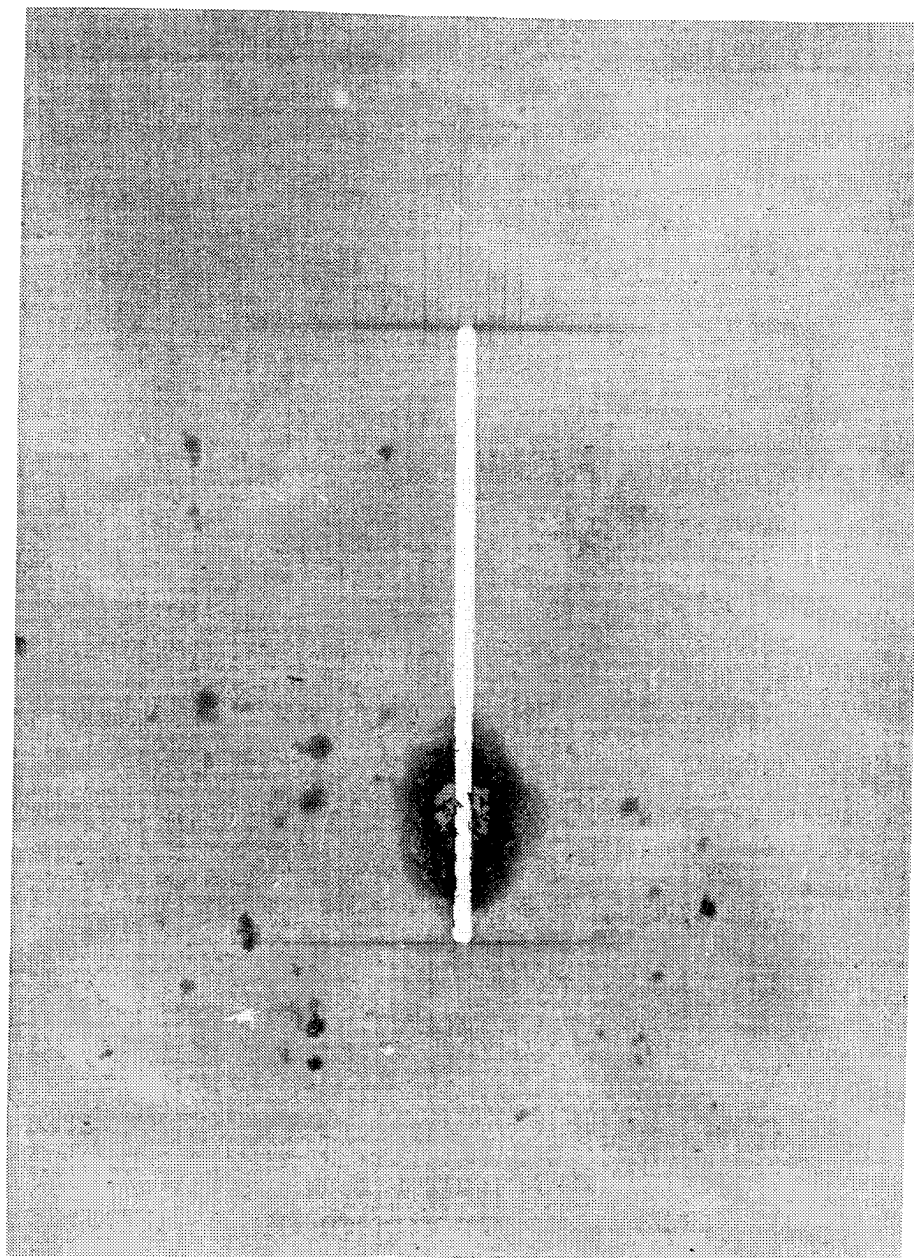


Figure 5.24 Crack Tip Damage in a $[0/90]_{2s}$ Specimen at 60% of Failing Load (Center-Cracked Tension Specimen)

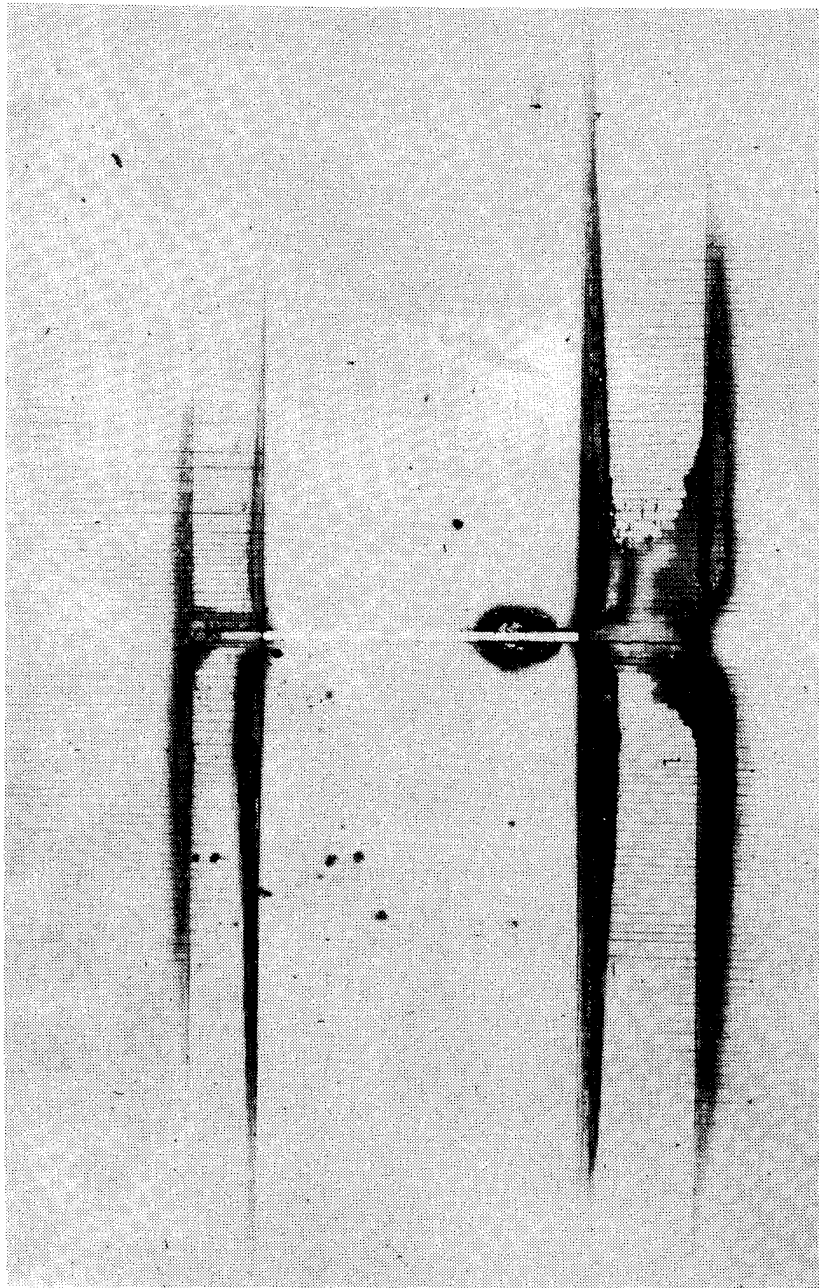


Figure 5.25 Crack Tip Damage in a $[0/90]_{2s}$ Specimen at 92% of Failing Load (Center-Cracked Tension Specimen)

understand this effect, the variation in damage through the thickness of the 8 ply specimen must be established. Figure 5.26 shows the x-ray photograph of damage in an 8 ply specimen selected for depley with $2a/W = 0.5$ and at a damage level similar to that of the specimen shown in Figure 5.25 at 92% of the maximum load. The documentation of the depley study is shown in Figure 5.27. The ply-to-ply examination shows the damage to be symmetric with respect to the laminate midplane. The major axial splits form in the outside 0° plies and the regions of delamination occur at the outer $0/90$ and $90/0$ interfaces. Lines of broken fibers extend collinear with the starter notch in each 0° ply. Notice that the fiber breaks occur at notch tips where the axial splits do not form, and vice versa. In the interior two 0° plies, there are no axial splits at the tip of the starter notch. (It is of interest to note that the fiber breaks form in the outermost 90° ply parallel to the major axial split in the adjacent 0° ply.) In summary, the depley study of this 8 ply specimen shows that the axial splitting occurs primarily in the outside 0° plies which are only partially constrained by an adjacent 90° ply. The interior 0° plies with 90° constraint plies on both sides do not split extensively. So the axial splitting in the $[0/90]_{2s}$ laminate is predominantly a surface effect.

Additional evidence that the axial splitting in the $[0/90]_{ns}$ laminate is a surface effect is obtained by comparing the load versus COD records of the 8 ply and 32 ply laminates. (The 32 ply specimen was selected for this comparison so that both load records could be plotted on the same axis.) Typical load versus COD records are shown in Figure 5.28. There are two significant differences. First, the critical load for the 8 ply specimen is a much lower percentage (60%) of the maximum

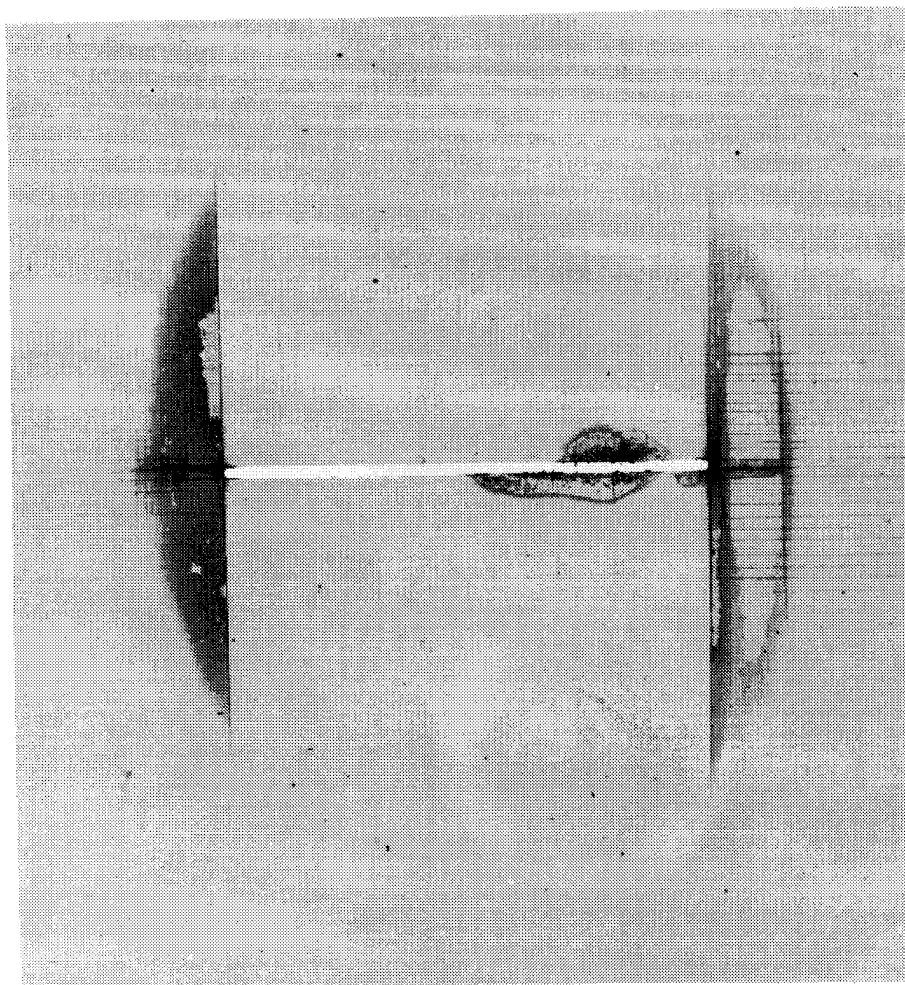


Figure 5.26 X-ray Radiograph of the $[0/90]_{2s}$ Specimen Before
Deply at 71% of Average Failing Load (Center-Cracked
Tension Specimen)

Outside 0 Ply 0/90 Interface	
90 Ply 90/0 Interface	
0 Ply 0/90 Interface	
Midplane 2@90 90/0 Interface	
0 Ply 0/90 Interface	
90 Ply 90/0 Interface	
Outside 0 Ply 90/0 Interface	

Figure 5.27 Documentation of the Through-The-Thickness Damage in the $[0/90]_{2s}$ Specimen by Depley at 71% of Average Failing Load (Not Drawn to Scale), (Center-Cracked Tension Specimen)

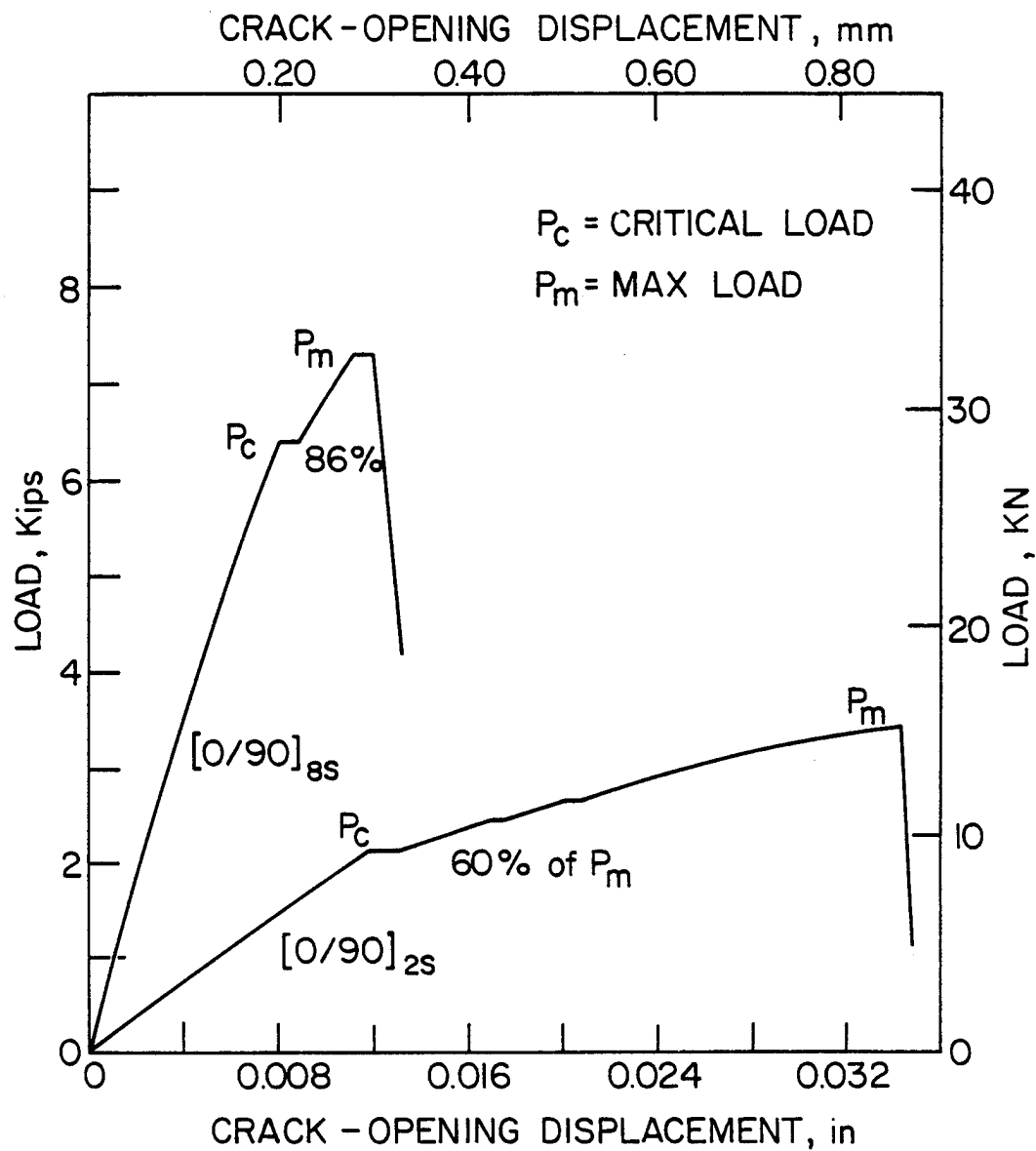


Figure 5.28 Comparison of the Load Versus COD Record for an 8 Ply and 32 Ply $[0/90]_{ns}$ Specimen (Center-Cracked Tension Specimen)

load than is the case for the 32 ply specimen (86%). Second, the crack-opening displacement at fracture is much higher for the 8 ply specimen than for the 32 ply specimen. Table 5.7 compares the fracture toughness and COD in the 8 ply specimens at the onset of splitting, P_c (60% of the maximum load), to the fracture toughness and COD at the maximum load for the 32 ply specimens. The COD values are essentially the same. This implies that the 8 ply specimens exhibit a splitting and crack arrest mechanism while the 32 ply specimens do not. The final fracture surface of the 32 ply specimen was smooth and the only evidence of splitting was in the outside 0° plies. In fact this description of the final fracture surface applies to all specimens thicker than 8 plies. Figures 5.29 and 30 show the fracture surface of an 8 ply and 120 ply specimen, respectively.

It should be noted before proceeding that the 120 ply specimens did not exhibit discontinuities in the load-COD records. This means that very little subcritical damage forms at the crack tip prior to final fracture. A 120 ply specimen was loaded to 91% of the failure load of the other specimens for examination. The x-ray radiograph revealed very little crack tip damage. The deply examination revealed no fiber breaks and matrix splits about .016 in. (.4 mm) in length in the surface boundary layer plies.

Figure 5.31 shows the subcritical damage region in a 96 ply specimen taken at 96% of the maximum load. By contrasting the damage in this thick specimen to the damage in the 8 ply specimen at 92% of the maximum load, Figure 5.25, one sees further evidence of the diminished role of axial splitting in the thicker specimens. The fact that the axial splitting and delamination in the thick specimen, shown in Figure 5.31,

Table 5.7 Test Data for the $[0/90]_{2S}$ and $[0/90]_{8S}$ Laminates

SPECIMEN ID	THICKNESS # OF PLIES	MAX LOAD		CRITICAL LOAD	
		K_{max} Ksi $\sqrt{in.}$ (MPa \sqrt{mm})	COD_{max} in. (mm)	K_C Ksi $\sqrt{in.}$ (MPa \sqrt{mm})	COD_C in. (mm)
18-3	8			31.3 (1088)	.0095 (0.24)
18-4	8			38.2 (1327)	.012 (0.30)
18-5	8			36.9 (1282)	.012 (0.30)
18-6	8			37.8 (1314)	.012 (0.30)
AVERAGE				36.1 (1253)	.011 (.29)
19-1	32	32.5 (1129)	.011 (0.28)		
19-2	32	30.8 (1070)	.010 (0.25)		
19-3	32	32.4 (1126)	.010 (0.25)		
19-4	32	32.4 (1126)	.011 (0.28)		
AVERAGE		32.0 (1113)	.011 (.29)		

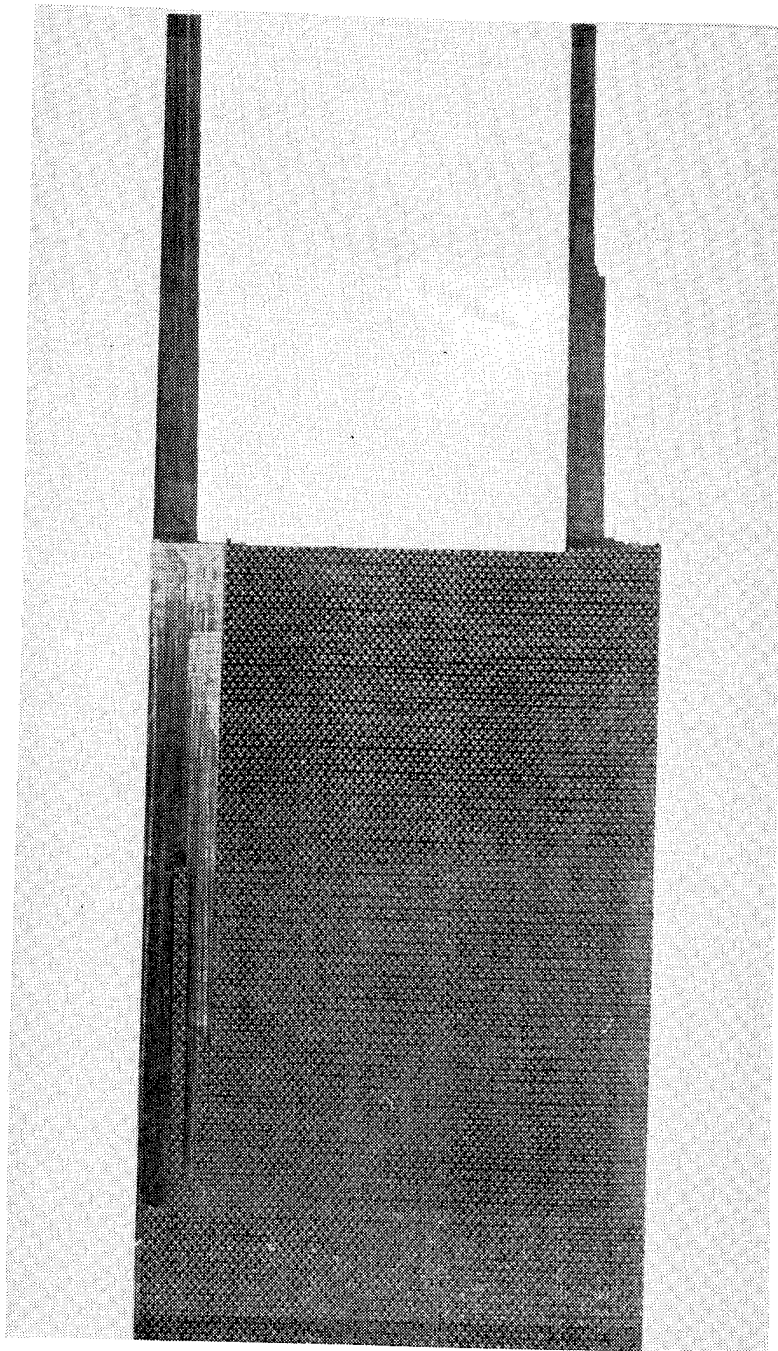


Figure 5.29 Photograph of a Fractured $[0/90]_{2s}$ Specimen

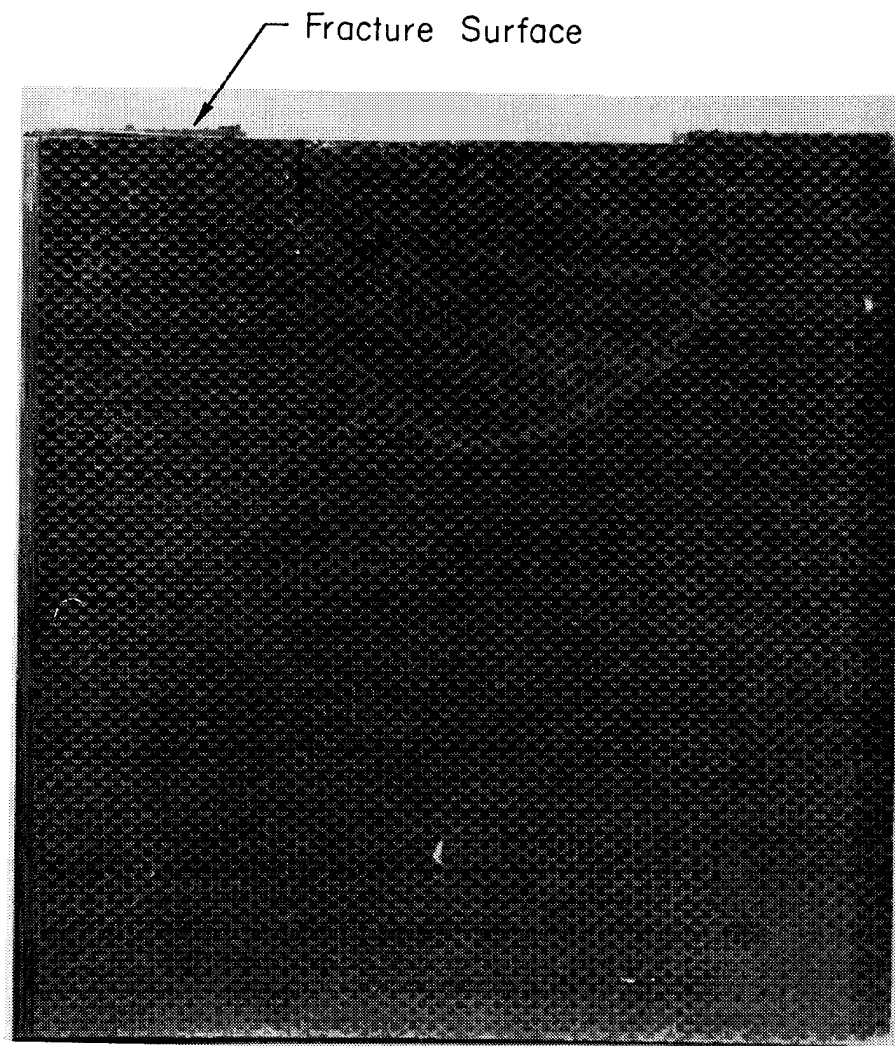


Figure 5.30 Photograph of the Fracture Surface
of a $[0/90]_{30s}$ Specimen

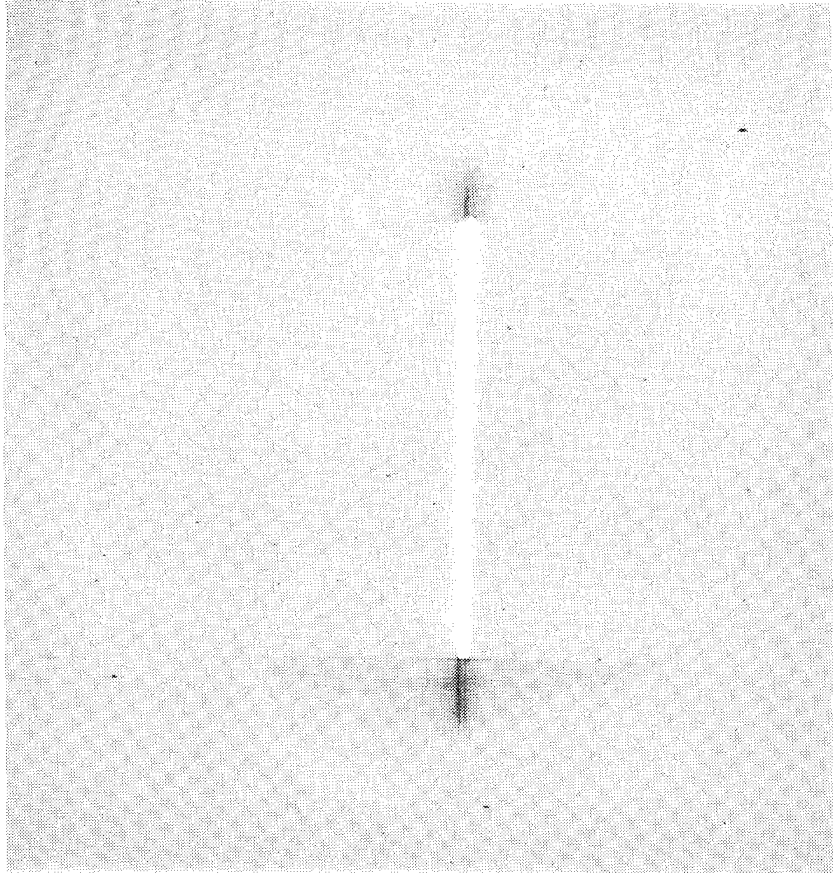


Figure 5.31 X-ray Radiograph of a $[0/90]_{24s}$ Specimen
at 96% of the Failing Load

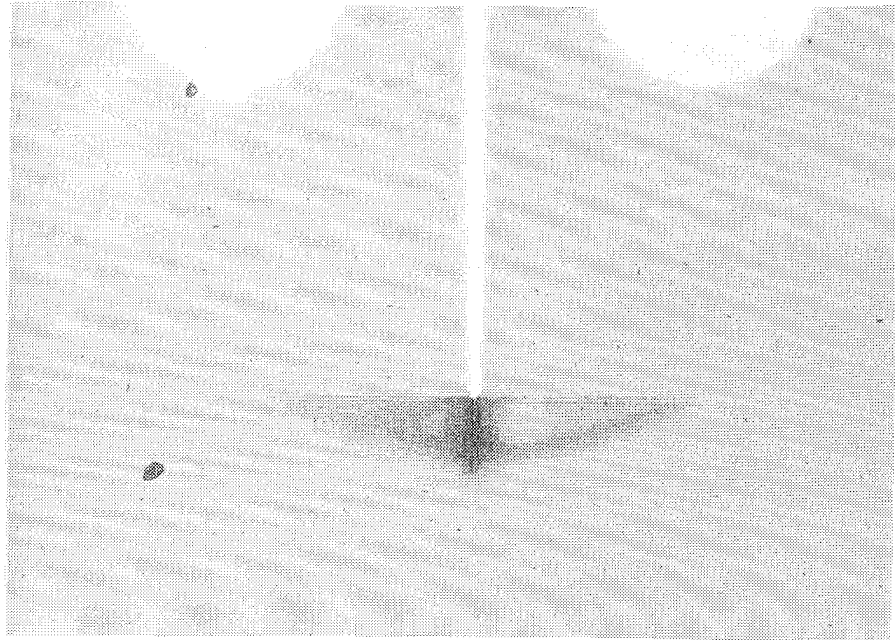
is strictly a surface effect is illustrated by the x-ray photographs of Figure 5.32. Figure 5.32(a) shows the crack tip damage in a 96 ply compact tension specimen just prior to the maximum load. The damage in the compact tension specimen is identical to the damage in the center-cracked tension specimen of Figure 5.31. After the maximum load has been reached, the compact tension specimens do not fail catastrophically because of the existence of a compression region on the surface opposite the crack front. After loading the compact tension specimens to their maximum load the axial splits are so extensive in the outside surface 0° plies that they delaminate from the adjacent 90° plies and can be easily peeled away. The x-ray photograph in Figure 5.32(b) shows the remaining interior damage after peeling the two outside 0° plies. Clearly the crack has extended in a self-similar manner, collinear with the starter notch. There is no evidence of splitting or delaminations at the tip of the starter notch in the interior of the specimen.

In summary, the variation of fracture toughness of the $[0/90]_{ns}$ laminate with crack size and laminate thickness is due to the role of axial splits that form at the starter crack tip. Axial splitting elevates the fracture toughness of the 8 ply laminate by reducing the strength of the crack tip stress singularity. These axial splits have been shown to be a surface effect in thicker laminates and do not significantly affect the fracture behavior.

5.3.3 The $[0/\pm 45]_{ns}$ Laminates

The fracture toughness of the $[0/\pm 45]_{ns}$ laminate varies with laminate thickness as does the toughness of the $[0/\pm 45/90]_{ns}$ and $[0/90]_{ns}$ laminates. However, in sharp contrast to the behavior of the first two

(a)



(b)

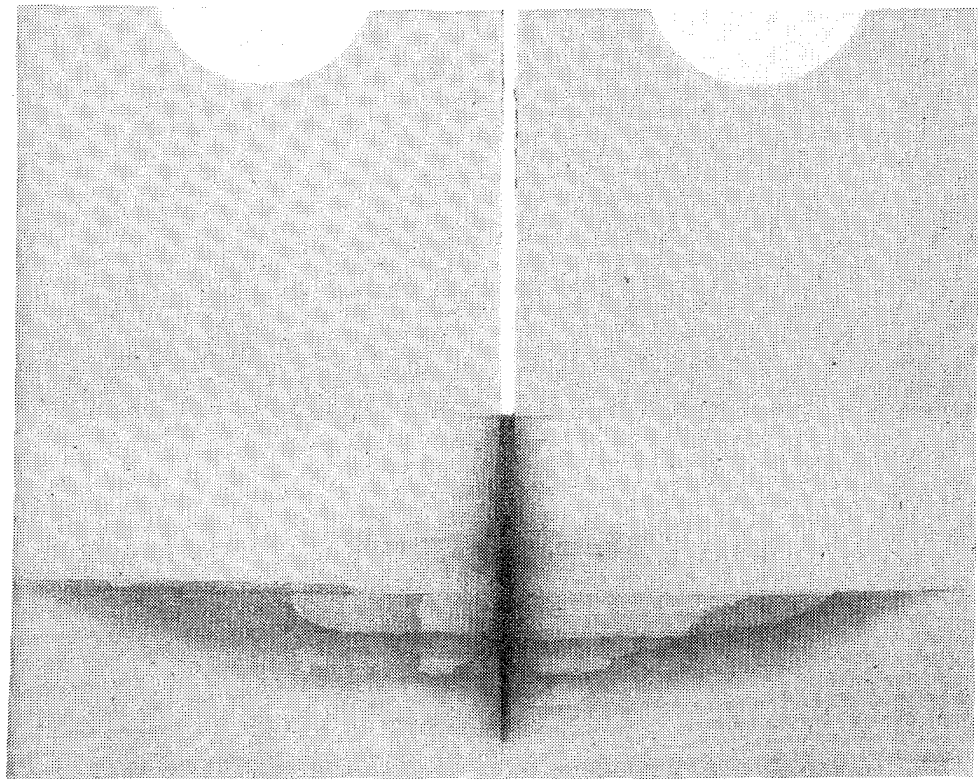


Figure 5.32 X-ray Radiograph of Crack Tip Damage in a $[0/90]_{24s}$ Compact Tension Specimen (a) Just After the First Load Reduction (b) After Final Load Reduction with Surface Ply Partially Peeled

laminates, the fracture toughness at the maximum load of the $[0/\pm 45]_{ns}$ laminate increases initially with increasing laminate thickness and then asymptotically approaches a plateau value of approximately $40 \text{ ksi}\sqrt{\text{in}}$ ($1390 \text{ MPa}\sqrt{\text{mm}}$). Fracture toughness as a function of laminate thickness is shown in Figure 5.33 for $\frac{2a}{W} = 0.5$. There is virtually no difference in the fracture of the laminates at 30 plies and thicker. Fracture toughness as a function of crack length was a test variable at laminate thicknesses of 6 plies and 90 plies. Fracture toughness at $\frac{2a}{W}$ values of 0.25, 0.375, 0.50 and 0.625 are presented in Figure 5.34. As shown in Figure 5.33, the fracture toughness of the 90 ply laminate is higher than the fracture toughness of the 6 ply laminate. Fracture toughness is relatively independent of crack size for both the 6 and 90 ply laminates. (Fracture toughness at $\frac{2a}{W} = 0.25$ for the 90 ply specimen is not available because one 90 ply panel was layed up incorrectly.) In addition to the differences in fracture toughness, the type of damage and mode of final fracture of the 6 ply laminate is entirely different from those of the thicker laminates. These differences are described in detail in the following paragraphs which document the damage examinations.

A comparison of the load versus COD records of the thin and thick laminates provides some insight into the role subcritical damage plays in the final fracture. Figure 5.35 shows the records for a typical 6, 60 and 120 ply specimen. Notice that the COD scales are the same in each plot but the load scales are different. There is one obvious difference between these load records and those of the $[0/\pm 45/90]_{ns}$ laminates shown in Figure 5.7. The first discontinuity in the load record of the $[0/\pm 45]_s$ laminate occurs at a much higher percentage of the failure load. This implies that the subcritical damage that forms

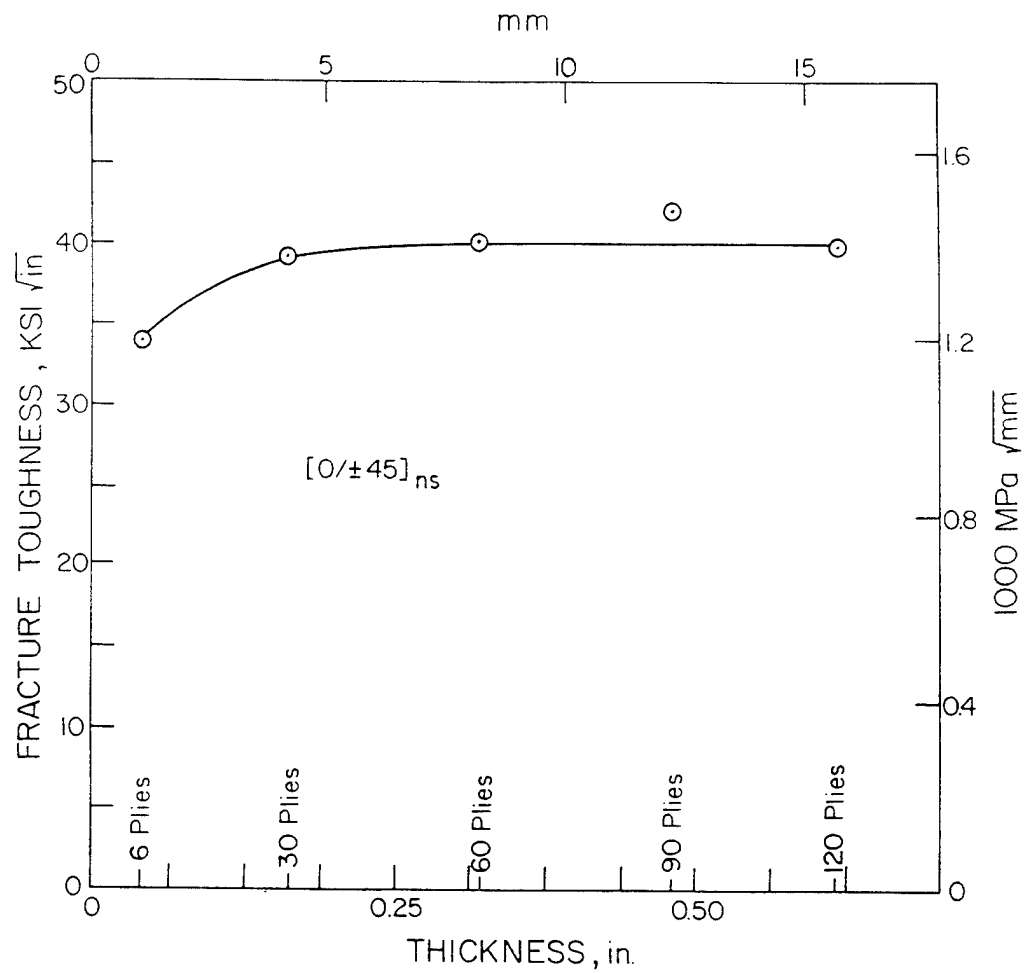


Figure 5.33 Fracture Toughness Versus Laminate Thickness for the $[0/\pm 45]_{ns}$ Laminate (Center-Cracked Tension Specimen)

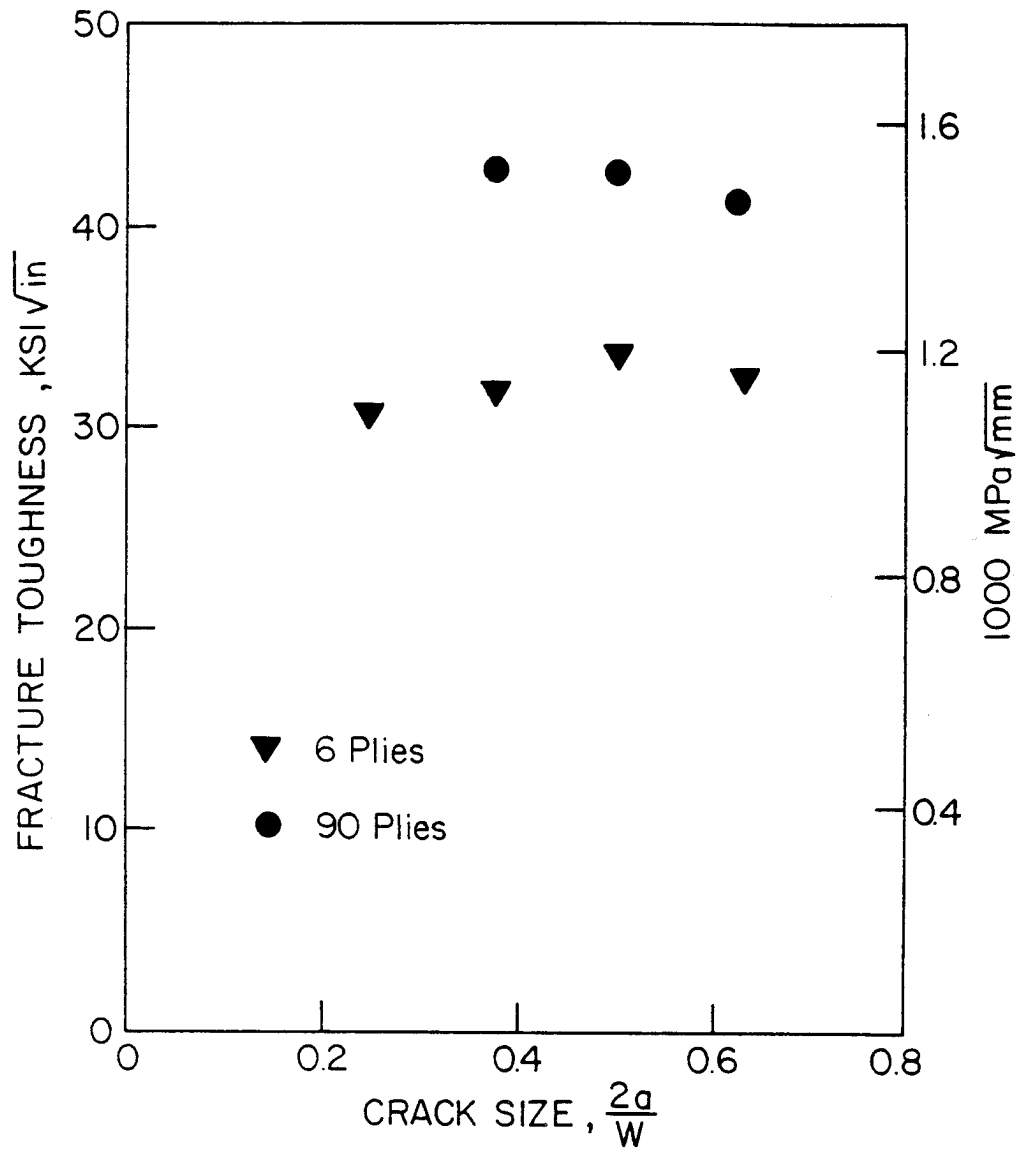


Figure 5.34 Fracture Toughness as a Function of $\frac{2a}{W}$ for the $[0/\pm 45]_{ns}$ Laminates (Center-Cracked Tension Specimen)

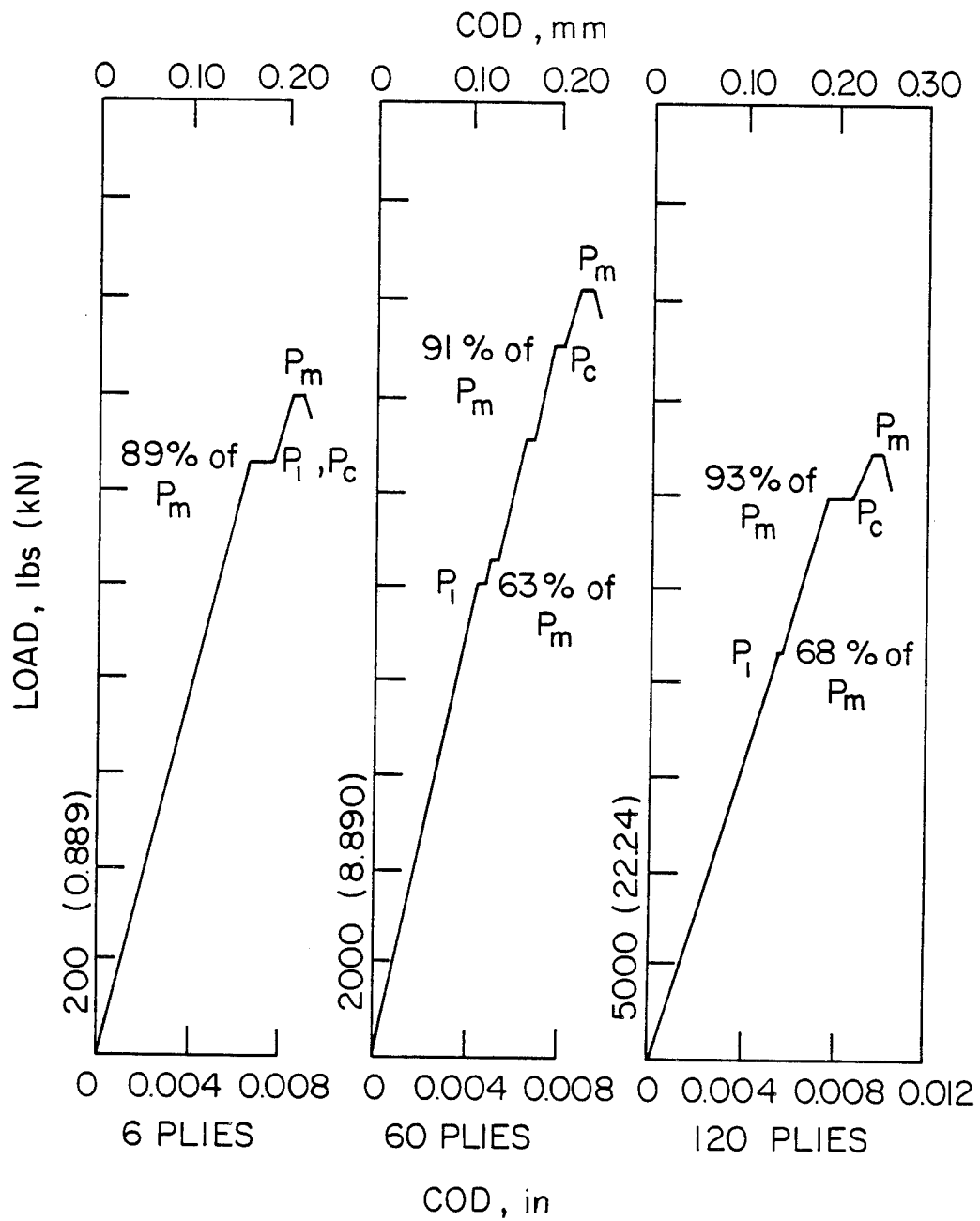


Figure 5.35 Comparison of Typical Load Versus COD Records for the 6, 60 and 120 Ply $[0/\pm 45]_{ns}$ Laminates (Center-Cracked Tension Specimen)

at the crack tip in the $[0/\pm 45]_S$ laminate did not have the same blunting or crack growth resistance effect as did the subcritical damage in the $[0/\pm 45/90]_S$ or $[0/90]_{2S}$ thin laminates.

The size of the damage zone in various thicknesses of $[0/\pm 45]_{nS}$ and $[0/\pm 45/90]_{nS}$ laminates are given in Table 5.8. The size of the damage was obtained by measuring the diameter of a circle surrounding the crack tip damage shown in x-ray examinations at various intermediate loads. The 6 ply specimen at $\frac{2a}{W} = 0.375$ and the 60 ply specimen at $\frac{2a}{W} = 0.50$ provide a good comparison because x-rays were taken at two comparable intermediate load levels for each specimen. It is obvious that the damage zone size in the 60 ply specimen is greater than the damage zone size in the 6 ply specimen at both 60% and 89% of the maximum (failing) load. By comparing the damage of the $[0/\pm 45]_S$ laminate to the damage in the $[0/\pm 45/90]_S$ at comparable load levels, it is obvious that the damage in the 6 ply $[0/\pm 45]_S$ laminate is less extensive. However, at 120 plies the size of the damage zone at about 92% of the specimen failing load is about the same for both the laminate types. Assuming that the subcritical damage zone at the crack tip has some analogy to the plastic zone at the crack tip of an isotropic metal, then larger subcritical damage zones provide higher crack growth resistance and a correspondingly higher fracture toughness.

An x-ray of the damage in the 6 ply specimen selected for the deply study is shown in Figure 5.36. The deply results, Figure 5.37, show the damage to consist of matrix cracks parallel to the fibers in each ply, delaminations at the $0/+45$ and $45/-45$ interfaces, and a line of fiber breaks at 45° to the starter notch in the outside 0° plies. Furthermore, the line of fiber breaks in the 0° plies and the matrix cracks in

Table 5.8 Crack Tip Damage Zone Size

Laminate Type	Number of Plies	Crack Size $\frac{2a}{W}$	Percent of Max load	Damage Zone Size in.(mm)	Comment
[0/±45/90]	8	0.50	77%	0.160"(4.06)	De ply
	8	0.50	85%	0.430"(10.9)	
	120	0.50	91%	0.110"(2.79)	De ply
[0/±45]	6	0.25	82%	0.067"(1.70)	
	6	0.375	63% 93%	0.023"(0.58) 0.115"(2.92)	
	6	0.50	80%	0.070"(1.78)	
	6	0.50	83%	0.085"(2.16)	De ply
	60	0.50	60% 89%	0.091"(2.31) 0.356"(9.04)	
	120	0.50	92%	0.192"(4.88)	De ply

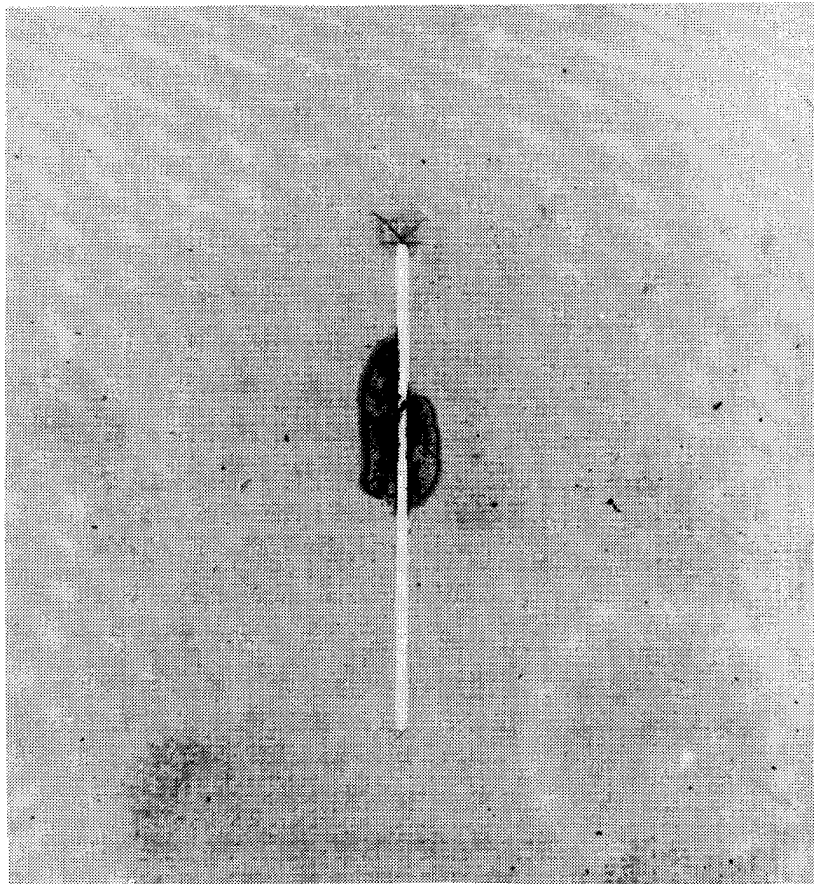


Figure 5.36 X-ray Radiograph of the $[0/\pm 45]_s$ Specimen Before Deploy at 83% of Average Failing Load (Center-Cracked Tension Specimen)

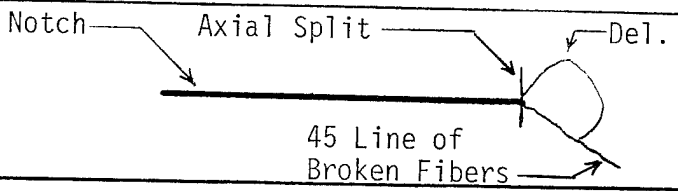
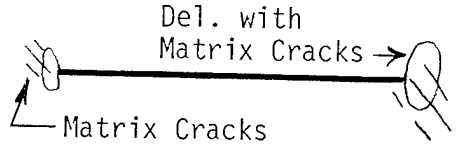



Outside 0 Ply 0/+45 Interface	 <p>Notch</p> <p>Axial Split</p> <p>Del.</p> <p>45 Line of Broken Fibers</p>
+45 Ply +45/-45 Interface	 <p>Del. with Matrix Cracks</p> <p>Matrix Cracks</p>
Midplane 2@-45 -45/+45 Interface	
+45 Ply +45/0 Interface	
Outside 0 Ply +45/0 Interface	

Figure 5.37 Documentation of the Through-the-Thickness Damage in the $[0/\pm 45]_s$ Specimen by Deply at 83% of Average Failing Load (Not Drawn to Scale), (Center-Cracked Tension Specimen)

the $\pm 45^\circ$ plies extend beyond the delamination regions at the crack tip. The final fracture of the typical 6 ply specimens, regardless of starter crack size, shown in Figure 5.38, is not self-similar (collinear with the starter notch). The final fracture surface is an extension of the damage seen in the deply study. The 0° outer plies fail by broken fibers extending from the starter notch tip to the specimen edge parallel to the fibers in the adjacent $+45^\circ$ ply. The $+45^\circ$ ply failed by matrix splitting. The two interior -45° plies delaminated from the adjacent $+45^\circ$ plies and also failed by matrix splitting. (There were essentially no fiber breaks in the $+45^\circ$ plies of the 6 ply laminate.) These examinations suggest the following laminate failure mechanism: Fibers in the surface 0° plies break along a line paralleling matrix splitting in the adjacent $+45^\circ$ plies. The $+45^\circ$ ply delaminates from the adjacent -45° ply thus uncoupling the two outside 0° , $+45^\circ$ plies at each surface from the two inside -45° plies. The strength of the laminate is then determined by the remaining intact 0° fibers. Once the uncoupling occurs, there is little crack growth resistance available so final fracture follows shortly thereafter.

The damage at intermediate loads and the final fracture of the 120 ply $[0/\pm 45]_{ns}$ specimens are entirely different from those of the 6 ply specimen. The x-ray of the crack tip damage in the 120 ply specimen is shown in Figure 5.39 and the results of the deply examination are documented in Figure 5.40. At both surfaces of the 120 ply specimen the damage is exactly like that of the 6 ply specimen. Matrix cracks occur parallel to the fibers in each ply. Delaminations are present at the $0/+45$ and $+45/-45$ interfaces. A line of fiber breaks in the outside 0° ply extends from the starter notch tip in a $+45^\circ$ direction. The size of

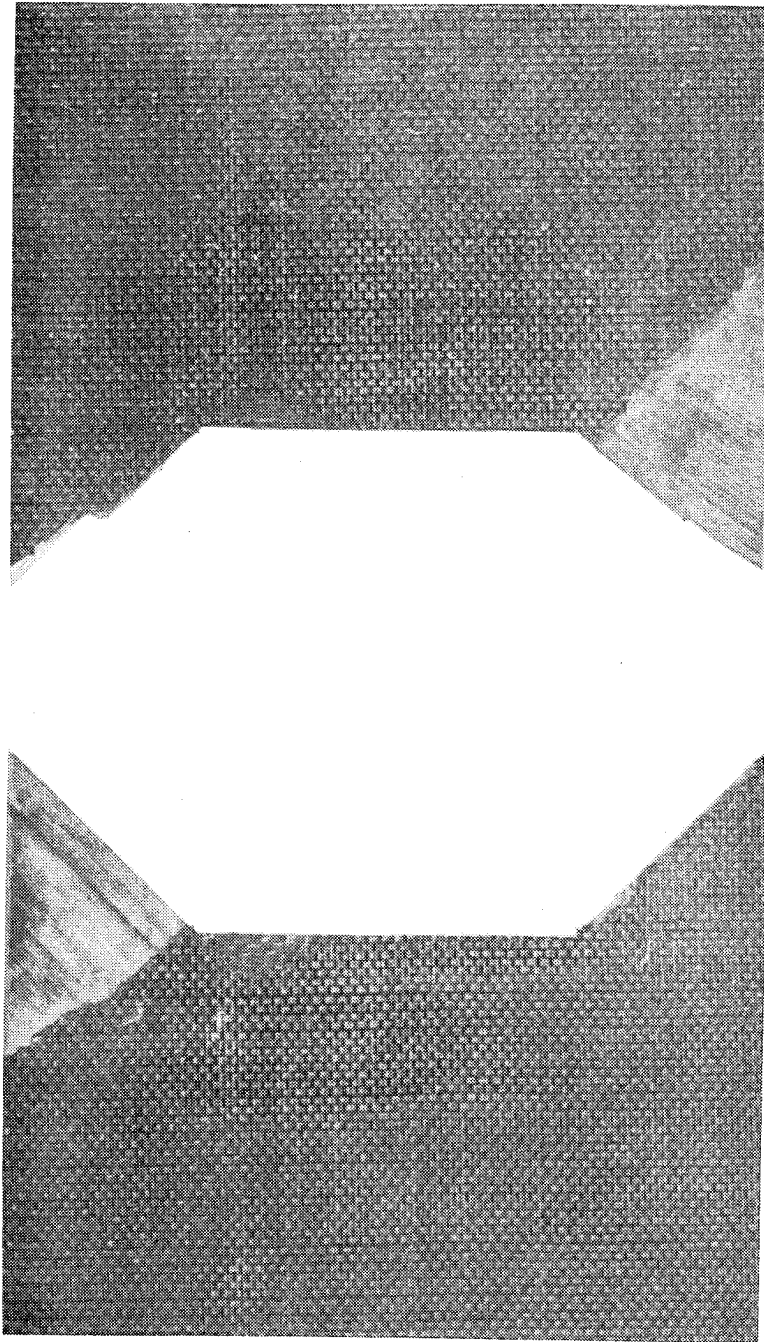


Figure 5.38 Photograph of a Fractured $[0/\pm 45]_S$ Specimen

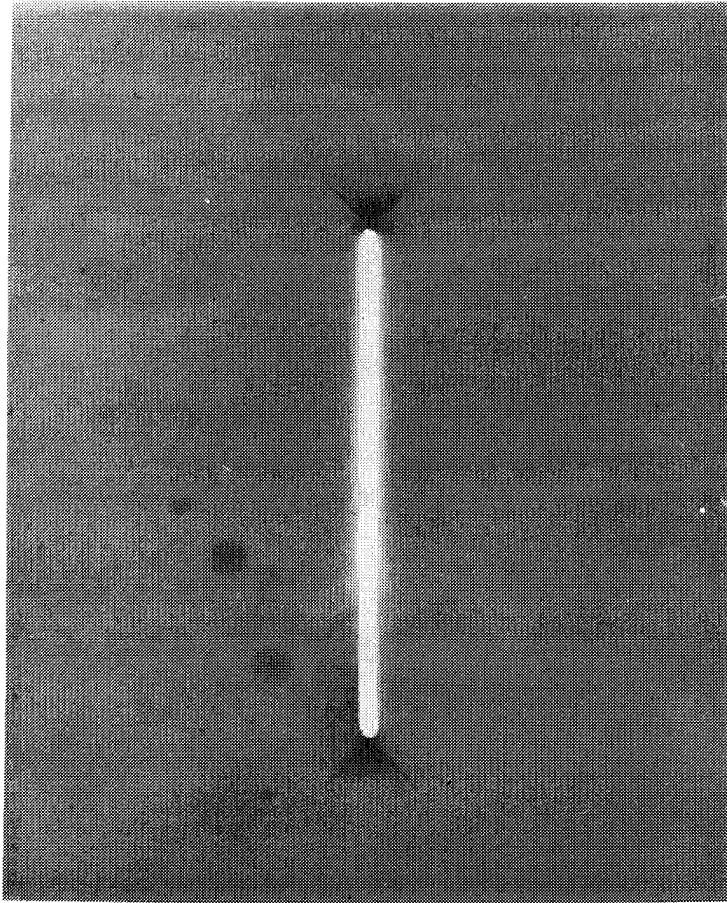
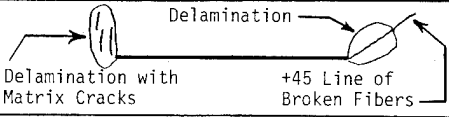

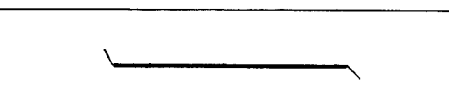
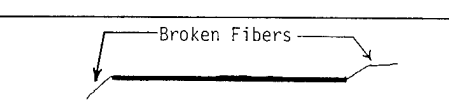
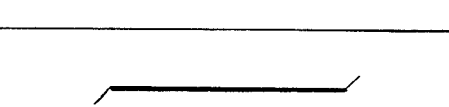
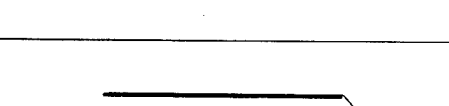
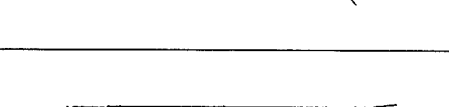
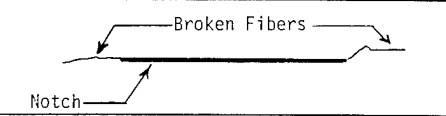
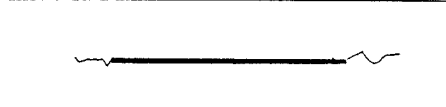
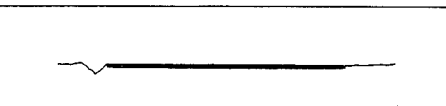
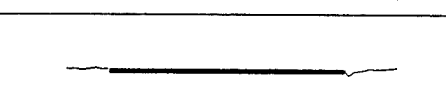
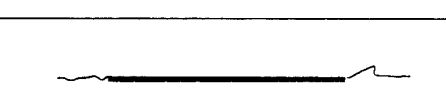
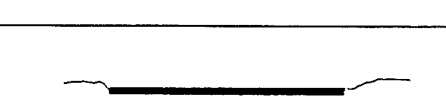


Figure 5.39 X-ray Radiograph of the 120 Ply $[0/\pm 45]_{ns}$ Specimen Before
Deply at 92% of Average Failing Load (Center-Cracked
Tension Specimen)

Outside 0 Ply 0/+45 Interface	 <p>Delamination with Matrix Cracks</p> <p>Delamination</p> <p>+45 Line of Broken Fibers</p>
#2 +45 Ply +45/-45 Interface	 <p>Notch</p>
#3 -45 Ply -45/0 Interface	
#4 0 Ply 0/+45 Interface	 <p>Broken Fibers</p>
#5 +45 Ply +45/-45 Interface	
#6 -45 Ply -45/0 Interface	
#7 0 Ply 0/+45 Interface	

a. First 7 Plies from the Surface

#43 0 Ply 0/+45 Interface	 <p>Broken Fibers</p> <p>Notch</p>
#46 0 Ply 0/+45 Interface	
#49 0 Ply 0/+45 Interface	
#52 0 Ply 0/+45 Interface	
#55 0 Ply 0/+45 Interface	
#58 0 Ply 0/+45 Interface	

b. Interior 6 0 Plies from the Midplane

Figure 5.40 Documentation of the Through-the-Thickness Damage in the $(0/\pm 45)_{20s}$ Specimen by Deply at 92% of Average Failing Load (Not Drawn to Scale), (Center-Cracked Tension Specimen)

the damage zone in this surface "boundary layer" is about 0.192" (4.9 mm). Outside of the boundary layer the damage is strictly in the form of matrix cracking and fiber breaks in the 0° plies. The 0° plies are constrained by a $+45^\circ$ ply on one surface and a -45° ply on the other surface. The fiber breaks in a 0° ply appear to be equally influenced by the adjacent 45° plies and extend in a line collinear with the starter notch. (This was the same behavior exhibited by the $[0/\pm 45/90]_{ns}$ thick laminates.) In the interior of the specimen the fiber breaks in the 0° plies are uniform in direction and length, about 0.050" (1.27 mm) long and slightly longer at one crack tip than the other. This is tantamount to a subcritical extension of the starter notch in a self-similar manner. The final fracture surfaces of the thick specimens bear this out. The fracture surface of the 120 ply specimens, Figure 5.41, are relatively smooth and directly collinear with the original starter notch. As was the case with the 120 ply $[0/\pm 45/90]_{ns}$ specimens, the 120 ply $[0/\pm 45]_{ns}$ specimens exhibit "shear lips" where the 0° fibers fracture in a $+45^\circ$ direction and the delaminations in the boundary layer are visible. Because of the absence of delaminations in the interior of the 120 ply specimen and the self-similar fracture, apparently the uncoupling mechanism of the 6 ply specimen does not occur in the 120 ply specimen. It seems intuitive, then, that more energy would be required for this self-similar fracture in which fibers are broken in each ply than would be required to fracture the 6 ply specimen exhibiting the ply uncoupling mechanism. Although based on somewhat limited examinations, this uncoupling mechanism is believed to be the primary reason the fracture toughness of the 6 ply laminate is lower than that of the thick laminates.

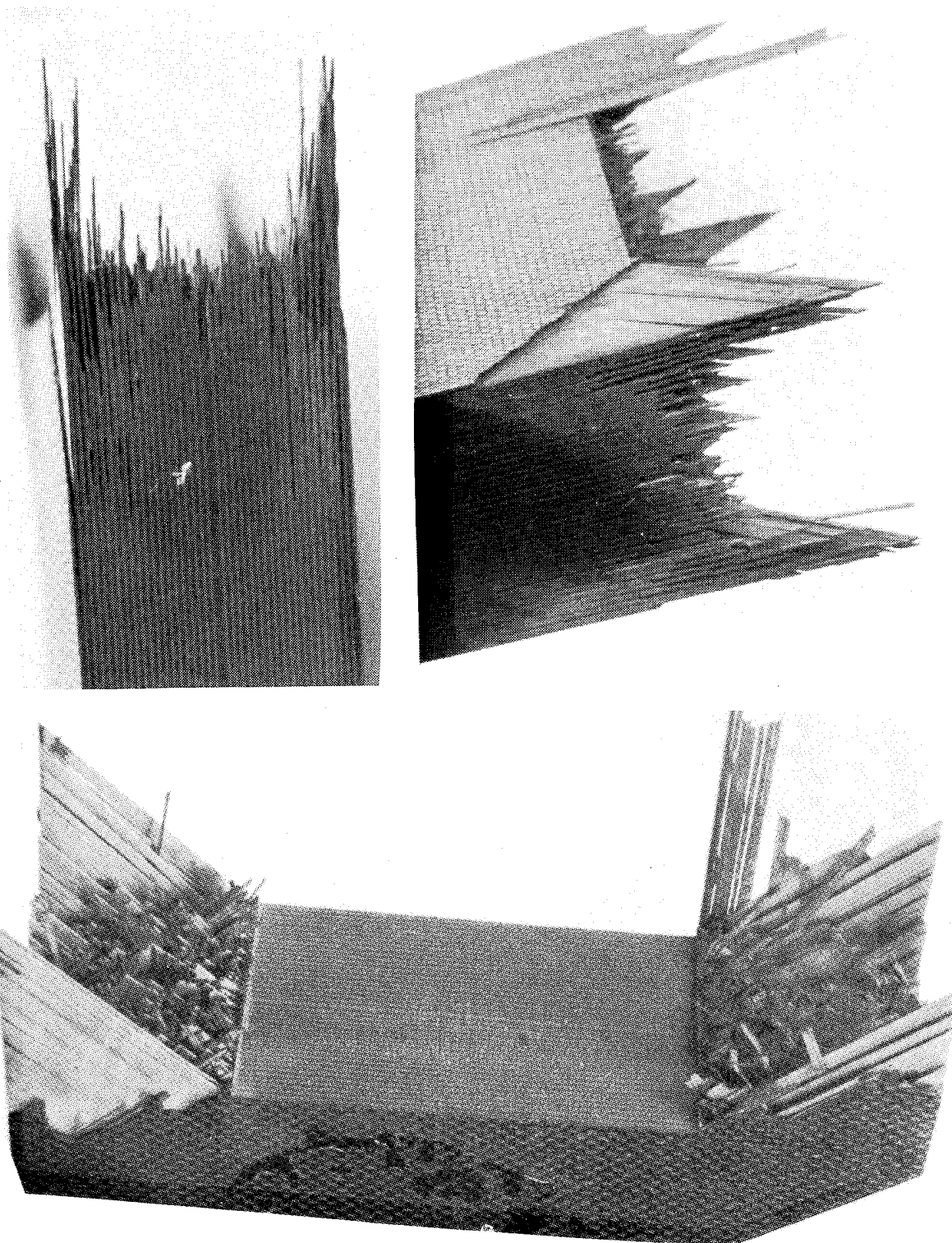


Figure 5.41 Photographs of the Fracture Surface of Several 120 Ply $[0/\pm 45]_{ns}$ Specimens

5.4 Comparison of the Test Results from the Center-Cracked Tension, Compact Tension and Three-Point Bend Specimen Types

For the past ten years the compact tension and three point bend specimens have been accepted by the ASTM [2,39] as the standard specimens for plane strain fracture toughness testing. These two specimens represent the same mode of fracture and same crack-tip stress state as does the center-cracked tension specimen. However, they require substantially less material than does the center-cracked tension specimen and they fail at much lower test loads. The gripping of thick specimens of a laminated composite is a major test problem that can be avoided by testing the three-point bend or compact tension specimens. But an even more important issue is the comparison of the test results obtained from the three specimen configurations. For fracture toughness to be used as a material property in design applications the three specimen configurations must yield similar results. As presented in the literature review of Chapter 2, earlier limited investigations have at times yielded results that indicate that the fracture toughness of the three specimen types may be different and even the fracture modes may differ. In this study the objective was to compare results from the three specimen configurations for the thicker laminates (60-120 plies). This avoided the out-of-plane deformation and local point load deformation problems associated with testing three point bend and compact tension specimens prepared from thin laminates. The test results are described below.

The fracture test procedure was described in Section 4.1. However, the compact tension and three-point bend specimens present several unique testing problems that must be addressed. The method of loading the compact tension specimen is through loading (dowel) pins. (The

specimen loading holes are shown in Figures 3.1 and 4.2.) The pin loading concentrates the load over a localized region which can lead to localized damage and distortion of the specimen in the loading region. Careful examination of the thick specimens of this study did not indicate that this was a problem. No significant localized damage occurred. Also thin compact tension specimens can "buckle" out-of-plane under the application of load. Again this was not observed to occur in the thick specimens of this study.

Local deformation and damage due to brinelling or crushing has also been observed to occur at the load and support points of the three point bend specimen. For the subject tests the radius of the loading ram (Figure 4.3) was 0.75 in. (19 mm) while the diameter of the supporting pins was 1.0 in. (25.4 mm). Careful examination of the contacting regions of failed specimens did not reveal significant damage. Finally, for fixed loading pins significant friction between the specimen and support may develop and can effect the test results. This problem was minimized by allowing the support pins to move outward during the load application. The rubber bands shown in Figure 4.3 insure the same initial support position for the specimen but are flexible enough to allow the outward support movement.

The load versus COD records of the three-point bend and compact tension specimens differ, characteristically, from the load-COD record of the center-cracked tension specimen. Typical load-COD records of the three specimen types are compared in Figure 5.42. When the maximum load in the center-cracked tension specimen is reached, the specimen fails catastrophically--splitting into two pieces. The compact tension and three-point bend specimens do not fail catastrophically. Significant

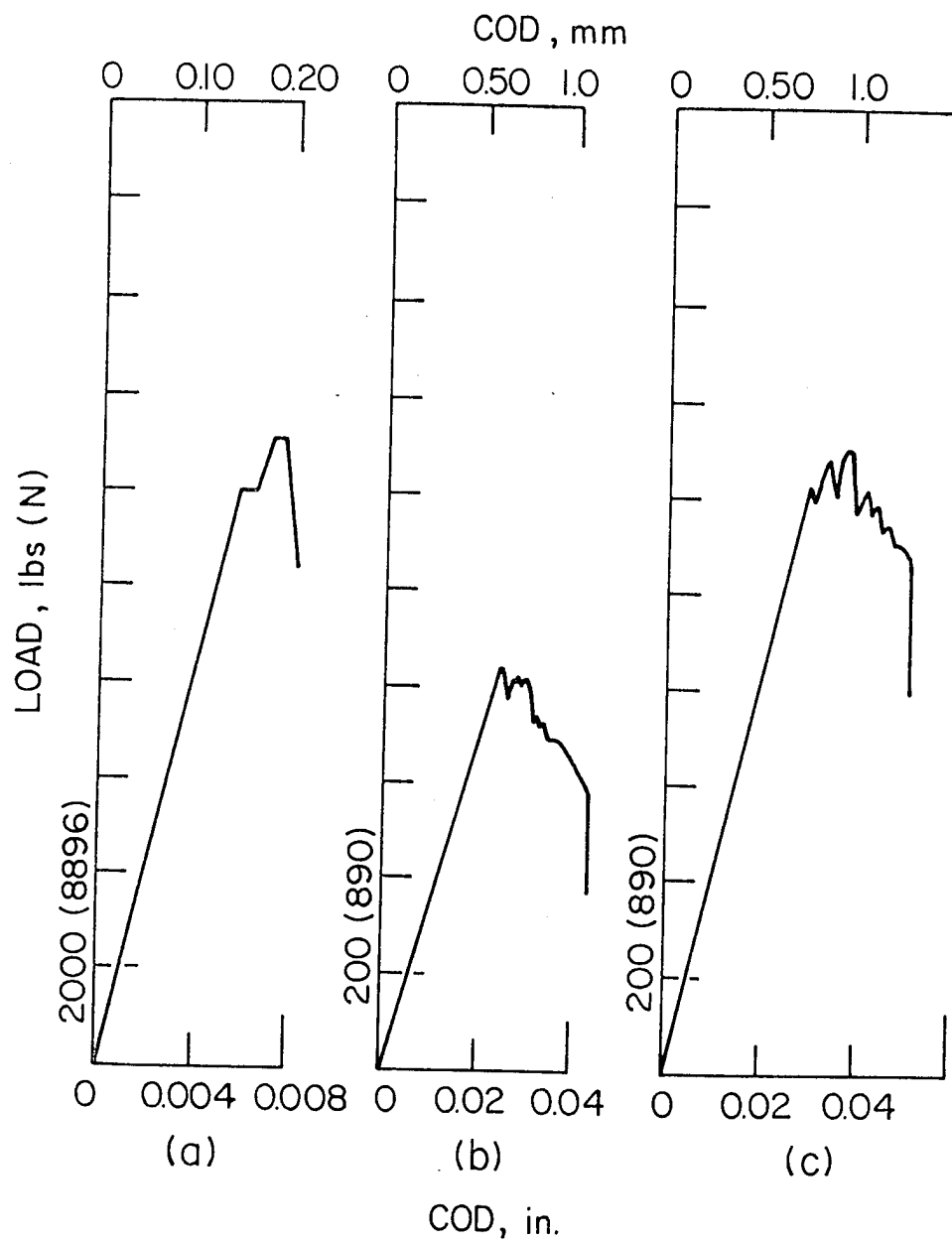


Figure 5.42 Comparison of Typical Load Versus COD for the $[0/\pm 45/90]_{8s}$

- (a) Center-Cracked Tension Specimen
- (b) Three Point Bend Specimen
- (c) Compact Tension Specimen

crack extension occurs, but the compression zone at the specimen edge, opposite the advancing crack front, causes crack arrest to occur. The first load reduction exhibited by the load-COD records of the compact tension and three point bend specimens is analogous to the large COD discontinuities in the load record of the center-cracked tension specimens. For example, the x-ray photographs of Figures 5.43 and 5.44 illustrate the similarity of the crack-tip damage of the three specimen types for the $[0/90]_{ns}$ and $[0/\pm 45/90]_{ns}$ laminates, respectively, at 64 plies. (The $[0/\pm 45]_{ns}$ laminate will be discussed later.) The damage examination in the center-cracked tension specimens were taken after the large COD discontinuity (P_c) just before the maximum load. The damage examination in the compact tension and three-point bend specimens were taken just after the first load reduction. It should be noted that the first load reduction was frequently the maximum test load.

The fracture toughness of each specimen type was computed by the finite element stress analysis method described in sections 4.4 and 5.1. The test results are shown in Figures 5.45-5.47 for the $[0/\pm 45/90]_{ns}$, $[0/90]_{ns}$, and the $[0/\pm 45]_{ns}$ laminates, respectively. Fracture toughness values from the three specimen configurations are compared at 64, 96 and 120 plies for each laminate type at a crack length-to-width ratio of 0.50. Each experimental value corresponds to the average of the four replicate tests. The three-point bend and compact tension specimens exhibited very repeatable results. The maximum deviation of fracture toughness from the mean value for a given set of four tests varied between 1% and 4%.

The three specimen configurations yielded very similar results for the $[0/\pm 45/90]_{ns}$ and $[0/90]_{ns}$ laminates. The maximum difference in

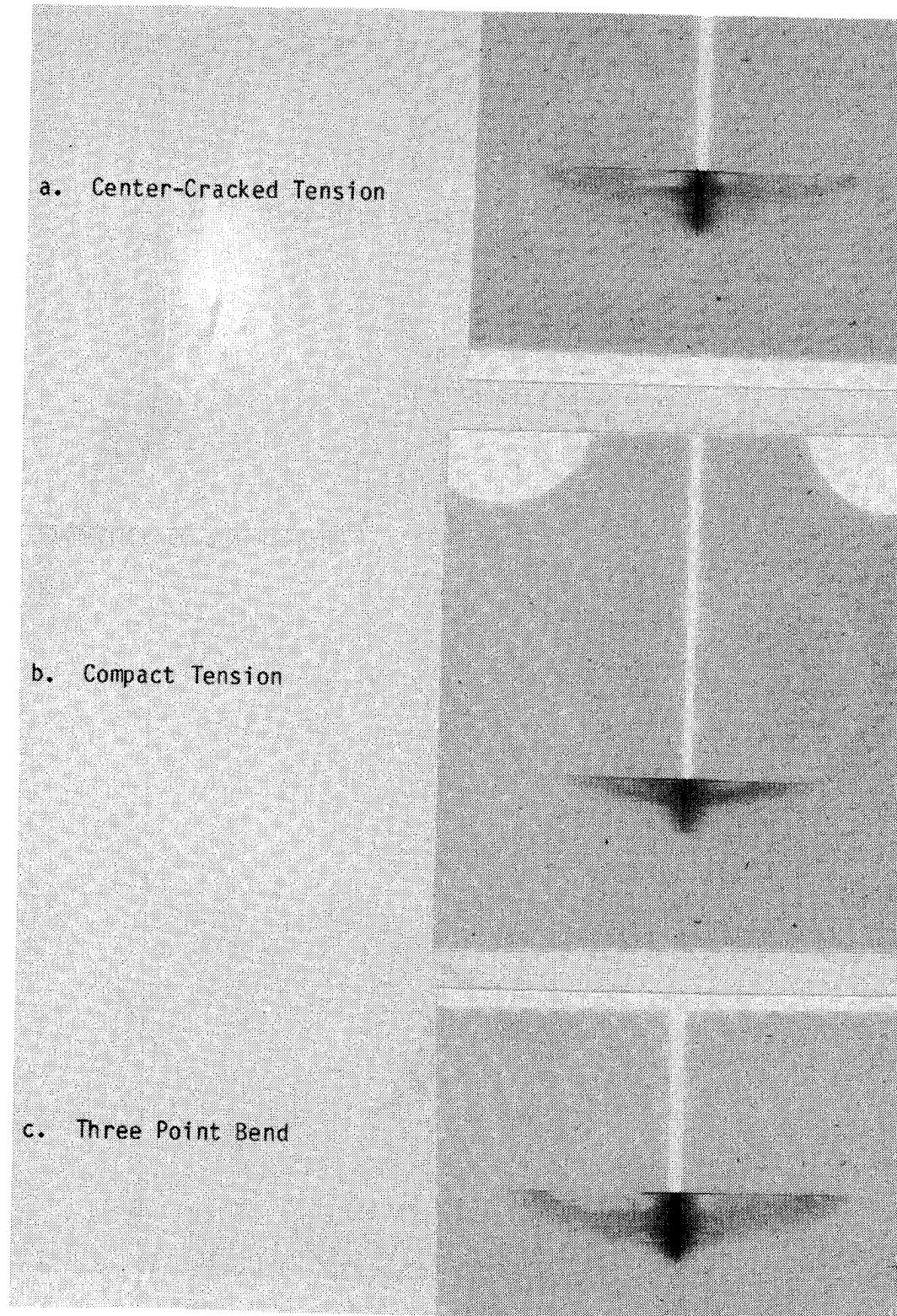


Figure 5.43 Comparison of Damage at the First COD Discontinuity for the $[0/90]_{ns}$ Laminate at 64 Plies

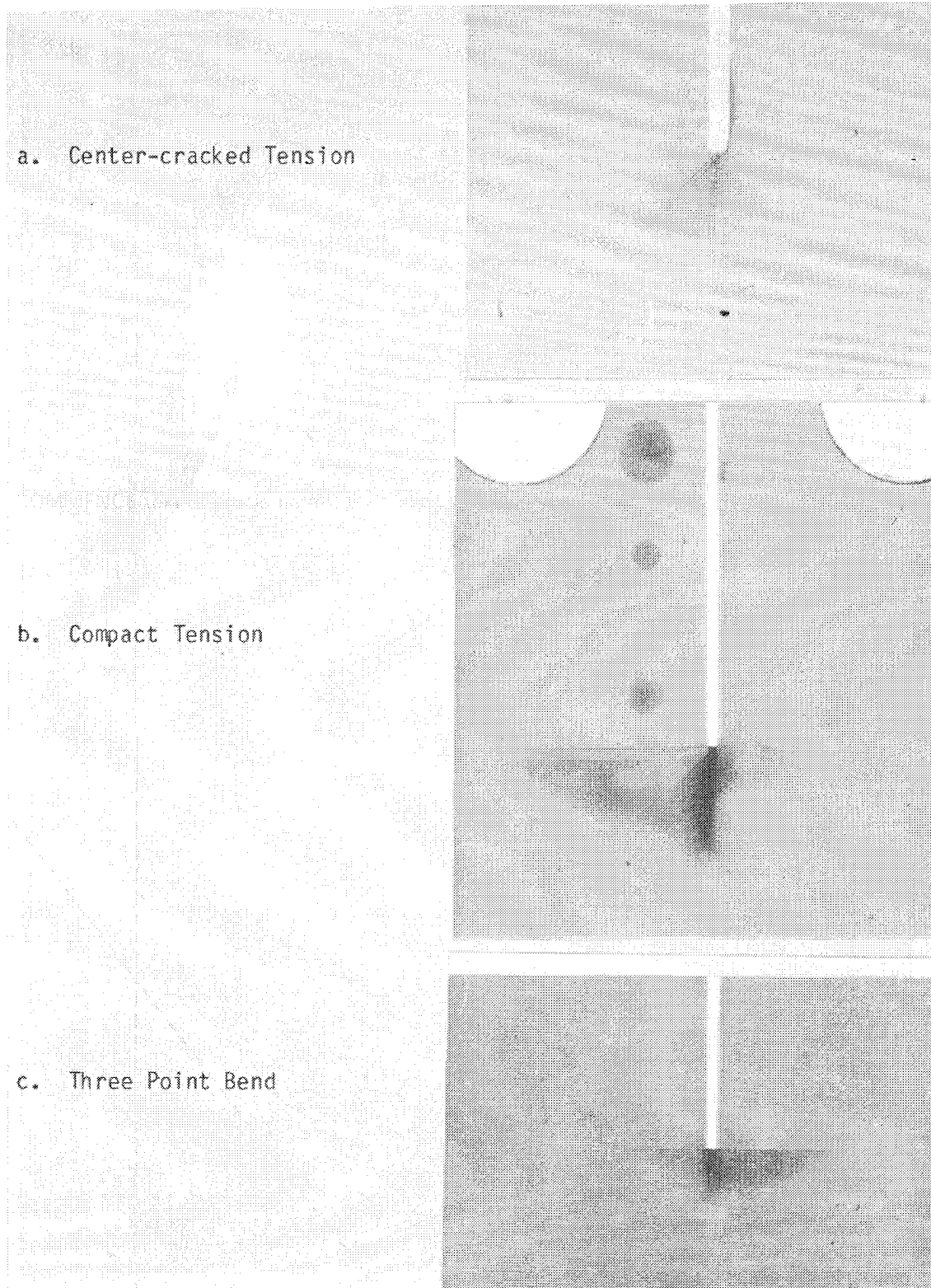


Figure 5.44 Comparison of Damage at the First COD Discontinuity for the $[0/\pm 45/90]_{ns}$ Laminate at 64 Plies

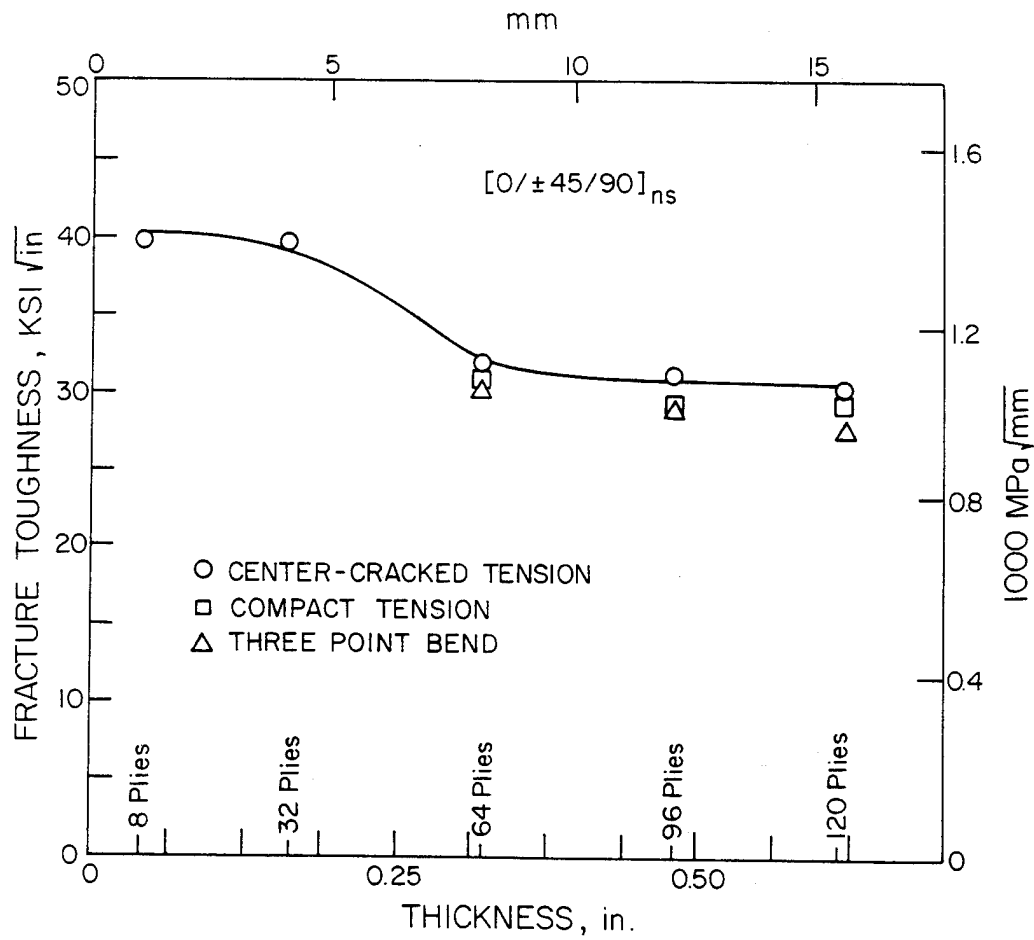


Figure 5.45 Comparison of the Fracture Toughness of the $[0/\pm 45/90]_{ns}$ Laminate for the Center-Cracked Tension, Compact Tension and the Three Point Bend Specimens; $2a/W = 0.50$.

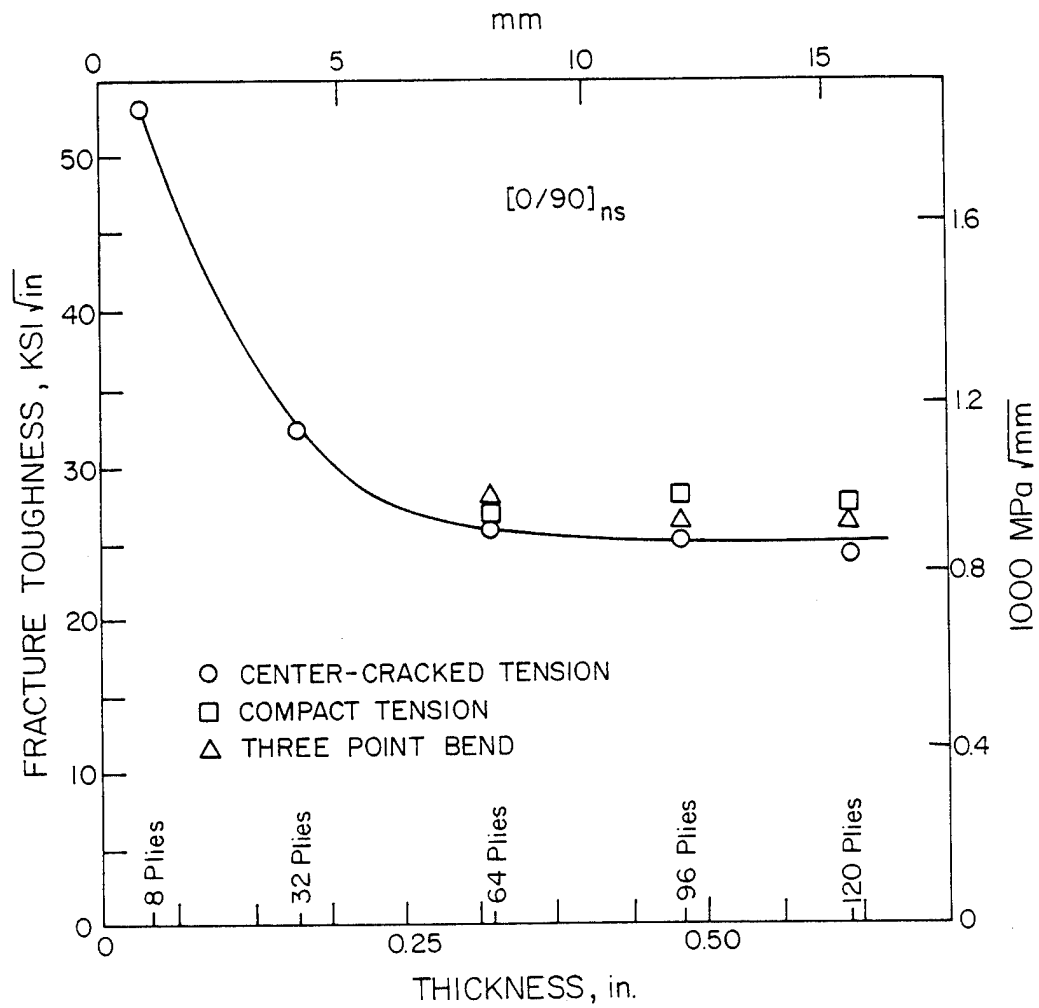


Figure 5.46 Comparison of the Fracture Toughness of the $[0/90]_{ns}$ Laminate for the Center-Cracked Tension, Compact Tension and the Three Point Bend Specimens; $2a/W = 0.50$.

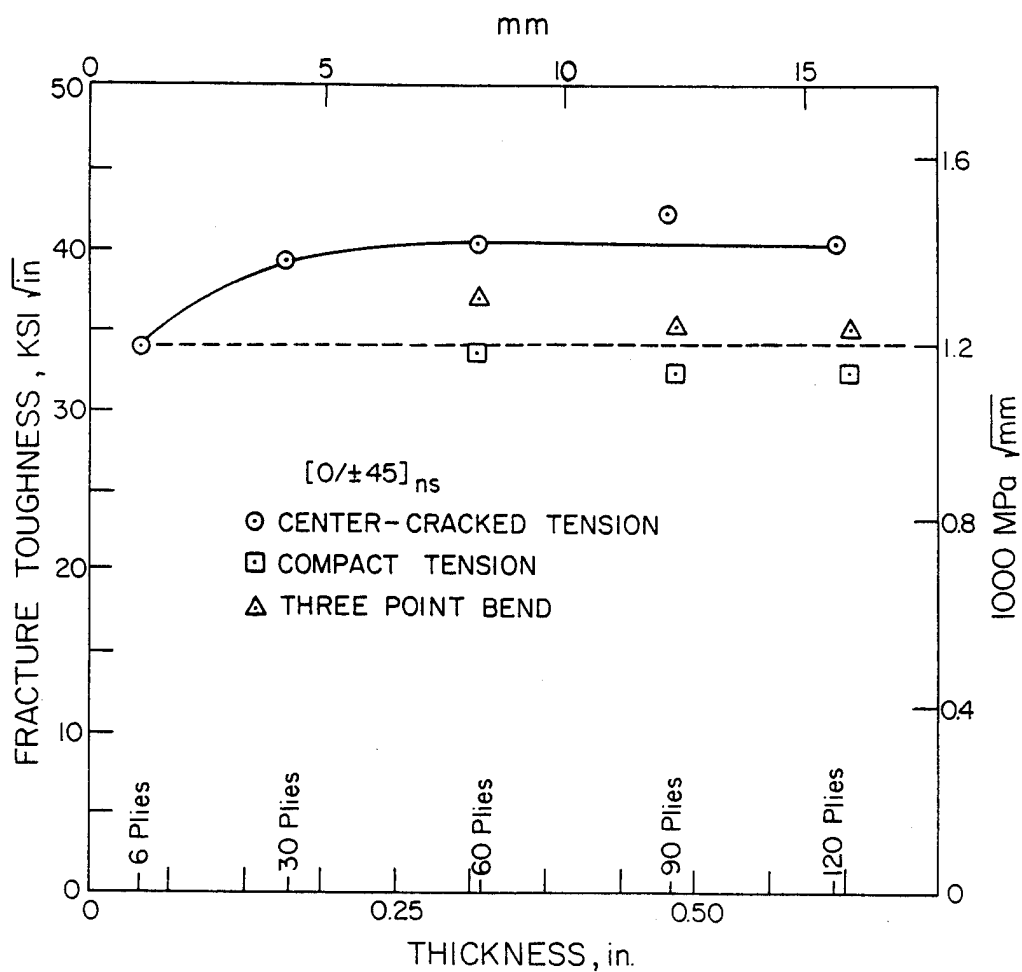


Figure 5.47 Comparison of the Fracture Toughness of the [0/±45]_{ns} Laminate for the Center-Cracked Tension, Compact Tension and the Three Point Bend Specimens; $2a/W = 0.50$.

fracture toughness values occurred at 120 plies for both laminate types. For the $[0/\pm 45/90]_{ns}$ laminate, the largest difference in fracture toughness between specimen types was 10%. For the $[0/90]_{ns}$ laminate the largest difference was 12%. As the comparisons of the x-ray photographs of damage shown in Figures 5.43 and 5.44 illustrate, the formation of damage in the three specimen types is similar in magnitude and type. Also much of the damage seen in the x-ray examinations is confined to the surface boundary layers in all three specimen types. (This was illustrated in Figure 5.32 and discussed in Article 5.3.2.) Furthermore, macroscopic crack extension was collinear with the original starter notch in each specimen type.

Test results of the $[0/\pm 45]_{ns}$ laminate for the three specimen configurations are somewhat different. The fracture toughness values obtained from the compact tension and the three point bend specimens are very close, as shown in Figure 5.47. (They differ by 6% at 120 plies.) However, their average values are about 15% below the fracture toughness of the center-cracked tension specimen. It appears that the compact tension and three-point bend specimens fall along one plateau at about $34 \text{ ksi}\sqrt{\text{in}}$ ($1182 \text{ MPa}\sqrt{\text{mm}}$) while the center-cracked tension specimens fall along another plateau at about $40 \text{ ksi}\sqrt{\text{in}}$ ($1390 \text{ MPa}\sqrt{\text{mm}}$).

Historically in the case of metals, the plane strain fracture toughness determined from compact tension or three-point bend specimens is compared to the "pop-in" fracture toughness exhibited by center-cracked tension specimens. Perhaps it is more appropriate to compare the fracture toughness values of the compact tension and three-point bend specimens to the values of stress intensity factor at the critical load of the center-cracked tension specimens. (There are differences in

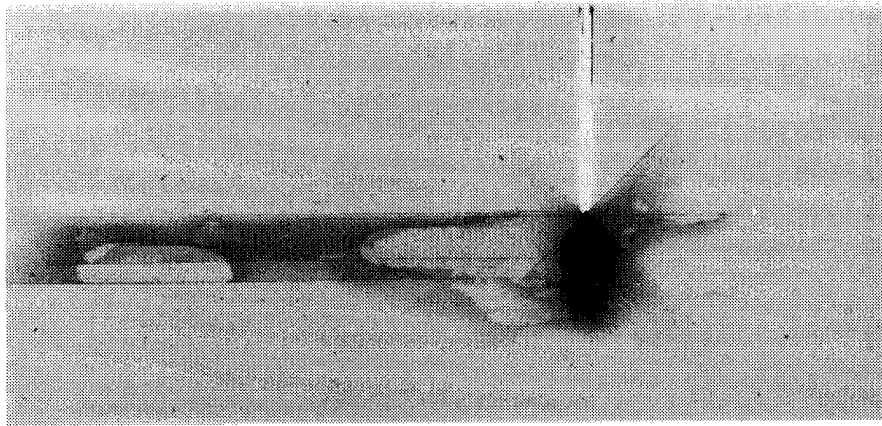
the specimen behavior beyond the critical load of the center-cracked tension specimens and after the first load reduction of the other two specimen configurations. These differences may give rise to discrepancies in the computed values of fracture toughness if the maximum load is used.) If the fracture toughness of the compact tension and three-point bend specimens (at the maximum load) are compared to the stress-intensity factor of the center-cracked tension specimens (at the critical load), the data from the three specimen configurations would coalesce. For example, this comparison can be made easily for the $[0/\pm 45/90]_{ns}$ laminate by comparing the data of Figure 5.10 and Figure 5.45. The difference between the maximum value and the minimum value is 2.0%, 4.3% and 6.0% at 60 plies, 96 plies and 120 plies, respectively. These percent differences are about half those shown in Figure 5.45. Similar results are obtained for the $[0/90]_{ns}$ and $[0/\pm 45]_{ns}$ laminates as well.

It is interesting to note that the fracture toughness of the compact tension and three point bend specimens are the same as the fracture toughness of the 6 ply center-cracked tension specimen, for the $[0/\pm 45]_{ns}$ laminate. This is similar to what Cruse and Osias [9] observed in an earlier investigation. They compared the fracture toughness of a $[0/\pm 45]_s$ graphite/epoxy laminate, with a thickness of 0.070 in. (1.78 mm), obtained by a center-cracked tension specimen to the fracture toughness of a three-point bend specimen with the same stacking sequence but a thickness of 0.363 in. (9.22 mm). The fracture toughness of the two specimens were the same. They reported the K_{IC} value of $36.2 \text{ ksi}\sqrt{\text{in}}$ ($1258 \text{ MPa}\sqrt{\text{mm}}$) for the $[0/\pm 45]_s$ laminate and concluded that there was no thickness effect.

Even though the fracture toughnesses of the $[0/\pm 45]_{ns}$ laminate as measured by the compact tension and three-point bend specimens are similar, the macroscopic crack extension of the two specimens is different. This is illustrated by the comparison of x-ray photographs of damage in typical 64 ply specimens shown in Figures 5.48 and 5.49. Figure 5.48 shows the damage in a three-point bend specimen just after the first load reduction (a) and just after the final load reduction (b) with the outside 0° ply partially peeled away. The heavy dark area represents extensive damage and is collinear with the original starter notch. The delamination regions are not very extensive, so this specimen is failing in a self-similar manner as did the thick center-cracked tension specimens. On the other hand, the macroscopic damage in the compact tension specimen, shown in Figure 5.49, is at a 45° angle to the original starter notch. The top x-ray, Figure 5.49(a), was taken just after the first load reduction and the bottom x-ray, Figure 5.49(b), was taken just after the final load reduction. The damage has clearly progressed at a 45° orientation. For both specimen types, the partial peeling of the outside 0° ply tends to confirm that the delaminations are confined to a surface boundary layer, as was the case with the other two specimen configurations.

The reasons why the fracture toughness of the $[0/\pm 45]_{ns}$ laminate measured by the three-point bend and compact tension specimens are identical in spite of the difference in the direction of crack extension are not known. The overall behavior of the $[0/\pm 45]_{ns}$ laminate warrants further study. One of the planned follow-on research activities includes a thorough investigation of the behavior of the $[0/\pm 45]_{ns}$ laminate and several other similar laminates. This research activity consists of a

(a)



(b)

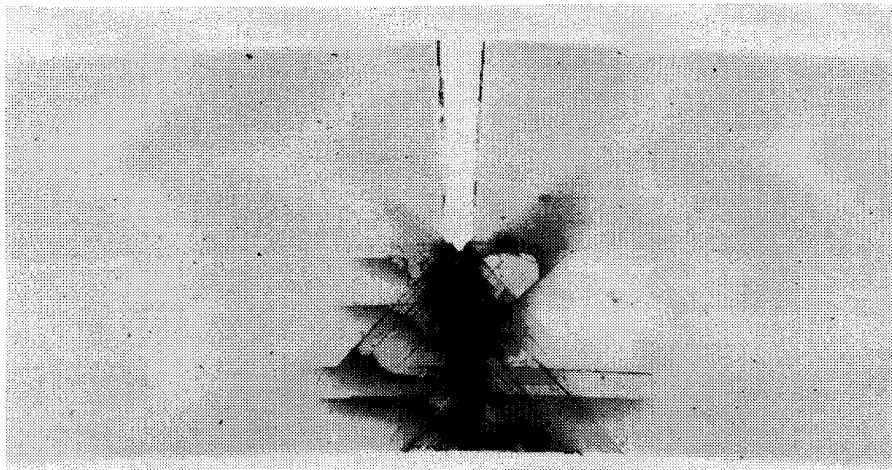


Figure 5.48 Development of Crack Tip Damage in the Three Point Bend Specimen of the $[0/\pm 45]_{ns}$ Laminate
(a) Just After the First Load Reduction,
(b) After the Final Load Reduction

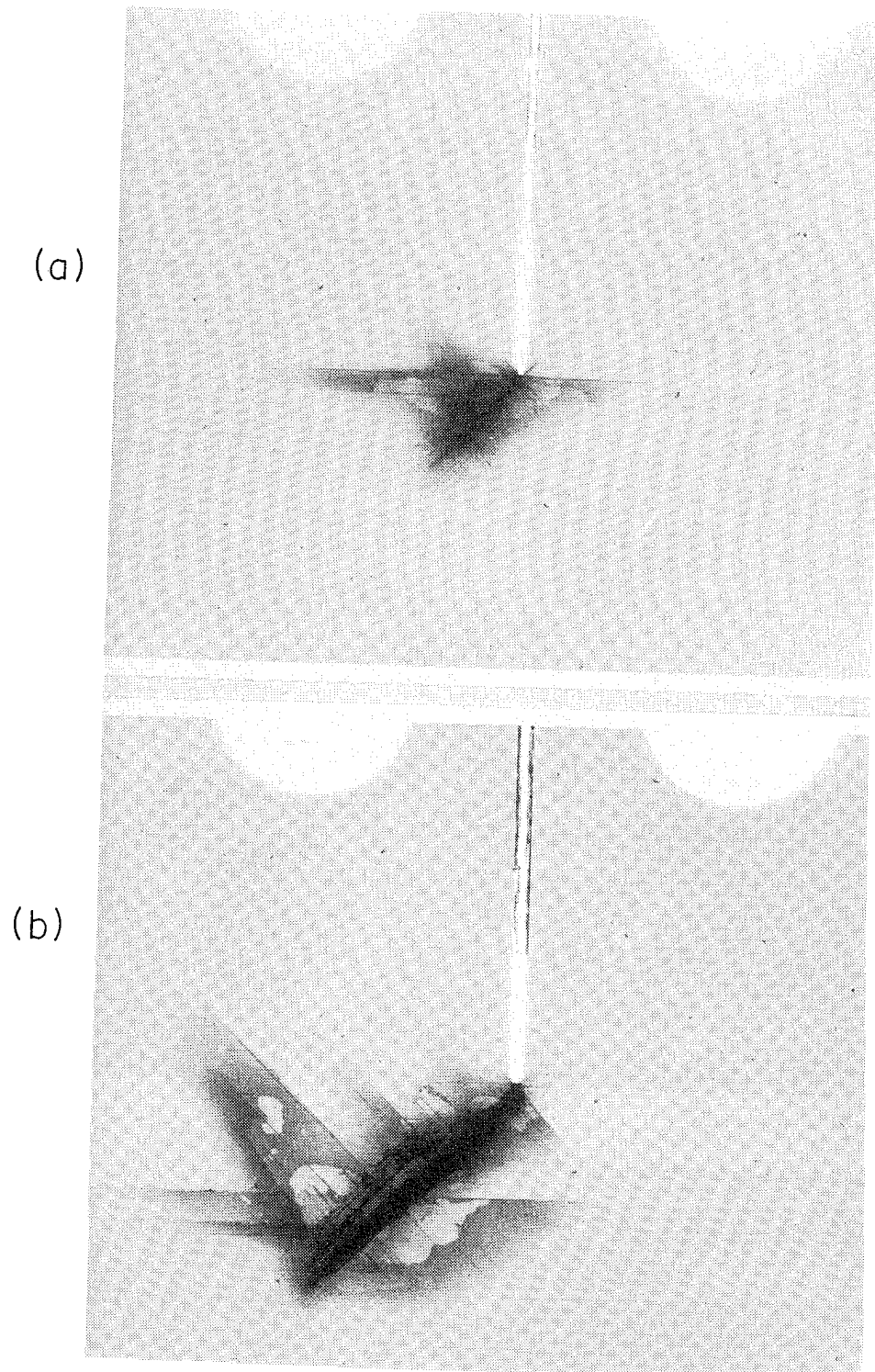


Figure 5.49 Development of Crack Tip Damage in the Compact Tension Specimen of the $[0/\pm 45]_{ns}$ Laminate
(a) Just After the First Load Reduction,
(b) Just After the Final Load Reduction

substantial depth study that will include several thicknesses and all three specimen configurations.

In conclusion, it is interesting to note the dramatic difference in the test loads required to fail the three specimen types. The 120 ply specimens of the $[0/90]_{NS}$ laminate provides a good comparison. A center-cracked tension specimen having a fracture toughness of $25.3 \text{ ksi}\sqrt{\text{in}}$ ($879 \text{ MPa}\sqrt{\text{mm}}$) failed at 21,600 lb (96.1 kN). The failure loads of a comparable compact tension and three point bend specimen, each of which had a fracture toughness of $26.6 \text{ ksi}\sqrt{\text{in}}$ ($924 \text{ MPa}\sqrt{\text{mm}}$), were 2,275 lb (10.1 kN) and 1,520 lb (6.76 kN), respectively. Therefore, for comparable sized specimens an order of magnitude reduction of the maximum test load can be achieved.

5.5 Concluding Comments

Before proceeding with the discussion of the postulated fracture criteria given in Chapter 6, it seems appropriate to conclude this chapter with a few comments concerning the fracture toughness of laminated composites. (The discussion in Chapter 6 will center around the prediction of notched laminate failure strength, determined by the center-cracked tension specimen, rather than fracture toughness.) The usefulness of fracture mechanics and, hence, fracture toughness to describe the failure of notched laminated composites has been a fundamental issue for many years. This is because sharp cracks do not nucleate and grow to critical proportions under fatigue loadings in laminated composites as they do in metals. Even though several of the failure criteria described in Chapter 2 were based on fracture mechanics concepts, notched laminate fracture strength was usually computed rather

than fracture toughness. However, currently there are several practical applications for fracture toughness. One such application is the prediction of the residual strength of laminates following foreign object impacts [40]. As the ability to design damage tolerant structures increases, a variety of structural applications will require thicker laminates. Perhaps these applications will increase the necessity for fracture toughness testing as has been described in this chapter. (As a part of a planned follow-on research activity, the application of the fracture toughness values reported herein to predict the fracture of laminates with part-through surface flaws will be assessed.)

6.0 A CRITICAL ASSESSMENT OF THE APPLICABILITY OF CURRENT POSTULATED FRACTURE MODELS TO THICK LAMINATES

In section 2.1 of the Literature Review a number of failure criteria with associated mathematical models were presented that attempted to predict the fracture of notched laminated composites. In this chapter an assessment of the application of several of these criteria to the prediction of fracture of the thick laminates will be made. Because of the limited development of micromechanical models, only the more widely used macromechanical models will be addressed herein. Fracture predictions will be made using the following failure criteria: the inherent flaw model of Waddoups, Eisenmann and Kaminski [5], the point stress model and average stress model of Whitney and Nuismer [6], the general toughness parameter model of Poe [13] and the Mar-Lin curve fit model [41]. Each model will be briefly described, then used to predict the fracture strength of both thin and thick laminates.

The models described below and all subsequent discussions of this chapter center around the prediction of notched laminate strength. Experimental values of notched laminate strength were determined from the center-cracked tension specimen as described in section 6.1.6. As will be shown later in this chapter, values of notched laminate strength were affected by laminate thickness exactly as was the fracture toughness results of Chapter 5.

6.1 Description of Models

This section provides a description of each failure criteria and the associated mathematical models. Also given are the values of un-notched laminate strength and the method for experimentally computing notched laminate strength.

6.1.1 The Inherent Flaw Model

Waddoups, Eisenmann and Kaminski [5] postulated the existence of a "high intensity energy region" adjacent to the holes and at the tip of notches which could be represented by a characteristic dimension, a , see Figure 6.1. The characteristic dimension was then utilized much like Irwin's plastic zone correction factor for isotropic materials to modify the stress intensity factors and hence the stress distributions near the notch. The stress intensity factor at the notch tip is given by [5]

$$K_I = Y\sigma\sqrt{\pi(L + a)} \quad (1)$$

where Y = finite width correction factor (see article 6.1.6)

σ = applied stress

L = crack half length

and a = size of intense energy region at the crack tip.

By setting $L = 0$ and $\sigma = \sigma_0$ in equation (1) the following expression for a is obtained:

$$a = \frac{L}{\left(\frac{\sigma_0}{Y\sigma_f}\right)^2 - 1} \quad (2)$$

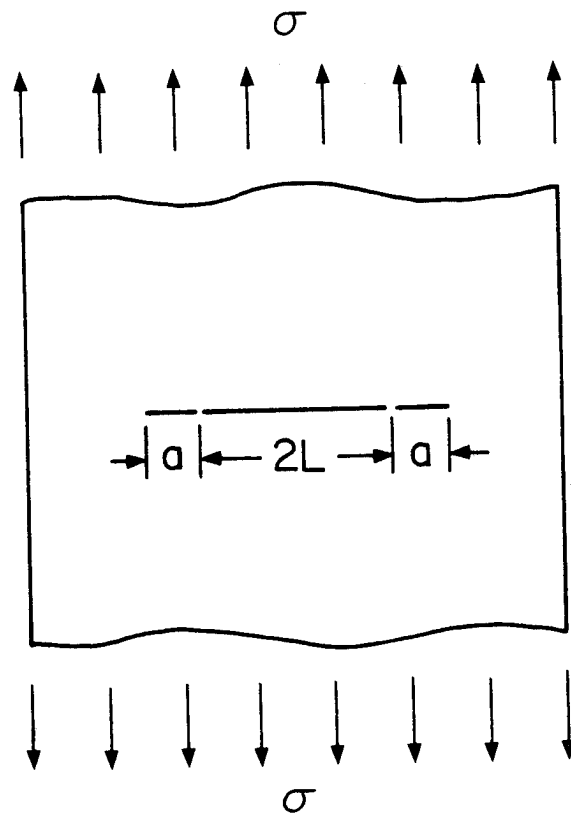


Figure 6.1 "High Intensity Energy Zones" Postulated by Waddoups, Eisenmann and Kaminski [5]

where σ_0 = unnotched laminate strength

σ_f = notched laminate strength (see article 6.1.6)

For a given laminate the value of a is obtained experimentally by conducting notched and unnotched strength tests. Rearranging equation (2), the expression for the notched strength of a finite width plate is

$$Y\sigma_f = \frac{\sigma_0}{\left(\frac{L}{a} + 1\right)^{1/2}} \quad (3)$$

Assuming the unnotched laminate strength and intense energy region are material properties, the failure strength of the laminate for any size notch can be predicted by equation (3).

6.1.2 The Point Stress Model

Rather than using a fracture mechanics approach as did Waddoups, et al., Whitney and Nuismer [6] used strength criteria to develop the point stress criterion and the average stress criterion (described in article 6.1.3). The point stress criterion utilizes the stress distribution adjacent to a discontinuity such as a hole or slot and postulates failure to occur when the stress at some distance, d_0 (Figure 6.2) from the discontinuity reaches the critical, unnotched laminate strength, σ_0 . For a crack the critical stress intensity factor is given by [6]

$$K_Q = \sigma_0 \sqrt{\pi c (1 - \xi_3^2)} \quad (4)$$

where c = crack half length

$$\xi_3 = \frac{c}{c + d_0}$$

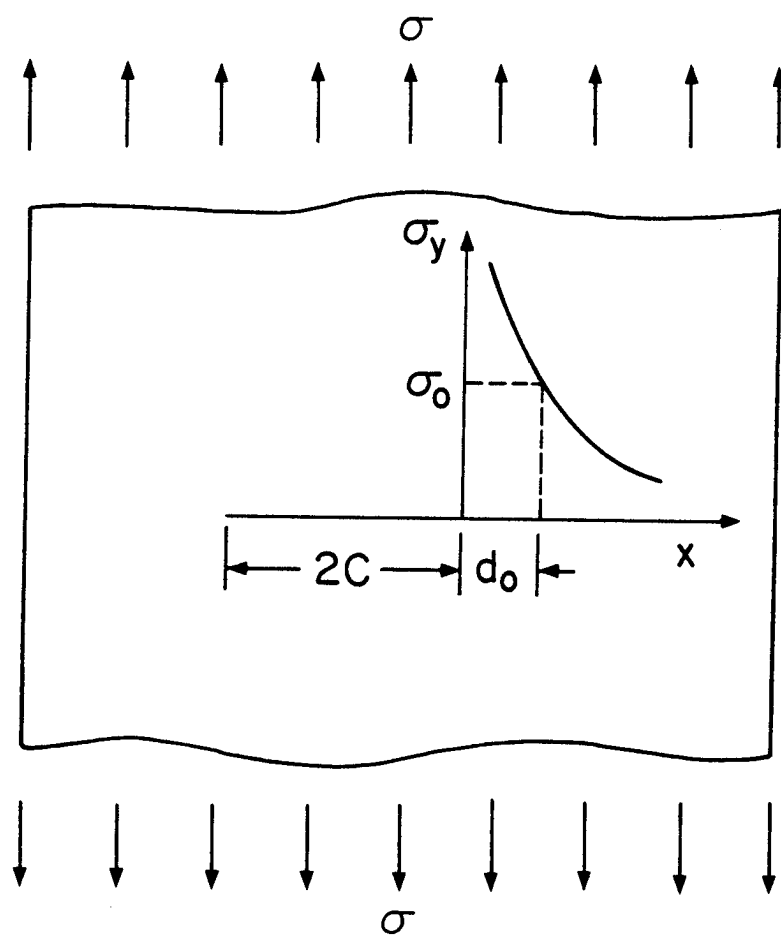


Figure 6.2 Point Stress Model of Whitney and Nuismer [6]

Rewriting equation (4) results in the following expression

$$d_0 = c \{ [1 - (\frac{Y\sigma_f}{\sigma_0})^2]^{-1/2} - 1 \} \quad (5)$$

where Y and σ_f have the same meaning as in equation (2).

The value of d_0 for a given laminate is obtained experimentally by conducting notched and unnotched laminate strength tests. Rearranging equation (5) yields the following expression for the notched strength:

$$Y\sigma_f = \sigma_0 [1 - (\frac{c}{c + d_0})^2]^{1/2} \quad (6)$$

Therefore, if the unnotched laminate strength and the characteristic distance are material properties, the notched failure strength for the laminate with any notch length can be predicted by equation (6).

6.1.3 The Average Stress Model

The average stress model of Whitney and Nuismer [6] is similar to the point stress model except failure is postulated to occur when the average stress some distance, a_0 , (Figure 6.3) from the discontinuity reaches the critical, unnotched laminate strength. For a crack the critical stress intensity factor is

$$K_Q = \sigma_0 \sqrt{\pi a_0 \xi_4} \quad (7)$$

where $\xi_4 = \frac{c}{2c + a_0}$.

Rewriting equation (7) one obtains

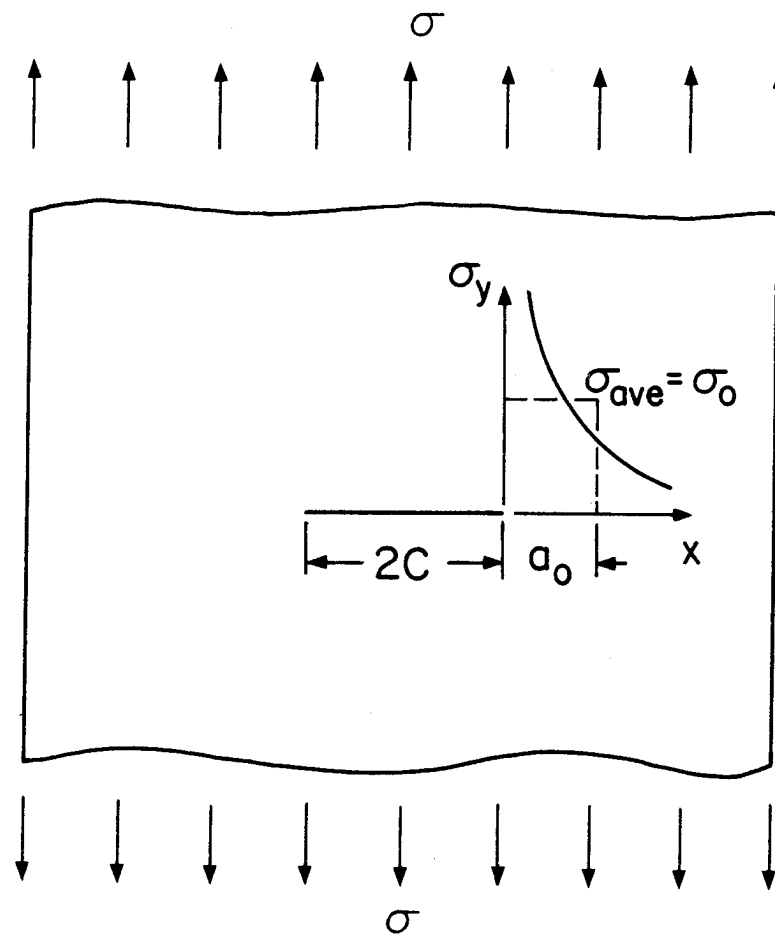


Figure 6.3 Average Stress Model of Whitney and Nuismer [6]

$$a_0 = 2c \frac{\left(\frac{Y\sigma_f}{\sigma_0}\right)^2}{\left[1 - \left(\frac{Y\sigma_f}{\sigma_0}\right)^2\right]} \quad (8)$$

As with the previous two models, a_0 is determined experimentally by conducting notched and unnotched strength tests. Rearranging equation (8), the notched failure strength is

$$Y\sigma_f = \sigma_0 \left[\frac{a_0}{2c + a_0} \right]^{1/2}. \quad (9)$$

Once σ_0 and a_0 are determined for a given laminate, the notched failure strength for any crack size can be predicted by equation (9).

6.1.4 General Toughness Parameter

A "general toughness parameter" based on a critical strain criterion was developed by Poe [13]. Based on experimental observations, Poe postulated that laminate failure occurs whenever the fiber strains reach a critical value in the principle load-carrying laminae. Using the linear elastic fracture mechanics expressions for strain in the singular zone at a crack tip for an orthotropic material and the strain failure criterion, a constant toughness parameter, Q_c , is defined as [13]

$$Q_c = K_0 (\xi_1)_i / E_y \quad (10)$$

where K_0 = stress intensity factor at failure

$$(\xi_1)_i = (1 - \nu_{yx}) \sqrt{\frac{E_x}{E_y}} \left(\sqrt{\frac{E_y}{E_x}} \sin^2 \alpha + \cos^2 \alpha \right) \quad (11)$$

ν_{yx} , E_x and E_y are the laminate engineering stiffness constants with y being the loading direction.

α = fiber angle from y -axis of principle load-carrying laminae.

Q_c is independent of laminate orientation and depends only on the laminate engineering stiffness constants. Poe found that when the toughness parameter is divided by the ultimate tensile strain of the fibers, ϵ_{tuf} , the resulting ratio, $\frac{Q_c}{\epsilon_{tuf}}$, (hereinafter referred to as the general toughness parameter) appeared to be a constant value of $1.5\sqrt{\text{mm}}$. This was based on a statistical analysis of all available fracture toughness data, regardless of laminate stacking sequence or material type.

While $\frac{Q_c}{\epsilon_{tuf}} = 1.5\sqrt{\text{mm}}$ is a statistical mean to a substantial data base, it is most valid for those laminates that fracture in a self-similar manner. It is less accurate for laminates that split extensively or exhibit substantial delamination. A more precise value of $\frac{Q_c}{\epsilon_{tuf}}$ for a given laminate can be obtained by using equations (10) and (11) along with experimentally determined values of K_Q . Finally by manipulating the basic equations an expression for notched failure strength is given by [13]

$$Y\sigma_f = \sigma_0 \{1 + \pi a [(\xi_1)_i \sigma_0 / Q_c E_y]^2\}^{-1/2} \quad (12)$$

Therefore, once σ_0 and Q_c are determined experimentally (or the general Q_c value is used) the notched failure strength of any laminate for any crack size can be predicted by equation (12).

6.1.5 Mar-Lin Curve Fit Model

Mar and Lin [41] have postulated a "curve fit" model for predicting fracture strength. The form of the model is taken from isotropic metals behavior and is given by

$$\frac{\sigma_f}{\sigma_0} = M \left(\frac{2a}{W} \right)^{-m} \quad (13)$$

where $2a$ = crack length
 W = specimen width
 M, m = curve fit parameters

When the strength ratio and $\frac{2a}{W}$ values are plotted on a log-log scale, M is the intercept and m is the slope of the resulting straight line. M may be analogous to the material fracture toughness and m may be related to the strength of the crack tip singular zone. (For an isotropic material, $M = K_{IC}$ and $m = 1/2$.) While a log-log curve fit of this type may have questionable quantitative value for predicting laminated composite fracture, it can be used in a qualitative manner to evaluate the notch sensitivity of various laminates. The Mar-Lin model will be used herein to compare the thin laminate and thick laminate fracture strength data as a function of crack size.

6.1.6 Determination of Strength and the Finite Width Correction Factor

The unnotched laminate strength utilized herein is estimated by multiplying the laminate engineering stiffness constant in the loading direction, E_y , by the ultimate fiber failing strain $\epsilon_{tuf} = 0.010$ [13]. Since the unnotched laminates of this study are approximately linear to

failure, this approximation is reasonable. The values of strength are tabulated below:

$[0/\pm 45/90]_{ns}$	$E_y = 8.057 \times 10^6 \text{ psi}$ (55.6 GPa)	$\sigma_o = 80.6 \text{ ksi}$ (556 MPa)
$[0/90]_{ns}$	$E_y = 11.07 \times 10^6 \text{ psi}$ (76.3 GPa)	$\sigma_o = 110.7 \text{ ksi}$ (763 MPa)
$[0/\pm 45]_{ns}$	$E_y = 8.952 \times 10^6 \text{ psi}$ (61.7 GPa)	$\sigma_o = 89.5 \text{ ksi}$ (617 MPa)

where values of E_y are obtained from Table 5.2 of section 5.1. (The validity of this approach for estimating the strength of T300/5208 laminates was provided by the work of Garber [42].)

It has long been recognized that the stress distribution adjacent to a notch in a finite width plate is different from the distribution in an infinite width plate. In order to relate notched laminate strength (finite width) to unnotched laminate strength (infinite width), the "finite width correction factor" [3] must be applied to the notched laminate strength.

The notched laminate strength is taken to be the stress away from the crack. For the center-cracked tension specimen, the failing stress is computed by

$$\sigma_f = \frac{P}{Wt}$$

where P = load at failure
 W = specimen width
 t = specimen thickness

The finite width correction factor utilized herein is the isotropic correction factor. For the center-cracked tension specimen geometry, ASTM 410 [1] provides the following polynomial expression for the finite width correction factor:

$$Y = 1 + 0.1282 \left(\frac{2a}{W}\right) - 0.2881 \left(\frac{2a}{W}\right)^2 + 1.5254 \left(\frac{2a}{W}\right)^3$$

For the $\frac{2a}{W}$ values included in this study, the finite width correction factors are tabulated below:

$\frac{2a}{W}$	Y
0.25	1.038
0.375	1.088
0.50	1.183
0.625	1.340

Section 5.1 presents the solutions for the stress intensity factors for the three laminate types and the center-cracked tension specimen geometries. The differences between the orthotropic and isotropic solutions were small, as shown in Table 5.6. For purposes of evaluating the failure criteria herein, the differences are not considered significant. Therefore, the isotropic correction factor is utilized.

6.2 Prediction of Notched Strength of Thin Laminates

The laminate modeling parameters determined from the thin laminate test data are tabulated in Table 6.1. Utilizing equations (2), (5), and (8), the characteristic distances were computed for the inherent flaw, point stress and average stress models. The general toughness parameter, $\frac{Q_c}{\epsilon_{tuf}}$, was computed from equations (10) and (11) using the experimentally determined values of K_Q . The characteristic distance values are comparable to previously reported values. Whitney and Nuismer [6] reported a value of $d_0 = 0.04$ in. (1.02 mm) and $a_0 = 0.15$ in. (3.81 mm) for a T300/5208 $[0/\pm 45]_S$ laminate. Hahn and Morris [26] reported an average stress model parameter of $a_0 = 0.10$ in. (2.54 mm) for a T300/5208 $[0/\pm 45]_S$ laminate. The average value of a_0 is 0.094 in. (2.39 mm) for the T300/5208 $[0/\pm 45]_S$ laminate reported herein. The general toughness parameter values are comparable to those reported by Poe [13] for T300/5208 graphite/epoxy laminates. Poe reported values of $\frac{Q_c}{\epsilon_{tuf}} = 1.60, 1.09$ and $2.25\sqrt{\text{mm}}$ for the $[0/\pm 45/90]_S$, $[0/\pm 45]_{2S}$ and $[0/90]_{4S}$ laminates, respectively. The corresponding experimental values reported herein are 1.72, 1.0 and $2.00\sqrt{\text{mm}}$.

The average characteristic distance values along with equations (3), (6) and (9) were used to compute the notched fracture strength of the three laminates for the inherent flaw, point stress and average stress models. The notched fracture strength predictions are shown graphically in Figures 6.4-6.6 for the $[0/\pm 45/90]_S$, $[0/90]_S$ and $[0/\pm 45]_S$ laminates, respectively. (The thick laminate strength values shown in these figures will be discussed in the next section.) No distinction could be made between the predictions from the three models, so the solid line represents the strength prediction as a function of crack

Table 6.1 Characteristic Distances Computed From Thin Laminate Data

Laminate Type	$\frac{2a}{W}$	$\frac{Y\sigma_f}{\sigma_0}$	Inherent Flaw a in.(mm)	Point Stress d_0 in.(mm)	Average Stress a_0 in.(mm)	General Toughness Parameter $\frac{Q_c}{\epsilon_{tuf}} \sqrt{\text{mm}}$
[0/±45/90] _s	0.25	0.533	0.100(2.54)	0.0456(1.16)	0.198(5.03)	1.63
	0.375	0.462	0.101(2.57)	0.0477(1.21)	0.204(5.18)	1.78
	0.50	0.388	0.089(2.26)	0.0426(1.08)	0.177(4.50)	1.72
	0.625	0.344	0.084(2.13)	0.0405(1.03)	0.168(4.27)	1.75
Average			0.094(2.39)	0.044(1.12)	0.187(4.75)	1.72
[0/±45] _s	0.25	0.388	0.0442(1.12)	0.0212(.538)	0.088(2.24)	0.95
	0.375	0.335	0.0475(1.21)	0.0230(.589)	0.095(2.41)	0.99
	0.50	0.306	0.0517(1.31)	0.0252(.640)	0.103(2.62)	1.04
	0.625	0.259	0.0450(1.14)	0.0221(.561)	0.090(2.29)	1.01
Average			0.047(1.19)	0.023(.584)	0.094(2.39)	1.00
[0/90] _{2s}	0.25	0.423	0.0543(1.38)	0.0258(.655)	0.109(2.77)	1.65
	0.375	0.386	0.0659(1.67)	0.0316(.803)	0.132(3.35)	1.86
	0.50	0.417	0.1053(2.67)	0.0501(1.27)	0.211(5.36)	2.34
	0.625	0.334	0.0786(2.00)	0.0381(.968)	0.157(3.99)	2.13
Average			0.076(1.93)	0.036(.914)	0.152(3.86)	2.00

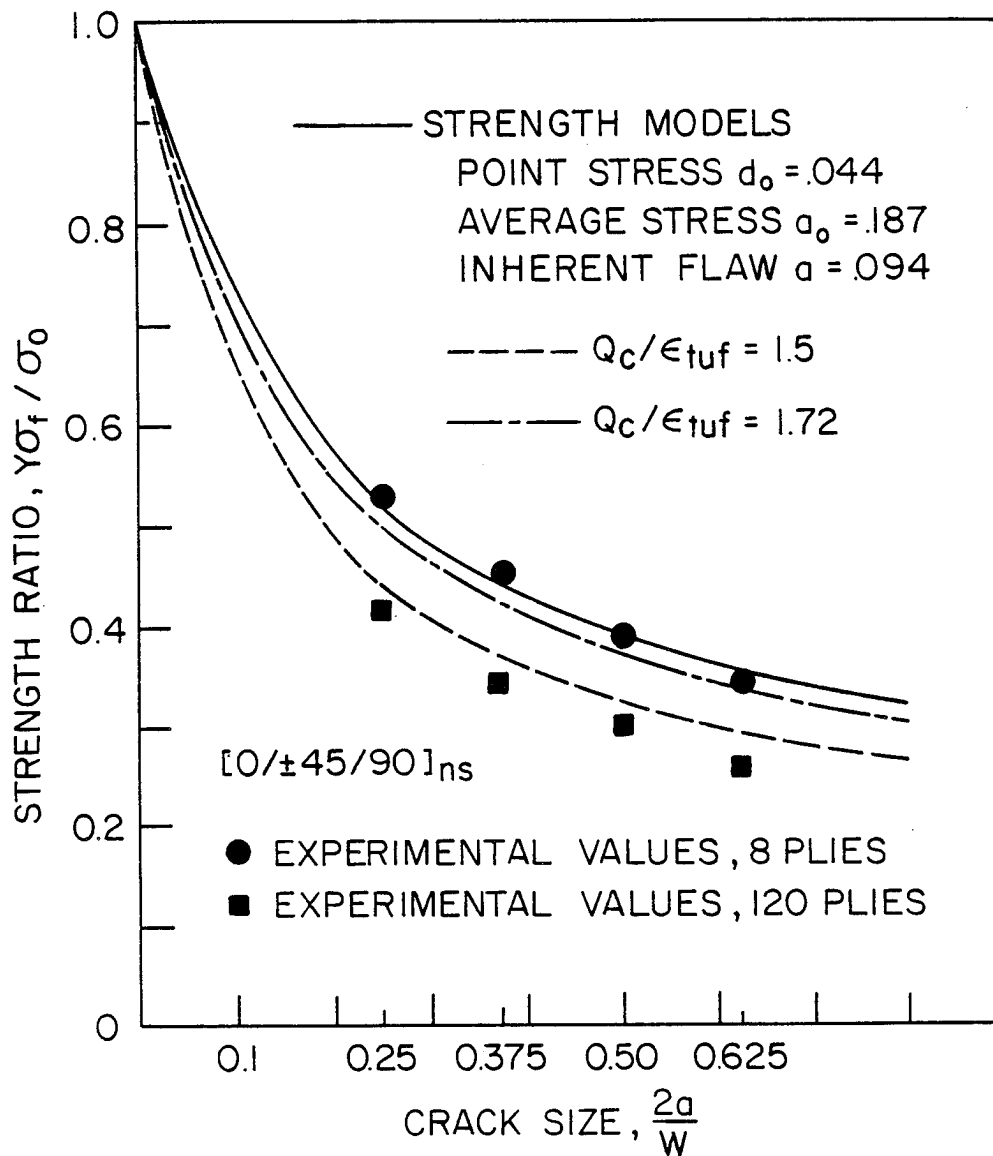


Figure 6.4 Comparison of Experimental and Predicted Values of Notched Laminate Strength of the 8 Ply and 120 Ply $[0/\pm 45/90]_{ns}$ Laminates

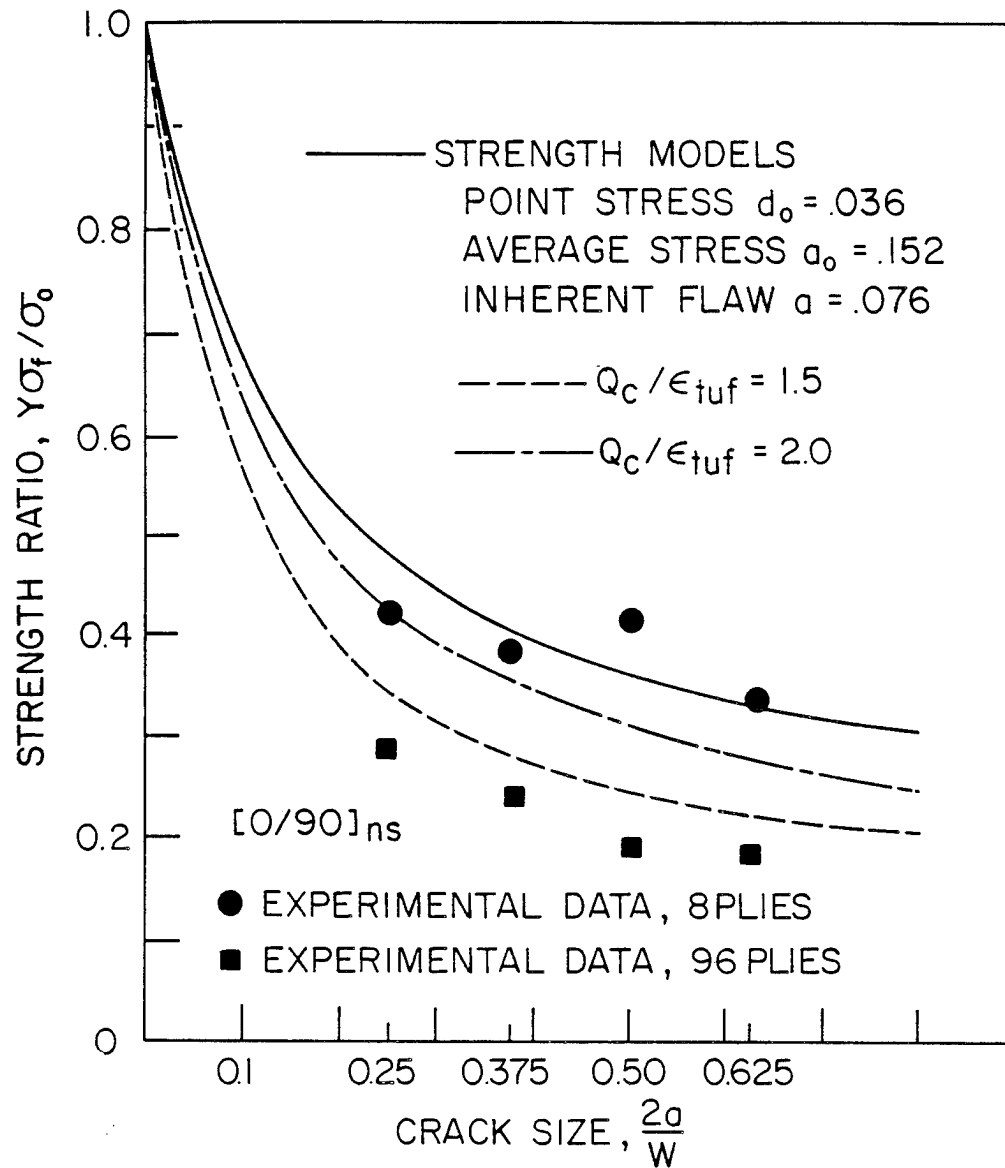


Figure 6.5 Comparison of Experimental and Predicted Values of Notched Laminate Strength of the 8 Ply and 96 Ply [0/90]_{ns} Laminates

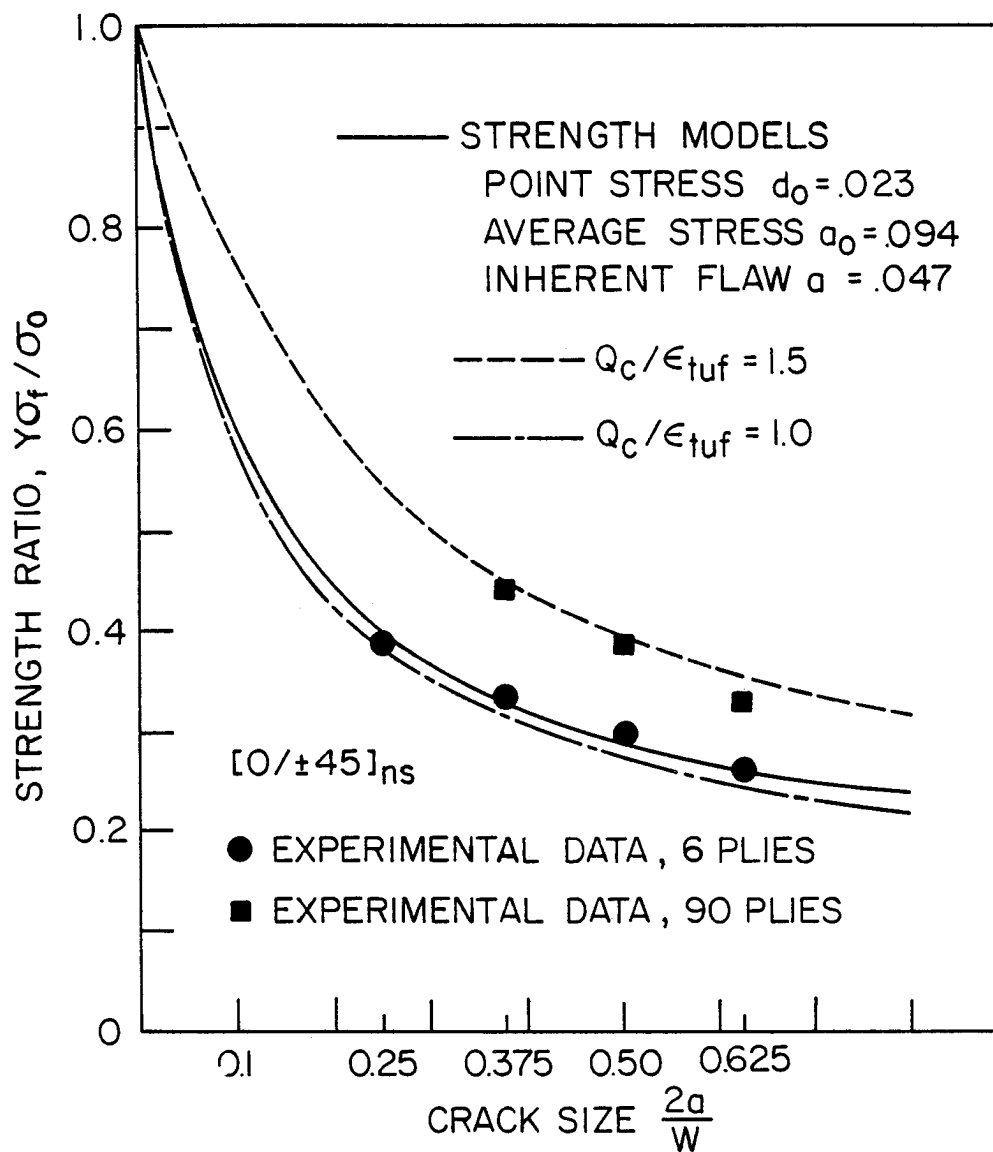


Figure 6.6 Comparison of the Experimental and Predicted Values of Notched Laminate Strength of the 6 Ply and 90 Ply [0/±45]_{ns} Laminates

half-length, a , from each model. (This will be referred to hereinafter as the strength model predictions.) Also shown are the notched fracture strength predictions of the general toughness parameter using equation (12) and both the experimentally determined values of $\frac{Q_c}{\epsilon_{tuf}}$ and the universal value of $\frac{Q_c}{\epsilon_{tuf}} = 1.5 \sqrt{\text{mm}}$. Shown for comparison purposes are the experimentally determined values of notched fracture strength. Figures 6.4 and 6.6 clearly show that the strength models and experimental general toughness parameter provide very accurate predictions of notched fracture strength for the $[0/\pm 45/90]_S$ and $[0/\pm 45]_S$ laminates. Because of the substantial axial splitting at the notch tips of the $[0/90]_{2S}$ laminates, none of the models accurately predicted the fracture strength. It should be noted that if the fracture strength and model parameters of the $[0/90]_{2S}$ laminate are computed at the onset of splitting (critical load) rather than at the maximum load, then both the strength models and the experimental general toughness parameter accurately predict the fracture strength. This is illustrated in Figure 6.7. Finally the universal general toughness parameter value of $\frac{Q_c}{\epsilon_{tuf}} = 1.5 \sqrt{\text{mm}}$ substantially underestimates the fracture strength of the $[0/\pm 45/90]_S$ and $[0/90]_{2S}$ laminates while substantially overestimating the strength of the $[0/\pm 45]_S$ laminate. However, one should keep in mind that the value of $1.5 \sqrt{\text{mm}}$ was determined for many different materials of various laminate orientations, and should not be expected to fit the data as well as a value of Q_c/ϵ_{tuf} found for the data presented herein.

The Mar-Lin curve fits are shown in Figure 6.8. The experimental values of strength ratio are plotted versus $\frac{2a}{W}$ on a log-log scale at both the critical test load and maximum test load. A straight line of the form of equation (13) was placed through the data. The value of the

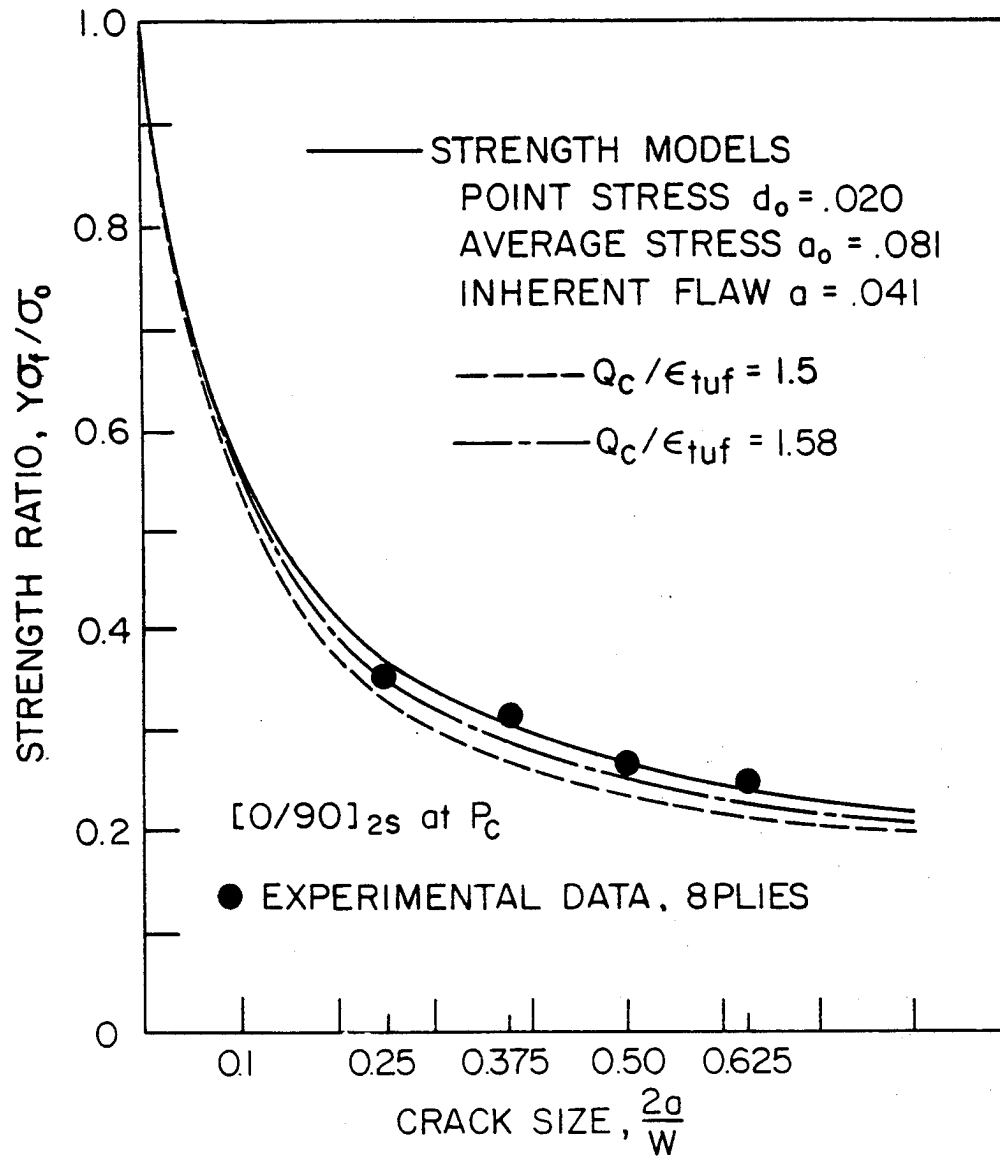


Figure 6.7 Comparison of Experimental and Predicted Values of Notched Laminate Strength at the Critical Load for the [0/90]_{2s} Laminate

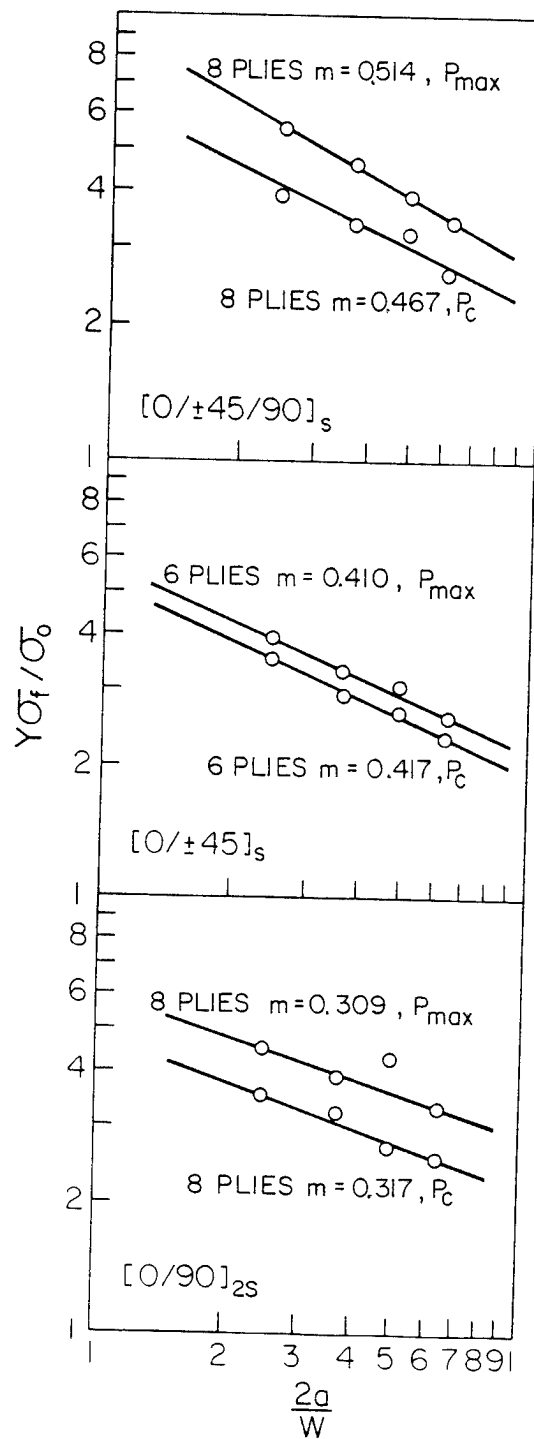


Figure 6.8 Comparison of the Mar-Lin Curve Fit at the Critical Load and Maximum Load for the Thin Laminates

slope was computed and is shown on the figure. Two qualitative conclusions can be reached by comparing the two lines. First, there is very little difference in the slopes of the lines through the critical load values and the maximum load values. This indicates that the strength of the crack tip singularity is similar at P_c and P_m . Second, the slope of the line through the $[0/90]_{2S}$ data is substantially lower than the slopes for the $[0/\pm 45/90]_S$ and $[0/\pm 45]_S$ laminates. This indicates that the $[0/90]_{2S}$ laminate is less notch sensitive than the other two laminates. This result is to be expected because the $[0/90]_{2S}$ laminates split extensively at the notch tips, therefore reducing the strength of the singularity at the crack tip.

6.3 Application to Thick Laminates

In this section we will address the issue of predicting the fracture of the thick laminates utilizing thin laminate data and the previously described failure criteria. There are two fundamental issues that must be addressed before proceeding with this task. First, for the failure criteria developed for thin laminates to be applicable to thick laminates, the fracture phenomenon or process must be the same. Fracture of the 8 ply and 120 ply $[0/\pm 45/90]_{nS}$ laminates are the same. Both the thin and thick laminates fracture in a generally self-similar manner. However, this is not the case with the other two laminates. To predict the fracture of the $[0/90]_{nS}$ laminates the criteria must be able to address the role of axial splitting at the crack tip. This dominates the thin laminate fracture and has little if any effect on the fracture strength of thick laminates. The $[0/\pm 45]_S$ laminate fractures in a mixed mode manner with fibers breaks in the 0° plies oriented at 45° to the

starter notch and the ± 45 cross-ply delaminate and fail by matrix splitting. At the other extreme the 120 ply $[0/\pm 45]_{ns}$ laminates fracture in a self-similar manner with fiber breaks collinear with the starter notch with very little delamination present. These differences may have no effect on the applicability of the strength criteria but may be significant when using a fracture mechanics criterion such as the general toughness parameter.

Assuming that the thin and thick fracture phenomenon are the same, how then is the thickness effect, such as for the $[0/\pm 45/90]_{ns}$ laminate, incorporated into the mathematical model of fracture? Obviously there is no explicit thickness effect built into any of the models. Perhaps the unnotched strength and characteristic distances are a function of laminate thickness. There are no experimental values of unnotched strength as a function of laminate thickness. Therefore, computing a characteristic distance from the thick laminate notched test results is not possible because the corresponding notched laminate strengths are not available. Finally, is there a plane stress versus plane strain effect in laminated composites as there is in isotropic metals that may account for the thickness effect? Assuming that the thick laminates are behaving in a plane strain manner, only the general toughness parameter model can be modified from plane stress to plane strain. This is accomplished primarily by replacing $\sqrt{\frac{E_x}{E_y}}$ in equation (11) by

$$\sqrt{\frac{E_x}{E_y}} \left\{ \sqrt{\frac{1 - \frac{E_z}{E_y} (\nu_{yz})^2}{1 - \frac{E_z}{E_x} (\nu_{xz})^2}} \right\}.$$

By assuming transverse isotropy, the E_z , ν_{yz} and ν_{xz} laminate stiffness properties were estimated as described in section 5.1.3. The differences in $\frac{Q_c}{\epsilon_{tuf}}$ between plane stress and plane strain were computed to be 5.7%, 3.5% and 9.2% for the $[0/\pm 45/90]_{ns}$, $[0/90]_{ns}$ and $[0/\pm 45]_{ns}$ laminates, respectively, with the plane strain value being lower. These differences are obviously not nearly enough to account for the changes in fracture strength between the thin and thick laminates of this study, as shown in Figures 6.4-6.6.

The conclusion reached from the foregoing discussion is that there are no modifications of thin laminate failure criteria that address the thickness effect. (This statement is made in the absence of unnotched strength versus laminate thickness data.) The experimental values of notched strength are shown in Figures 6.4-6.6 at 120 plies, 96 plies and 90 plies for the $[0/\pm 45/90]_{ns}$, $[0/90]_{ns}$, and $[0/\pm 45]_{ns}$ laminates, respectively. Also shown in these figures were the thin laminate experimental strength data and the thin laminate strength predictions. The strength model predictions substantially overestimated the notched strength of the $[0/\pm 45/90]_{ns}$ and $[0/90]_{ns}$ thick laminates, while the thick $[0/\pm 45]_{ns}$ laminate strength was substantially underestimated. However, the universal value of $\frac{Q_c}{\epsilon_{tuf}} = 1.5 \sqrt{\text{mm}}$ is a very close prediction of the experimental notched strength of the thick laminates for all three laminate types. Furthermore if the plane strain values of $\frac{Q_c}{\epsilon_{tuf}}$ given in the previous paragraph are used rather than $1.5 \sqrt{\text{mm}}$ the prediction curves pass directly through the experimental data. This is not just a fortuitous result and a review of the basis for establishing the universal value of $\frac{Q_c}{\epsilon_{tuf}}$ indicates why this is a consistent result. A large body of laminated composite data of a variety of material systems

and stacking sequences were statistically analyzed [13]. The value of $\frac{Q_c}{\epsilon_{tuf}} = 1.5 \sqrt{\text{mm}}$ is the mean value between the 20th (1.25) and 73rd (1.75) percentile [13] within which the coefficient of variation was 0.10. The laminates that fell within this range fractured in a self-similar manner and those outside the range exhibited substantial splitting such as the $[0/90]_{2S}$ laminate or substantial delamination such as the $[0/\pm 45]_S$ laminate. However, the fracture of the thick laminates of each of these two laminate types was self-similar. Splitting and delaminations were confined to a surface or boundary layer. Therefore, the thick laminates of all three laminate types fractured in a manner totally consistent with the statistical basis of $\frac{Q_c}{\epsilon_{tuf}} = 1.5 \sqrt{\text{mm}}$.

In conclusion, the Mar-Lin curve fit for the thick laminate data is shown in Figure 6.9. The thick laminate curves are shown along with the thin laminate curves for comparison purposes. The 8 ply and 120 ply data for the $[0/\pm 45/90]_{NS}$ laminate fall along parallel lines. This indicates that both the thin and thick laminates are equally notch sensitive as would be inferred from the test results. The 90 ply curve for the $[0/\pm 45]_{NS}$ laminate is slightly steeper than its 6 ply counterpart. This suggests that the thick laminate is more notch sensitive than the thin laminate. One would expect the slopes to be different because of the dramatically different failure modes of the 6 ply and 90 ply specimens. Also the curve fit to the 96 ply $[0/90]_{NS}$ data is steeper than the curve fit to the 8 ply data. The 8 ply laminate is less notch sensitive than the 96 ply laminate because of the dominant role of axial splits that form in the 0° plies at the crack tip. Therefore, the Mar-Lin curve fit does provide a good qualitative correlation with the test results. Finally, it is interesting to note that the exponent, m , which

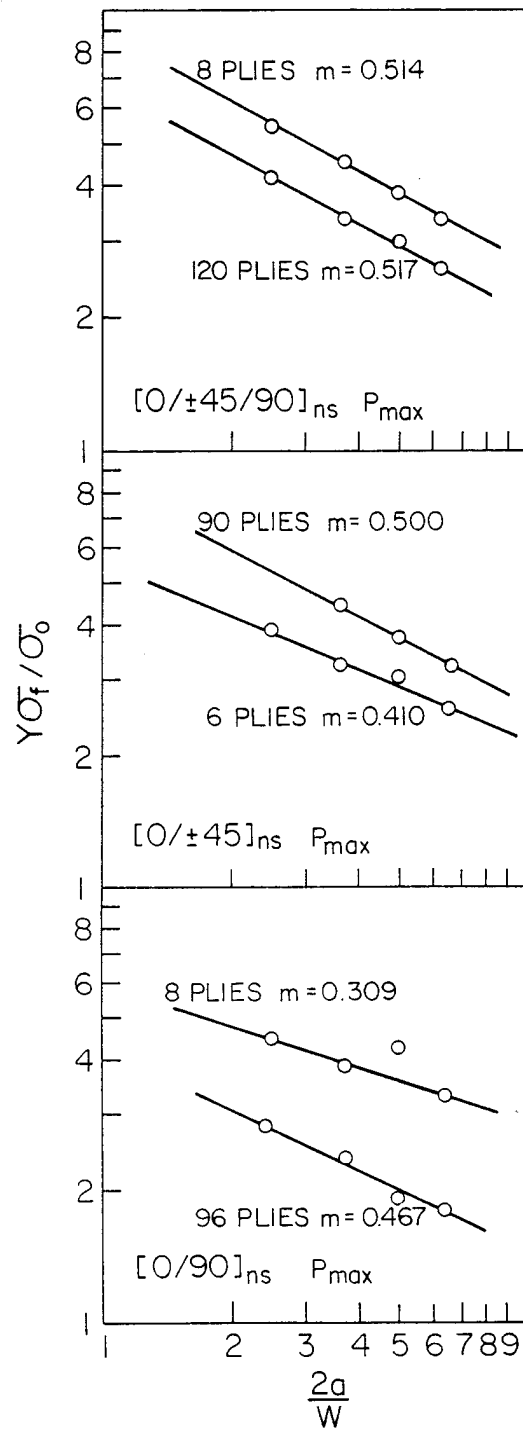


Figure 6.9 Comparison of the Mar-Lin Curve Fit at the Maximum Load for the Thin and Thick Laminates

may be interpreted as the strength of the crack tip singularity is close to $1/2$ for all three thick laminates which fractured in a self-similar manner.

7.0 SUMMARY AND CONCLUSIONS

The effect of laminate thickness on the fracture behavior of graphite/epoxy laminated composites has been studied. The predominantly experimental research program included the study of $[0/\pm 45/90]_{ns}$ and $[0/90]_{ns}$ laminates with thicknesses of 8, 32, 64, 96 and 120 plies and the $[0/\pm 45]_{ns}$ laminate at thicknesses of 6, 30, 60, 90 and 120 plies. The research concentrated on the measurement of fracture toughness utilizing the center-cracked tension, compact tension, and three point bend specimen configurations. The development of subcritical damage at the crack tip was studied using the enhanced x-ray radiography nondestructive technique and the laminate deply destructive technique. The deply technique provided a complete record of the individual ply damage and ply interface delaminations through the laminate thickness. A finite element analysis of each specimen configuration yielded expressions for the stress intensity factors by treating the composite as homogeneous and anisotropic. The final activity was the assessment of the ability of several candidate thin laminate fracture criteria to predict the failure of thick notched laminates.

The test results clearly show fracture toughness and notched laminate failure strength to be significantly influenced by laminate thickness. The substantial matrix splitting and delaminations that occurred in the 6 and 8 ply laminates greatly influenced their fracture behavior. The thick laminates exhibited a surface boundary layer in which the crack tip matrix splitting and delaminations were just like those in the thin laminates. However, outside of this boundary layer the interior region of the specimen exhibited a self-similar fracture that was uniform and relatively free of delaminations.

The general toughness parameter model, a strain criterion developed by C. C. Poe, Jr. [13], was the only candidate thin laminate failure criterion that was successful in using thin laminate parameters to predict the fracture of thick laminates. The "universal" general toughness parameter value of $1.5 \sqrt{\text{mm}}$ quite closely predicted the fracture of the thick laminates. The Mar-Lin curve fit [41] was found to be a useful qualitative tool in assessing the relative notch sensitivity of thin and thick laminates as well as different laminate types.

The $[0/\pm 45/90]_{ns}$ quasi-isotropic laminate exhibited a reduction in fracture toughness with increasing laminate thickness. Toughness appeared to asymptotically approach a lower bound toughness of $30 \text{ ksi}\sqrt{\text{in}}$ ($1043 \text{ MPa}\sqrt{\text{mm}}$) beyond 64 plies. Fracture toughness was independent of crack size for both the 8 ply and 120 ply laminates. There was little difference in the type of damage or the final fracture of the thin and thick laminates. Only the relative size of the subcritical damage zone at comparable percentages of the failing load appeared different. The behavior of the quasi-isotropic laminate suggests a direct analogy to the fracture behavior of isotropic metals as a function of thickness.

The $[0/90]_{ns}$ laminate fracture behavior was greatly affected by the influence of laminate thickness on the axial splitting that formed at the crack tip in 0° plies and extended in the direction of applied load. The 8 ply laminate split extensively, with the longer starter cracks experiencing more extensive splitting. The axial splits decreased the strength of the crack tip singularity and, thus, elevated the fracture toughness. The 8 ply laminate exhibited a sharp increase in fracture toughness with increasing starter crack size. Examinations of the thick laminates revealed the splitting to be a surface phenomenon. The in-

terior region of the specimen exhibited self-similar fracture with a very smooth fracture surface. The fracture toughness decreased sharply with increasing laminate thickness and asymptotically approached a lower bound value of $25 \text{ ksi}\sqrt{\text{in}}$ ($869 \text{ MPa}\sqrt{\text{mm}}$) beyond 64 plies. At 96 plies the fracture toughness was independent of starter crack size.

The fracture behavior of the $[0/\pm 45]_{ns}$ laminate was in sharp contrast to the behavior of the other two laminate types. The fracture toughness of the $[0/\pm 45]_{ns}$ laminate increased sharply, initially, with increasing thickness but asymptotically approached a plateau value of $40 \text{ ksi}\sqrt{\text{in}}$ ($1390 \text{ MPa}\sqrt{\text{mm}}$) at 30 plies. The 6 ply laminate failed differently from the thick laminates as well. The outside 0° plies exhibited fiber breaks along a $+45^\circ$ line--parallel to matrix splitting in the adjacent ply. The $+45^\circ$ plies delaminated from the two interior -45° plies, thus, resulting in an uncoupling of the two outside plies from the two inside plies. The two -45° plies failed by matrix splitting along a -45° line. The thick laminate (120 plies) exhibited a surface boundary layer where the $+45^\circ$ fiber breaks, matrix splits and delaminations were present. However, the interior of the specimen exhibited very little evidence of delamination and the fracture was self-similar. Recognizing the somewhat limited examinations of this study, the uncoupling mechanism exhibited by the 6 ply $[0/\pm 45]_s$ laminate appears to be the likely reason for its sharp contrast to the behavior of the thicker laminates.

Finally, the center-cracked tension, compact tension and three-point bend specimens provided similar results. Comparisons were made at the greater laminate thicknesses. For the $[0/\pm 45/90]_{ns}$ and $[0/90]_{ns}$ laminates, the modes of damage and final fracture of the three specimen

types were the same. The fracture toughness values fell along the same toughness-thickness trend curve. For the $[0/\pm 45]_{ns}$ laminate the center-cracked tension specimens seemed to define one plateau at $40 \text{ ksi}\sqrt{\text{in}}$ ($1390 \text{ MPa}\sqrt{\text{mm}}$) while the compact tension and three point bend specimens defined a lower plateau at $34 \text{ ksi}\sqrt{\text{in}}$ ($1182 \text{ MPa}\sqrt{\text{mm}}$).

In conclusion this study has shown the fracture behavior of laminated composites to be influenced by laminate thickness. The fracture of thick laminates was relatively smooth and self-similar while their thin laminate counterparts may have failed in a "deviate" manner. Thick laminates exhibited a surface boundary layer where matrix splitting, delaminations and fiber breaks resembled their thin laminate counterparts. The principal damage mode in the interior of thick specimens was fiber breaks extending collinearly with the original starter cracks.

REFERENCES

1. Brown, W. F., Jr. and Srawley, J. E., editors, Plane Strain Crack Toughness Testing of High Strength Metallic Materials, ASTM STP 410, American Society for Testing and Materials, 1966.
2. Brown, W. F., Jr., Editor, Review of Developments in Plane Strain Fracture Toughness Testing, ASTM STP 463, American Society for Testing and Materials, 1970.
3. Paris, P. C., and Sih, G. C., "Stress Analysis of Cracks" in Fracture Toughness Testing and Its Applications. ASTM STP 381, American Society for Testing and Materials, c.1965, pp. 30-83.
4. Wu, E. M., "Fracture Mechanics of Anisotropic Plates," in Composite Materials Workshop, S. W. Tsai, J. C. Halpin, and J. F. Pagano, Eds., Technomic Publishing Co., 1968, pp. 20-43.
5. Waddoups, M. E., Eisenmann, J. R., and Kaminski, B. E., "Macroscopic Fracture Mechanics of Advanced Composite Materials," Journal of Composite Materials, Vol. 5, Oct. 1971, pp. 446-454.
6. Whitney, J. M., and Nuismer, R. J., "Stress Fracture Criteria for Laminated Composites Containing Stress Concentrations," Journal of Composite Materials, Vol. 8, July 1974, pp. 253-265.
7. Whitney, J. M., and Nuismer, R. J., "Uniaxial Failure of Composite Laminates Containing Stress Concentrations," in Fracture Mechanics of Composites, ASTM STP 593, American Society for Testing and Materials, 1975, pp. 117-142.
8. Mandell, J. F., Wang, S. S., and McGarry, F. J., "Fracture of Graphite Fiber Reinforced Composites," Air Force Materials Laboratory Report AFML-TR-73-142, 1973.
9. Cruse, T. A., and Osias, J. R., "Exploratory Development on Fracture Mechanics of Composite Materials," Air Force Materials Laboratory Report AFML-TR-74-111, 1974.
10. Zweben, C., "An Approximate Method of Analysis for Notched Unidirectional Composites," Engineering Fracture Mechanics, Vol. 6, no. 1, 1974, pp. 1-10.
11. Goree, J. G. and Gross, R. S., "Analysis of a Unidirectional Composite Containing Broken Fibers and Matrix Damage," Engineering Fracture Mechanics, Vol. 13, 1979, pp. 563-578.
12. Zweben, C., "Fracture Mechanics and Composite Materials: A Critical Analysis," in Analysis of the Test Methods for High Modulus Fibers and Composites, ASTM STP 521, American Society for Testing and Materials, 1973, pp. 65-97.

13. Poe, Jr., C. C., "A Unifying Strain Criterion for Fracture of Fibrous Composite Laminates," Engineering Fracture Mechanics, Vol. 17, 1983, pp. 153-171.
14. Yeow, Y. T., Morris, D. H., and Brinson, H. F., "A Correlative Study Between Analysis and Experiment on the Fracture Behavior of Graphite/Epoxy Composites," Journal of Testing and Evaluation, Vol. 7, No. 2, 1979, pp. 117-125.
15. Snyder, M. D., and Cruse, T. A., "Boundary-Integral Equation Analysis of Cracked Anisotropic Plates," International Journal of Fracture, Vol. 11, 1975, pp. 315-328.
16. Snyder, M. D., and Cruse, T. A., "Crack Tip Stress Intensity Factors in Finite Anisotropic Plates," Air Force Materials Laboratory, Report AFML-TR-73-209, 1973.
17. Sih, G. C., Hilton, P. D., Badaliance, R., Shenberger, P. S., and Villarreal, G., "Fracture Mechanics for Fibrous Composites," in Analysis of the Test Methods for High Modulus Fibers and Composites, ASTM STP 521, American Society for Testing and Materials, 1973, pp. 98-132.
18. Griffith, W. I., Kanninen, M. F., and Rybicki, E. F., "A Fracture Mechanics Approach to the Analysis of Graphite/Epoxy Laminated Pre-cracked Tension Panel," in Nondestructive Evaluation and Flaw Criticality for Composite Materials, ASTM STP 696, American Society for Testing and Materials, 1979, pp. 185-201.
19. Ueng, C. E., Aberson, J. A., and Lafitte, B. A., "Tensile Analysis of an Edge Notch in a Unidirectional Composite," Journal of Composite Materials, Vol. 11, April 1977, pp. 222-234.
20. Poe, Jr., C. C., and Sova, J. A., "Fracture Toughness of Boron/Aluminum Laminates With Various Proportions of 0° and $\pm 45^\circ$ Plies," NASA TP-1707, 1980.
21. Whitney, J. M., and Knight, M., "The Relationship Between Tensile Strength and Flexure Strength in Fiber-Reinforced Composites," Experimental Mechanics, Vol. 20, June 1980, pp. 211-216.
22. Bullock, R. E., "Strength Ratios of Composite Materials in Flexure and Tension," Journal of Composite Materials, Vol. 8, 1974, p. 200.
23. Slepetz, J. M., and Carlson, L., "Fracture of Composite Compact Tension Specimens," in Fracture Mechanics of Composites, ASTM STP 593, American Society for Testing and Materials, 1975, pp. 143-162.
24. Owen, M. J., and Cann, R. J., "Fracture Toughness and Crack-Growth Measurements in GRP," Journal of Material Science, Vol. 14, Aug. 1979, pp. 1982-1996.

25. Sun, C. T., and Prewo, K. M., "The Fracture Toughness of Boron Aluminum Composites," Journal of Composite Materials, Vol. 11, April 1977, pp. 164-175.
26. Hahn, H. T., and Morris, D. H., "Fracture Resistance Characterization of Graphite/Epoxy Composites," in Composite Materials: Testing and Design (Fourth Conference), ASTM STP 617, American Society for Testing and Materials, 1977, pp. 5-17.
27. Prewo, K. M., "The Effect of Ply Lay-up Sequence on the Fracture Toughness of Boron Aluminum," Journal of Composite Materials Vol. 12, Jan. 1978, pp. 40-52.
28. Yeow, Y. T., Morris, D. H., and Brinson, H. F., "The Fracture Behavior of Graphite/Epoxy Laminates," Experimental Mechanics, Vol. 19, Jan. 1979, pp. 1-8.
29. Reedy, E. D., Jr., "On the Specimen Dependence of Unidirectional Boron/Aluminum Fracture Toughness," Journal of Composite Materials Supplement, Vol. 14, 1980, pp. 118-131.
30. Shih, T. T., and Logsdon, W. A., "Fracture Behavior of a Thick-Section Graphite/Epoxy Composite," Fracture Mechanics: Thirteenth Conference, ASTM STP 743, Richard Roberts, Ed., American Society for Testing and Materials, 1981, pp. 316-337.
31. Freeman, S. M., "Characterization of Lamina and Interlaminar Damage in Graphite-Epoxy Composites by the Deply Technique," Composite Materials: Testing and Design (Sixth Conference), ASTM 787, I. M. Daniel, Ed., American Society for Testing and Materials, 1982, pp. 50-62.
32. Kobayashi, A. S., Editor, Experimental Techniques in Fracture Mechanics, published by the Iowa State University Press and the Society for Experimental Stress Analysis, 1973.
33. Kanninen, M. F., Rybicki, E. F., and Brinson, H. F., "A Critical Look at Current Applications of Fracture Mechanics to the Failure of Fibre-Reinforced Composites," Composites, January 1977, pp. 17-22.
34. Jones, R. M., Mechanics of Composite Materials, McGraw-Hill Book Company, New York, 1975.
35. Chu, C. S., Anderson, J. M., Batdorf, W. J. and Aberson, J. A., "Finite Element Computer Program To Analyze Cracked Orthotropic Sheets" NASA CR-2698, 1976.
36. Rosen, B. W., "A Simple Procedure for Experimental Determination of the Longitudinal Shear Modulus of Unidirectional Composites," Journal of Composite Materials, Vol. 6, Oct. 1972, pp. 552-554.

37. Kaufman, J. C., "Progress in Fracture Testing of Metallic Materials," Review of Developments in Plane Strain Fracture Toughness Testing, ASTM STP 463, American Society for Testing and Materials, 1970, pp. 3-21.
38. Jones, M. H. and Brown, W. F., Jr., "The Influence of Crack Length and Thickness in Plane Strain Fracture Toughness Tests," Review of Developments in Plane Strain Fracture Toughness Tests, ASTM STP 463, American Society for Testing and Materials, 1970, pp. 63-101.
39. 1982 Annual Book of ASTM Standards, Part 10, American Society for Testing and Materials, Philadelphia, PA.
40. Avery, J. G. and Porter, T. R., "Comparisons of the Ballistic Impact Response of Metals and Composites for Military Aircraft Applications," in Foreign Object Impact Damage to Composites, ASTM STP 568, American Society for Testing and Materials, 1975, pp. 3-29.
41. Mar, J. W. and Lin, K. Y., "Fracture of Boron/Aluminum Composites with Discontinuities," Journal of Composite Materials, Vol. 11, Oct. 1977, pp. 405-421.
42. Garber, D. P., "Tensile Stress-Strain Behavior of Graphite/ Epoxy Laminates," NASA CR-3592, 1982.

APPENDIX A

This appendix contains a tabulation of the measured data from the notched specimen tests. The dimensions of the three specimen types are shown in Fig.

3.1. The width, crack length and thickness of each specimen was measured.

The following nomenclature is used to distinguish the three specimen configurations:

CCT = Center-Cracked Tension

CT = Compact Tension

TPB = Three-Point Bend

The "Panel ID Number" identifies the 14" x 14" panel from which the specimens were cut. The panel number and sequential specimen number uniquely identify each specimen.

The critical load, P_c , and the maximum load, P_m , are shown schematically in the load-COD records of Figures 5.15, 5.36 and 5.43 for the $[0/\pm 45/90]_{ns}$, $[0/90]_{ns}$ and $[0/\pm 45]_{ns}$ laminates, respectively. The determination of the critical load is somewhat subjective. It is defined, herein, as the load corresponding to the first pronounced discontinuity in the load record. This corresponds to a change in the specimen compliance brought about by the formation of substantial subcritical crack-tip damage.

The values of fracture toughness were computed at the maximum load by using the plane stress, anisotropic stress intensity factors, listed in Table 5.6, which were modified by the model accuracy percentages listed in Table 5.5. The stress intensity factors in Table 5.6 correspond to a unit load and unit thickness. Because these are plane stress values they are linear with applied load and inversely linear with specimen thickness.

Table A-1: Notched Specimen Test Data for the $[0/\pm 45/90]_{ns}$ Laminates

SPECIMEN ID		CRACK SIZE in. (mm)	MEASURED DIMENSIONS			LOADS		FRACTURE TOUGHNESS AT MAX LOAD K_{max} ksi \sqrt{in} (MPa \sqrt{mm})
			THICKNESS		WIDTH in. (mm)	CRITICAL LOAD P_c kips (KN)	MAX LOAD P_{max} kips (KN)	
TYPE CCT CT TPB	Panel ID Number		Number of Plies	Thickness in. (mm)				
CCT	1-1	0.50 (12.7)	8	.0385 (.978)	2.000 (50.8)	-	2.84 (12.63)	35.2 (1230)
	1-2	0.50 (12.7)	8	.0388 (.986)	2.000 (50.8)	2.40 (10.68)	3.14 (13.97)	38.6 (1349)
	1-3	0.50 (12.7)	8	.0395 (1.003)	2.000 (50.8)	2.75 (12.23)	3.37 (14.99)	40.7 (1422)
	1-4	0.50 (12.7)	8	.0392 (.996)	2.000 (50.8)	2.24 (9.96)	3.56 (15.83)	43.3 (1513)
CCT	1-5	0.75 (19.05)	8	.0398 (1.011)	2.000 (50.8)	2.04 (9.07)	2.83 (12.59)	43.7 (1527)
	1-6	0.75 (19.05)	8	.0382 (.970)	2.000 (50.8)	1.98 (8.81)	2.37 (10.54)	38.1 (1332)
	2-1	0.75 (19.05)	8	.0385 (.978)	2.000 (50.8)	2.10 (9.34)	2.88 (12.81)	46.0 (1608)
	2-2	0.75 (19.05)	8	.0392 (.996)	2.000 (50.8)	1.96 (8.72)	2.56 (11.39)	40.1 (1401)
CCT	2-3	1.0 (25.4)	8	.0397 (1.008)	2.000 (50.8)	1.73 (7.70)	2.11 (9.39)	40.7 (1422)
	2-4	1.0 (25.4)	8	.0388 (0.986)	2.000 (50.8)	-	1.97 (8.76)	38.9 (1360)
	2-5	1.0 (25.4)	8	.0398 (1.011)	2.000 (50.8)	-	2.12 (9.43)	40.8 (1426)
	2-6	1.0 (25.4)	8	.0375 (0.953)	2.000 (50.8)	1.63 (7.25)	2.02 (8.98)	41.3 (1443)
CCT	27-3	1.25 (31.75)	8	.0390 (0.991)	1.999 (50.8)	-	1.37 (6.09)	34.1 (1192)
	27-4	1.25 (31.75)	8	.0395 (1.003)	1.998 (50.7)	-	1.57 (6.98)	38.6 (1349)
	27-5	1.25 (31.75)	8	.0393 (0.998)	1.999 (50.8)	1.25 (5.56)	1.93 (8.58)	47.7 (1667)
	27-6	1.25 (31.75)	8	.0395 (1.003)	2.000 (50.8)	1.63 (7.25)	1.65 (7.34)	40.6 (1419)
CCT	3-1	1.0 (25.4)	32	.154 (3.91)	1.999 (50.8)	7.40 (32.9)	8.80 (39.1)	43.8 (1531)
	3-2	1.0 (25.4)	32	.157 (3.99)	2.001 (50.80)	7.40 (32.9)	8.11 (36.1)	39.6 (1384)
	3-3	1.0 (25.4)	32	.154 (3.91)	2.002 (50.9)	7.23 (32.2)	7.75 (34.5)	38.5 (1346)
	3-4	1.0 (25.4)	32	.155 (3.94)	2.002 (50.9)	7.26 (32.3)	7.71 (34.3)	38.1 (1332)

Table A-1 (cont.)

SPECIMEN ID		CRACK SIZE in. (mm)	MEASURED DIMENSIONS			LOADS		FRACTURE TOUGHNESS AT MAX LOAD K_{max} ksi \sqrt{in} (MPa \sqrt{mm})
TYPE	Panel		THICKNESS		WIDTH	CRITICAL LOAD P_c kips (kN)	MAX LOAD P_{max} kips (kN)	
CCT	ID		Number	Thickness	in.			
CT	Number		of	in.	(mm)			
TPB			Plies	(mm)				
CCT	4-1	1.0 (25.4)	64	.315 (8.00)	2.001 (50.8)	11.90 (52.9)	13.10 (58.3)	31.9 (1115)
	4-2	1.0 (25.4)	64	.315 (8.00)	1.999 (50.8)	12.50 (55.6)	13.55 (60.3)	32.9 (1150)
	4-3	1.0 (25.4)	64	.316 (8.03)	2.001 (50.8)	13.00 (57.8)	14.40 (64.1)	34.9 (1220)
	4-4	1.0 (25.4)	64	.310 (7.87)	2.001 (50.8)	12.60 (56.0)	13.40 (59.6)	33.1 (1157)
CT	4-1	1.0 (25.4)	64	.312 (7.92)	-	1.350 (6.00)	1.405 (6.25)	31.3 (1094)
	4-2	1.0 (25.4)	64	.313 (7.95)	-	1.280 (5.69)	1.390 (6.18)	30.9 (1080)
	4-3	1.0 (25.4)	64	.314 (7.98)	-	1.290 (5.74)	1.435 (6.38)	31.8 (1111)
	4-4	1.0 (25.4)	64	.313 (7.95)	-	1.260 (5.60)	1.365 (6.07)	30.3 (1059)
TPB	4-1	0.50 (12.7)	64	.309 (7.85)	1.001 (25.4)	0.830 (3.69)	0.870 (3.87)	31.0 (1083)
	4-2	0.50 (12.7)	64	.313 (7.95)	1.001 (25.4)	0.850 (3.78)	0.890 (3.96)	31.3 (1094)
	4-3	0.50 (12.7)	64	.312 (7.92)	1.001 (25.4)	0.840 (3.74)	0.840 (3.74)	29.7 (1038)
	4-4	0.50 (12.7)	64	.312 (7.92)	1.000 (25.4)	0.860 (3.83)	0.860 (3.83)	30.4 (1062)
CCT	5-1	1.0 (25.4)	96	.476 (12.09)	2.001 (50.8)	18.40 (81.8)	19.40 (86.3)	31.2 (1090)
	5-2	1.0 (25.4)	96	.479 (12.17)	2.002 (50.9)	18.30 (81.4)	19.74 (87.8)	31.6 (1104)
	5-3	1.0 (25.4)	96	.478 (12.17)	2.002 (50.9)	20.30 (90.3)	21.16 (94.1)	33.9 (1185)
	5-4	1.0 (25.4)	96	.479 (12.17)	2.002 (50.9)	18.65 (83.0)	19.65 (87.4)	31.4 (1097)
CT	5-1	1.0 (25.4)	96	.468 (11.89)	-	1.510 (6.72)	1.510 (6.72)	22.4 (783)
	5-2	1.0 (25.4)	96	.475 (12.07)	-	2.000 (8.90)	2.100 (9.34)	30.7 (1073)
	5-3	1.0 (25.4)	96	.476 (12.09)	-	2.230 (9.92)	2.230 (9.92)	32.6 (1139)
	5-4	1.0 (25.4)	96	.469 (11.91)	-	2.040 (9.07)	2.040 (9.07)	30.2 (1055)

Table A-1 (cont.)

SPECIMEN ID		CRACK SIZE in. (mm)	MEASURED DIMENSIONS			LOADS		FRACTURE TOUGHNESS AT MAX LOAD K_{max} ksi/√in (MPa/√mm)
			THICKNESS		WIDTH in. (mm)	CRITICAL LOAD P_c kips (KN)	MAX LOAD P_{max} kips (KN)	
TYPE CCT CT TPB	Panel ID Number		Number of Plies	Thickness in. (mm)				
TPB	5-1	0.50 (12.7)	96	.467 (11.86)	1.002 (25.5)	1.200 (5.34)	1.200 (5.34)	28.3 (989)
	5-2	0.50 (12.7)	96	.471 (11.96)	1.001 (25.4)	1.280 (5.69)	1.295 (5.76)	30.3 (1059)
	5-3	0.50 (12.7)	96	.473 (12.01)	1.002 (25.5)	1.150 (5.12)	1.290 (5.74)	30.1 (1052)
	5-4	0.50 (12.7)	96	.472 (11.99)	1.001 (25.4)	1.170 (5.20)	1.170 (5.20)	27.3 (954)
CCT	6-1	00.50 (12.7)	120	.601 (15.27)	1.997 (50.7)	35.45 (157.7)	38.20 (169.9)	30.3 (1059)
	6-2	00.50 (12.7)	120	.605 (15.37)	2.000 (50.8)	36.30 (161.5)	39.80 (177.0)	31.4 (1097)
	6-3	0.50 (12.7)	120	.607 (15.42)	2.001 (50.8)	GRIPS SLIPPED SPECIMEN ENDS DAMAGED		
	6-4	0.50 (12.7)	120	.608 (15.44)	1.999 (50.8)	GRIPS SLIPPED SPECIMEN ENDS DAMAGED		
CCT	6-5	0.75 (19.05)	120	.608 (15.44)	2.001 (50.8)	28.2 (125.4)	31.1 (138.3)	31.4 (1097)
	6-6	0.75 (19.05)	120	.602 (15.29)	2.001 (50.8)	27.9 (124.1)	29.6 (131.7)	30.2 (1055)
	7-1	0.75 (19.05)	120	.597 (15.16)	2.000 (50.8)	29.3 (130.3)	31.6 (140.6)	32.5 (1136)
	7-2	0.75 (19.05)	120	.598 (15.19)	2.000 (50.8)	27.4 (121.9)	29.9 (133.0)	30.7 (1073)
CCT	7-3	1.0 (25.4)	120	.601 (15.27)	2.000 (50.8)	-	24.35 (108.3)	31.0 (1083)
	7-4	1.0 (25.4)	120	.600 (15.24)	2.000 (50.8)	DEPLIED AT		22.00 (97.9)
	7-5	1.0 (25.4)	120	.598 (13.19)	2.001 (50.8)	22.00 (97.9)	24.30 (108.1)	31.1 (1087)
	7-6	1.0 (25.4)	120	.594 (15.09)	2.001 (50.8)	22.60 (100.5)	24.20 (107.6)	31.2 (1090)
CCT	8-1	1.25 (31.75)	120	.607 (15.42)	2.002 (50.9)	18.10 (80.5)	18.88 (84.0)	30.2 (1055)
	8-2	1.25 (31.75)	120	.618 (15.70)	2.002 (50.9)	18.70 (83.2)	19.44 (86.5)	30.6 (1069)
	8-3	1.25 (31.75)	120	.613 (15.57)	2.002 (50.9)	17.60 (78.3)	18.66 (83.0)	29.6 (1035)
	8-4	1.25 (31.75)	120	.616 (15.65)	2.002 (50.9)	17.70 (78.8)	18.60 (82.7)	29.3 (1024)

Table A-1 (cont.)

SPECIMEN ID		CRACK SIZE in. (mm)	MEASURED DIMENSIONS			LOADS		FRACTURE TOUGHNESS AT MAX LOAD K_{max} $\frac{ksi\sqrt{in}}{(MPa\sqrt{mm})}$
			THICKNESS		WIDTH in. (mm)	CRITICAL LOAD P_c kips (KN)	MAX LOAD P_{max} kips (KN)	
TYPE CCT CT TPB	Panel ID Number		Number of Plies	Thickness in. (mm)				
CT	7-1	1.0 (25.4)	120	.597 (15.16)	-	2.395 (10.65)	2.530 (11.25)	29.5 (1031)
	7-2	1.0 (25.4)	120	.595 (15.11)	-	2.460 (10.94)	2.630 (11.70)	30.7 (1073)
	7-3	1.0 (25.4)	120	.596 (15.14)	-	2.230 (9.92)	2.570 (11.43)	30.0 (1049)
	7-4	1.0 (25.4)	120	.585 (14.86)	-	2.210 (9.83)	2.420 (10.76)	28.8 (1007)
TPB	8-1	0.50 (12.7)	120	.614 (15.60)	1.001 (25.4)	1.465 (6.52)	1.465 (6.52)	26.3 (919)
	8-2	0.50 (12.7)	120	.609 (15.47)	1.001 (25.4)	1.550 (6.89)	1.585 (7.05)	28.7 (1003)
	8-3	0.50 (12.7)	120	.614 (15.60)	1.001 (25.4)	1.585 (7.05)	1.585 (7.05)	28.5 (996)
	8-4	0.50 (12.7)	120	.614 (15.60)	1.001 (25.4)	1.465 (6.52)	1.575 (7.01)	28.3 (989)

Table A-2 Notched Specimen Test Data for the $[0/\pm 45]_{ns}$ Laminates

SPECIMEN ID		CRACK SIZE in. (mm)	MEASURED DIMENSIONS			LOADS		FRACTURE TOUGHNESS AT MAX LOAD K_{max} ksi \sqrt{in} (MPa \sqrt{mm})
TYPE CCT CT TPB	Panel ID Number		THICKNESS		WIDTH in. (mm)	CRITICAL LOAD P_c kips (KN)	MAX LOAD P_{max} kips (KN)	
			Number of Plies	Thickness in. (mm)				
CCT	9-1	0.50 (12.7)	6	.0297 (.754)	2.000 (50.8)	-	1.90 (8.45)	29.5 (1031)
	9-2	0.50 (12.7)	6	.0308 (.782)	2.000 (50.8)	1.95 (8.67)	2.10 (9.34)	31.5 (1101)
	9-3	0.50 (12.7)	6	.0305 (.775)	2.001 (50.8)	1.82 (8.10)	2.10 (9.34)	31.8 (1111)
	9-4	0.50 (12.7)	6	.0307 (.780)	2.000 (50.8)	-	2.01 (8.94)	30.2 (1055)
CCT	9-5	0.75 (19.05)	6	.0307 (.780)	2.000 (50.8)	1.48 (6.58)	1.72 (7.65)	33.2 (1160)
	9-6	0.75 (19.05)	6	.0287 (.729)	2.000 (50.8)	1.32 (5.87)	1.58 (7.03)	32.6 (1139)
	10-1	0.75 (19.05)	6	.0290 (.737)	2.001 (50.8)	1.52 (6.76)	1.58 (7.03)	32.2 (1125)
	10-2	0.75 (19.05)	6	.0307 (.780)	2.001 (50.8)	1.56 (6.94)	1.67 (7.43)	32.2 (1125)
CCT	10-3	1.0 (25.4)	6	.0300 (.762)	2.000 (50.8)	-	1.32 (5.87)	32.4 (1132)
	10-4	1.0 (25.4)	6	.0305 (.775)	2.000 (50.8)	1.25 (5.56)	1.40 (6.23)	33.8 (1181)
	10-5	1.0 (25.4)	6	.0300 (.762)	2.001 (50.8)	1.10 (4.89)	1.39 (6.18)	34.2 (1195)
	10-6	1.0 (25.4)	6	.0277 (.704)	2.000 (50.8)	1.17 (5.20)	1.43 (6.36)	38.1 (1332)
CCT	28-3	1.25 (31.75)	6	.0300 (.762)	2.001 (50.8)	1.00 (4.45)	1.08 (4.80)	34.1 (1192)
	28-4	1.25 (31.75)	6	.0298 (.757)	2.001 (50.8)	1.00 (4.45)	1.05 (4.67)	33.4 (1167)
	28-5	1.25 (31.75)	6	.0300 (.762)	2.000 (50.8)	1.00 (4.45)	1.05 (4.67)	33.1 (1157)
	28-6	1.25 (31.75)	6	.0295 (.749)	2.000 (50.8)	0.94 (4.18)	1.01 (4.49)	32.4 (1132)
CCT	11-1	1.0 (25.4)	30	.149 (3.78)	2.001 (50.8)	7.70 (34.2)	7.98 (35.5)	39.5 (1381)
	11-2	1.0 (25.4)	30	.151 (3.84)	2.001 (50.8)	7.68 (34.2)	7.95 (35.4)	38.8 (1356)
	11-3	1.0 (25.4)	30	.151 (3.84)	2.000 (50.8)	7.57 (33.7)	8.21 (36.5)	40.1 (1401)
	11-4	1.0 (25.4)	30	.151 (3.84)	2.000 (50.8)	7.68 (34.2)	7.98 (35.5)	39.0 (1363)

Table A-2 (cont.)

SPECIMEN ID		CRACK SIZE in. (mm)	MEASURED DIMENSIONS			LOADS		FRACTURE TOUGHNESS AT MAX LOAD K_{max} ksi√in (MPa√mm)
			THICKNESS		WIDTH in. (mm)	CRITICAL LOAD P_c kips (kN)	MAX LOAD P_{max} kips (kN)	
TYPE CCT CT TPB	Panel ID Number		Number of Plies	Thickness in. (mm)				
CCT	12-1	1.0 (25.4)	60	.303 (7.70)	2.001 (50.8)	15.10 (67.2)	16.03 (71.3)	39.0 (1363)
	12-2	1.0 (25.4)	60	.303 (7.70)	2.001 (50.8)	15.60 (69.4)	16.50 (73.4)	40.2 (1405)
	12-3	1.0 (25.4)	60	.301 (7.65)	2.002 (50.9)	16.70 (74.3)	17.08 (75.97)	41.8 (1461)
	12-4	1.0 (25.4)	60	.296 (7.52)	2.001 (50.8)	15.40 (68.5)	16.35 (72.72)	40.7 (1422)
CT	12-1	1.0 (25.4)	60	.301 (7.65)	-	1.350 (6.00)	1.605 (7.14)	35.2 (1230)
	12-2	1.0 (25.4)	60	.301 (7.65)	-	1.220 (5.43)	1.450 (6.45)	31.8 (1111)
	12-3	1.0 (25.4)	60	.303 (7.70)	-	1.440 (6.41)	1.520 (6.76)	33.1 (1157)
	12-4	1.0 (25.4)	60	.297 (7.54)	-	1.350 (6.00)	1.580 (7.03)	35.2 (1230)
TPB	12-1	0.50 (12.7)	60	.293 (7.44)	1.001 (25.4)	0.970 (4.31)	1.005 (4.47)	36.6 (1279)
	12-2	0.50 (12.7)	60	.298 (7.57)	1.001 (25.4)	0.975 (4.34)	1.000 (4.45)	35.8 (1251)
	12-3	0.50 (12.7)	60	.298 (7.57)	1.001 (25.4)	1.010 (4.49)	1.045 (4.65)	37.4 (1307)
	12-4	0.50 (12.7)	60	.303 (7.70)	1.002 (25.4)	1.015 (4.51)	1.070 (4.76)	37.6 (1314)
CCT	13-1	0.50 (12.7)	90	.451 (11.46)	2.001 (50.8)	PANEL NO GOOD		
	13-2	0.50 (12.7)	90	.453 (11.51)	2.000 (50.8)	PANEL NO GOOD		
	13-3	0.50 (12.7)	90	.455 (11.56)	2.001 (50.8)	PANEL NO GOOD		
	13-4	0.50 (12.7)	90	.456 (11.58)	2.001 (50.8)	PANEL NO GOOD		
CCT	13-5	0.75 (19.05)	90	.456 (11.58)	2.001 (50.8)	PANEL NO GOOD		
	13-6	0.75 (19.05)	90	.452 (11.48)	2.001 (50.8)	PANEL NO GOOD		
	14-1	0.75 (19.05)	90	.445 (11.30)	2.001 (50.8)	-	32.10 (142.8)	42.7 (1492)
	14-2	0.75 (19.05)	90	.448 (11.38)	2.000 (50.8)	-	32.30 (143.7)	42.7 (1492)

Table A-2 (cont.)

SPECIMEN ID		CRACK SIZE in. (mm)	MEASURED DIMENSIONS			LOADS		FRACTURE TOUGHNESS AT MAX LOAD K_{max} $\text{ksi}\sqrt{\text{in}}$ ($\text{MPa}\sqrt{\text{mm}}$)
TYPE	Panel		THICKNESS		WIDTH	CRITICAL LOAD P_c	MAX LOAD P_{max}	
CT TPB	ID Number	(mm)	Number of Plies	Thickness in. (mm)	in. (mm)	kips (KN)	kips (KN)	
CCT	14-3	1.0 (25.4)	90	.444 (11.28)	2.001 (50.8)	23.80 (105.86)	25.40 (112.98)	42.2 (1475)
	14-4	1.0 (25.4)	90	.443 (11.25)	2.001 (50.8)	24.30 (108.09)	25.40 (112.98)	42.3 (1478)
	14-5	1.0 (25.4)	90	.445 (11.30)	2.001 (50.8)	23.10 (102.75)	25.60 (113.87)	42.4 (1482)
	14-6	1.0 (25.4)	90	.442 (11.23)	2.000 (50.8)	24.30 (108.09)	24.60 (109.42)	41.0 (1433)
CCT	15-1	1.25 (31.75)	90	.442 (11.23)	2.001 (50.8)	18.10 (80.51)	19.28 (85.76)	41.3 (1443)
	15-2	1.25 (31.75)	90	.441 (11.20)	2.002 (50.8)	18.60 (82.73)	18.78 (83.53)	40.3 (1408)
	15-3	1.25 (31.75)	90	.441 (11.20)	2.001 (50.8)	18.80 (83.62)	19.82 (88.16)	42.6 (1489)
	15-4	1.25 (31.75)	90	.438 (11.13)	2.000 (50.8)	17.60 (78.28)	17.88 (79.53)	38.7 (1353)
CT	14-1	1.0 (25.4)	90	.446 (11.3)	-	2.075 (9.230)	2.075 (9.230)	30.7 (1073)
	14-3	1.0 (25.4)	90	.446 (11.33)	-	2.080 (9.252)	2.240 (9.964)	33.2 (1160)
	14-4	1.0 (25.4)	90	.441 (11.20)	-	1.900 (8.451)	2.150 (9.563)	32.2 (1125)
	15-1	1.0 (25.4)	90	.445 (11.30)	-	2.220 (9.875)	2.220 (9.875)	33.0 (1153)
TPB	15-1	0.50 (12.7)	90	.439 (11.15)	1.001 (25.4)	1.385 (6.160)	1.415 (6.294)	34.4 (1202)
	15-2	0.50 (12.7)	90	.441 (11.20)	1.002 (25.5)	1.490 (6.628)	1.490 (6.628)	36.0 (1258)
	15-3	0.50 (12.7)	90	.440 (11.18)	1.001 (25.4)	1.485 (6.605)	1.485 (6.605)	36.0 (1258)
	15-4	0.50 (12.7)	90	.446 (11.33)	1.001 (25.4)	1.450 (6.450)	1.450 (6.450)	34.7 (1213)
CCT	16-1	1.0 (25.4)	120	.602 (15.29)	2.001 (50.8)	29.00 (128.99)	32.40 (144.12)	39.7 (1388)
	16-2	1.0 (25.4)	120	.602 (15.29)	2.001 (50.8)	-	DEPLIED AT	30.00
	16-3	1.0 (25.4)	120	.602 (15.29)	2.001 (50.8)	30.40 (135.22)	32.70 (145.45)	40.0 (1398)

Table A-2 (concluded)

SPECIMEN ID		CRACK SIZE in. (mm)	MEASURED DIMENSIONS			LOADS		FRACTURE TOUGHNESS AT MAX LOAD K_{max} ksi \sqrt{in} (MPa \sqrt{mm})
			THICKNESS		WIDTH in. (mm)	CRITICAL LOAD P_c kips (KN)	MAX LOAD P_{max} kips (KN)	
TYPE CCT CT TPB	Panel ID Number		Number of Plies	Thickness in. (mm)				
CT	16-1	1.0 (25.4)	120	.595 (15.11)	-	2.95 (13.12)	2.95 (13.12)	32.8 (1146)
	16-2	1.0 (25.4)	120	.602 (15.29)	-	2.88 (12.81)	2.95 (13.12)	32.4 (1132)
	16-3	1.0 (25.4)	120	.598 (15.19)	-	2.75 (12.23)	2.825 (12.57)	31.2 (1090)
	16-4	1.0 (25.4)	120	.597 (15.16)	-	2.74 (12.19)	2.850 (12.68)	31.5 (1101)
TPB	16-1	0.50 (12.7)	120	.599 (15.21)	1.002 (25.5)	1.955 (8.696)	1.955 (8.696)	34.8 (1216)
	16-2	0.50 (12.7)	120	.594 (15.09)	1.001 (25.4)	1.950 (8.674)	1.950 (8.674)	35.0 (1223)
	16-3	0.50 (12.7)	120	.591 (15.01)	1.001 (25.4)	1.910 (8.496)	1.910 (8.496)	34.5 (1206)
	16-4	0.50 (12.7)	120	.598 (15.19)	1.001 (25.4)	2.005 (8.918)	2.005 (8.918)	35.7 (1248)

Table A-3 Notched Specimen Test Data for the $[0/90]_{ns}$ Laminates

SPECIMEN ID		CRACK SIZE in. (mm)	MEASURED DIMENSIONS			LOADS		FRACTURE TOUGHNESS AT MAX LOAD K_{max} ksi \sqrt{in} (MPa \sqrt{mm})
TYPE CCT CT TPB	Panel ID Number		THICKNESS		WIDTH in. (mm)	CRITICAL LOAD P_c kips (kN)	MAX LOAD P_{max} kips (kN)	
			Number of Plies	Thickness in. (mm)				
CCT	17-1	0.50 (12.7)	8	.0390 (.991)	2.004 (50.9)	3.02 (13.43)	3.12 (13.88)	33.9 (1185)
	17-2	0.50 (12.7)	8	.0393 (.998)	2.000 (50.8)	-	3.43 (15.26)	36.9 (1290)
	17-3	0.50 (12.7)	8	.0388 (.986)	2.003 (50.9)	3.30 (14.68)	3.75 (16.68)	40.9 (1429)
	17-4	0.50 (12.7)	8	.0403 (1.024)	2.002 (50.9)	2.72 (12.10)	3.98 (17.70)	41.8 (1461)
CCT	17-5	0.75 (19.05)	8	.0404 (1.026)	2.003 (50.9)	2.40 (10.68)	2.75 (12.23)	37.2 (1300)
	17-6	0.75 (19.05)	8	.0393 (.998)	2.000 (50.8)	2.38 (10.59)	2.69 (11.97)	37.4 (1307)
	18-1	0.75 (19.05)	8	.0393 (.998)	2.000 (50.8)	2.93 (13.03)	4.00 (17.79)	55.6 (1943)
	18-2	0.75 (19.05)	8	.0402 (1.021)	1.999 (50.8)	2.57 (11.43)	3.02 (13.43)	41.0 (1433)
CCT	18-3	1.0 (25.4)	8	.0383 (.973)	2.000 (50.8)	1.72 (7.65)	3.75 (16.68)	68.1 (2380)
	18-4	1.0 (25.4)	8	.0392 (.996)	2.000 (50.8)	2.15 (9.56)	2.98 (13.26)	52.9 (1849)
	18-5	1.0 (25.4)	8	.0402 (1.021)	2.000 (50.8)	-	2.12 (9.43)	36.7 (1283)
	18-6	1.0 (25.4)	8	.0388 (.986)	1.999 (50.8)	2.11 (9.39)	3.45 (15.35)	61.9 (2163)
CCT	29-3	1.25 (31.75)	8	.0388 (.986)	2.001 (50.8)	1.73 (7.70)	2.43 (10.81)	55.2 (1929)
	29-4	1.25 (31.75)	8	.0395 (1.003)	2.000 (50.8)	1.70 (7.56)	2.69 (11.97)	60.1 (2100)
	29-5	1.25 (31.75)	8	.0395 (1.003)	2.001 (50.8)	1.60 (7.12)	1.90 (8.45)	42.4 (1482)
	29-6	1.25 (31.75)	8	.0390 (.991)	2.001 (50.8)	-	1.69 (7.52)	38.2 (1335)
CCT	19-1	1.0 (25.4)	32	.154 (3.91)	2.001 (50.8)	6.47 (28.8)	7.19 (32.0)	32.5 (1136)
	19-2	1.0 (25.4)	32	.158 (4.01)	2.001 (50.8)	6.40 (28.5)	6.99 (31.09)	30.8 (1076)
	19-3	1.0 (25.4)	32	.159 (4.04)	2.001 (50.8)	-	7.39 (32.9)	32.3 (1129)
	19-4	1.0 (25.4)	32	.158 (4.01)	2.001 (50.8)	6.42 (28.6)	7.37 (32.8)	32.5 (1136)

Table A-3 (cont.)

SPECIMEN ID		CRACK SIZE in. (mm)	MEASURED DIMENSIONS			LOADS		FRACTURE TOUGHNESS AT MAX LOAD K_{max} ksi \sqrt{in} (MPa \sqrt{mm})
TYPE CCT CT TPB	Panel ID Number		THICKNESS		WIDTH in. (mm)	CRITICAL LOAD P_c kips (KN)	MAX LOAD P_{max} kips (KN)	
			Number of Plies	Thickness in. (mm)				
CCT	20-1	1.0 (25.4)	64	.327 (8.31)	2.001 (50.8)	-	12.61 (56.1)	26.8 (937)
	20-2	1.0 (25.4)	64	.327 (8.31)	2.001 (50.8)	-	13.14 (58.4)	28.0 (979)
	20-3	1.0 (25.4)	64	.326 (8.28)	2.001 (50.8)	10.80 (48.0)	11.30 (50.3)	24.1 (842)
	20-4	1.0 (25.4)	64	.325 (8.26)	2.001 (50.8)	-	11.80 (52.5)	25.3 (884)
CT	20-1	1.0 (25.4)	64	.324 (8.23)	-	1.250 (5.56)	1.250 (5.56)	27.2 (951)
	20-2	1.0 (25.4)	64	.328 (8.23)	-	1.250 (5.56)	1.250 (5.56)	26.8 (937)
	20-3	1.0 (25.4)	64	.327 (8.31)	-	1.245 (5.54)	1.245 (5.54)	26.8 (937)
	20-4	1.0 (25.4)	64	.321 (8.15)	-	1.230 (5.47)	1.230 (5.47)	27.0 (944)
TPB	20-1	0.50 (12.7)	64	.325 (8.26)	1.001 (25.4)	0.855 (3.80)	0.855 (3.80)	27.3 (954)
	20-2	0.50 (12.7)	64	.323 (8.20)	1.001 (25.4)	0.830 (3.69)	0.830 (3.69)	26.7 (933)
	20-3	0.50 (12.7)	64	.327 (8.31)	1.000 (25.4)	0.950 (4.23)	0.950 (4.23)	30.2 (1055)
	20-4	0.50 (12.7)	64	.323 (8.20)	1.001 (25.4)	0.840 (3.74)	0.840 (3.74)	27.0 (944)
CCT	21-1	0.50 (12.7)	96	.477 (12.12)	2.001 (50.8)	-	27.50 (122.3)	24.4 (853)
	21-2	0.50 (12.7)	96	.480 (12.19)	2.000 (50.8)	-	30.00 (133.4)	26.5 (926)
	21-3	0.50 (12.7)	96	.482 (12.24)	2.001 (50.8)	-	28.10 (125.0)	24.7 (863)
	21-4	0.50 (12.7)	96	.481 (12.22)	2.001 (50.8)	-	27.50 (122.3)	24.2 (846)
CCT	21-5	0.75 (19.05)	96	.481 (12.22)	2.002 (50.9)	-	23.70 (105.4)	26.9 (940)
	21-6	0.75 (19.05)	96	.480 (12.19)	2.001 (50.8)	-	24.00 (106.8)	27.3 (954)
	22-1	0.75 (19.05)	96	.475 (12.07)	2.000 (50.8)	-	22.60 (100.5)	26.0 (909)
	22-2	0.75 (19.05)	96	.479 (12.17)	2.000 (50.8)	21.00 (93.4)	22.80 (101.4)	26.0 (909)

Table A-3 (cont.)

SPECIMEN ID		CRACK SIZE in. (mm)	MEASURED DIMENSIONS			LOADS		FRACTURE TOUGHNESS AT MAX LOAD K_{max} ksi \sqrt{in} (MPa \sqrt{mm})
			THICKNESS		WIDTH in. (mm)	CRITICAL LOAD P_c kips (KN)	MAX LOAD P_{max} kips (KN)	
TYPE CCT CT TPB	Panel ID Number		Number of Plies	Thickness in. (mm)				
CCT	22-3	1.0 (25.4)	96	.479 (12.17)	1.999 (50.8)	-	17.55 (78.1)	25.5 (891)
	22-4	1.0 (25.4)	96	.479 (12.17)	2.000 (50.8)	-	18.30 (81.4)	26.6 (930)
	22-5	1.0 (25.4)	96	.478 (12.14)	1.999 (50.8)	-	16.40 (72.9)	23.9 (835)
	22-6	1.0 (25.4)	96	.477 (12.12)	2.000 (50.8)	-	17.30 (77.0)	25.2 (881)
CCT	23-1	1.25 (31.75)	96	.485 (12.32)	2.001 (50.8)	-	13.40 (59.6)	24.4 (853)
	23-2	1.25 (31.75)	96	.482 (12.24)	2.001 (50.8)	-	14.94 (66.5)	27.3 (954)
	23-3	1.25 (31.75)	96	.478 (12.14)	2.001 (50.8)	-	13.75 (61.2)	25.4 (888)
	23-4	1.25 (31.75)	96	.477 (12.12)	2.002 (50.9)	-	14.05 (62.5)	26.0 (909)
CT	22-1	1.0 (25.4)	96	.477 (12.12)	-	1.89 (8.41)	1.89 (8.41)	27.9 (975)
	22-2	1.0 (25.4)	96	.479 (12.17)	-	1.93 (8.58)	1.93 (8.58)	28.4 (993)
	22-3	1.0 (25.4)	96	.477 (12.12)	-	1.98 (8.81)	1.98 (8.81)	29.2 (1021)
	22-4	1.0 (25.4)	96	.472 (11.99)	-	2.05 (9.12)	2.05 (9.12)	30.6 (1069)
TPB	23-1	0.50 (12.7)	96	.478 (12.14)	1.001 (25.4)	1.240 (5.52)	1.240 (5.52)	26.9 (940)
	23-2	0.50 (12.7)	96	.479 (12.17)	1.001 (25.4)	1.225 (5.45)	1.225 (5.45)	26.6 (930)
	23-3	0.50 (12.7)	96	.482 (12.24)	1.000 (25.4)	1.335 (5.94)	1.335 (4.94)	28.8 (1007)
	23-4	0.50 (12.7)	96	.482 (12.24)	1.001 (25.4)	1.250 (5.56)	1.250 (5.56)	26.9 (940)
CCT	24-1	1.0 (25.4)	120	0.595 (15.11)	2.002 (50.9)	-	19.70 (87.6)	23.0 (804)
	24-2	1.0 (25.4)	120	0.595 (15.11)	2.002 (50.9)	-	21.60 (96.1)	25.3 (884)
	24-3	1.0 (25.4)	120	0.595 (15.11)	2.002 (50.9)	-	DEPLIED AT-18.00 (80.1)	

Table A-3 (concluded)

SPECIMEN ID		CRACK SIZE in. (mm)	MEASURED DIMENSIONS			LOADS		FRACTURE TOUGHNESS AT MAX LOAD K_{max} $\frac{\text{ksi}\sqrt{\text{in}}}{(\text{MPa}\sqrt{\text{mm}})}$
TYPE CCT	Panel ID Number		THICKNESS		WIDTH in. (mm)	CRITICAL LOAD P_c kips (KN)	MAX LOAD P_{max} kips (KN)	
			Number of Plies	Thickness in. (mm)				
CT	24-1	1.0 (25.4)	120	.586 (14.88)	-- --	2.27 (10.10)	2.27 (10.10)	27.3 (954)
	24-2	1.0 (25.4)	120	.598 (15.19)	-- --	2.30 (10.23)	2.30 (10.23)	27.1 (947)
	24-3	1.0 (25.4)	120	.603 (15.32)	-- --	2.22 (9.87)	2.280 (10.14)	26.6 (930)
	24-4	1.0 (25.4)	120	.599 (15.21)	-- --	2.440 (10.85)	2.440 (10.85)	28.7 (1003)
TPB	24-1	0.50 (12.7)	120	.589 (14.96)	1.001 (25.4)	1.520 (5.76)	1.520 (6.76)	26.8 (937)
	24-2	0.50 (12.7)	120	.588 (14.94)	1.001 (25.4)	1.565 (6.96)	1.565 (6.96)	27.6 (965)
	24-3	0.50 (12.7)	120	.595 (15.11)	1.001 (25.4)	1.550 (6.89)	1.550 (6.89)	27.0 (944)
	24-4	0.50 (12.7)	120	.598 (15.19)	1.002 (25.5)	1.440 (2.41)	1.440 (6.41)	25.0 (874)

1. Report No. NASA CR-3784		2. Government Accession No.		3. Recipient's Catalog No.	
4. Title and Subtitle FRACTURE BEHAVIOR OF THICK, LAMINATED GRAPHITE/EPOXY COMPOSITES				5. Report Date March 1984	
				6. Performing Organization Code	
7. Author(s) C. E. Harris and D.H. Morris				8. Performing Organization Report No.	
9. Performing Organization Name and Address Engineering Science and Mechanics Department Virginia Polytechnic Institute and State University Blacksburg, VA 24061				10. Work Unit No.	
				11. Contract or Grant No. NAG1-264	
12. Sponsoring Agency Name and Address National Aeronautics and Space Administration Washington, D.C. 20546				13. Type of Report and Period Covered Contractor Report	
				14. Sponsoring Agency Code	
15. Supplementary Notes Langley Technical Monitor: C. C. Poe, Jr.					
16. Abstract The effect of laminate thickness on the fracture behavior of laminated graphite epoxy (T300/5208) composites has been studied. The predominantly experimental research program included the study of the $[0/\pm 45/90]_{ns}$ and $[0/90]_{ns}$ laminates with thicknesses of 8,32,64,96 and 120 plies and the $[0/\pm 45]_{ns}$ laminate with thicknesses of 6,30,60,90 and 120 plies. The research concentrated on the measurement of fracture toughness utilizing the center-cracked tension, compact tension and three-point bend specimen configurations. The development of subcritical damage at the crack tip was studied nondestructively using enhanced x-ray radiography and destructively using the laminate delly technique. The test results showed fracture toughness to be a function of laminate thickness. The fracture toughness of the $[0/\pm 45/90]_{ns}$ and $[0/90]_{ns}$ laminates decreased with increasing thickness and asymptotically approached lower bound values of 30 ksi \sqrt{in} (1043 MPa \sqrt{mm}) and 25 ksi \sqrt{in} (869 MPa \sqrt{mm}) respectively. In contrast to the other two laminates, the fracture toughness of the $[0/\pm 45]_{ns}$ laminate increased sharply with increasing thickness but reached an upper plateau value of 40 ksi \sqrt{in} (1390 MPa \sqrt{mm}) at 30 plies. Fracture toughness was independent of crack size for both thin and thick laminates for all three laminate types except for the $[0/90]_{2s}$ laminate which split extensively. The center-cracked tension, three-point bend and compact tension specimens gave comparable results.					
17. Key Words (Suggested by Author(s)) Composite, Fracture, Thickness, Graphite/Epoxy, Fracture Toughness, Notched Laminates			18. Distribution Statement Unclassified - Unlimited Subject Category 24		
19. Security Classif. (of this report) Unclassified		20. Security Classif. (of this page) Unclassified		21. No. of Pages 100	
				22. Price A09	